Title

A revised chronostratigraphic framework for International Ocean Discovery Program Expedition 355 sites in Laxmi Basin, eastern Arabian Sea

Journal

GEOLOGICAL MAGAZINE, 157(6)

ISSN

0016-7568

Authors

Routledge, Claire M
Kulhanek, Denise K
Tauxe, Lisa
et al.

Publication Date

2020

DOI

10.1017/S0016756819000104

Peer reviewed

A revised chronostratigraphic framework for International Ocean Discovery Program Expedition 355 sites in Laxmi Basin, eastern Arabian Sea

Journal:	*Geological Magazine*
Manuscript ID	Draft
Manuscript Type:	Original Article
Date Submitted by the Author:	n/a
Complete List of Authors:	Routledge, Claire; University College London, Department of Earth Sciences Kulhanek, Denise K.; Texas A&M University, International Ocean Discovery Program Tauxe, Lisa; Scripps Institution of Oceanography Scardia, Giancarlo; Universidade Estadual Paulista, Instituto de Geociências e Ciências Exatas Singh, Arun Deo ; Banaras Hindu University Faculty of Science, geology Steinke, Stephan; Xiamen University Griffith, Elizabeth; Ohio State University, Earth Sciences Saraswat, Rajeev; Geological Oceanography Division, National Institute of Oceanography, Goa, India
Keywords:	biostratigraphy, magnetostratigraphy, IODP Site U1456, IODP Site U1457, Indus Fan, Neogene

A revised chronostratigraphic framework for International Ocean Discovery Program Expedition 355 sites in Laxmi Basin, eastern Arabian Sea

Claire M. Routledge[1], Denise K. Kulhanek[2,*], Lisa Tauxe[3], Giancarlo Scardia[4], Arun D. Singh[5], Stephan Steinke[6], Elizabeth M. Griffith[7] & Rajeev Saraswat[8]

[1]Department of Earth Sciences, University College London, London WC1E 6BT, UK

[2]International Ocean Discovery Program, Texas A&M University, College Station, TX 77845, USA

[3]Scripps Institution of Oceanography, University of California San Diego, La Jolla, CA 92093-0220, USA

[4]Instituto de Geociências e Ciências Exatas, Universidade Estadual Paulista, Rio Claro 19014-020, Brazil

[5]Department of Geology, Banaras Hindu University, Varanasi 221005, India

[6]Department of Geological Oceanography, Xiamen University, Xiamen 361005, China

[7]School of Earth Sciences, The Ohio State University, Columbus, OH 43210, USA

[8]Geological Oceanography Division, National Institute of Oceanography, Dona Paula, Goa 403004, India

*Corresponding author: [kulhanek@iodp.tamu.edu]

Short title: Revised age models for IODP Expedition 355 sites

Abstract

International Ocean Discovery Program Expedition 355 drilled Sites U1456 and U1457 in Laxmi Basin (eastern Arabian Sea) to document the impact that the South Asian monsoon had on weathering and erosion of the Himalayas. We revised the chronostratigraphic framework for these sites using a combination of bio-, magneto- and strontium-isotope stratigraphy. The sedimentary section at both sites is similar and we divide it into six units bounded by unconformities or emplaced as a mass transport deposit (MTD). Unit 1 underlies the MTD and is of early–middle Miocene age at Site U1456 and early Paleocene age at Site U1457. An unconformity (U1) created by emplacement of the MTD (unit 2) in the late Miocene between ~9.83 and 9.69 Ma separates units 1 and 2 and is identified by a marked change in lithology. Unit 3 consists of hemipelagic sediment with thin interbeds of graded sandstone of late Miocene age, separated from unit 4 by a second unconformity (U2) of 0.5–0.9 million year duration. Unit 4 consists of upper Miocene interbedded mudstone and sandstone and hemipelagic chalk deposited between ~8 and 6 Ma. A ~1.4–1.6 million year hiatus (U3) encompasses the Miocene/Pliocene boundary and separates unit 4 from unit 5. Unit 5 includes upper Pliocene to lower Pleistocene siliciclastic sediment that is separated from unit 6 by a ~0.45 million year hiatus (U4) in the lower Pleistocene. Unit 6 includes a thick package of rapidly deposited Pleistocene sand and mud overlain by predominantly hemipelagic sediment deposited since ~1.2 Ma.

Keywords: biostratigraphy, magnetostratigraphy, IODP Site U1456, IODP Site U1457, Indus Fan, Neogene

1. Introduction

The initiation of Himalayan uplift occurred at ~50 Ma when India and Eurasia collided (Matthews *et al*., 2016). The Indus River subsequently formed, carrying sediment from the Western Himalayas, Karakoram and Hindu Kush, and depositing it in the Indus Fan in the Arabian Sea (Clift *et al*., 2000, 2002; Briggs, 2003). Provenance studies indicate that the Indus River and its associated tributaries have primarily fed the fan since the collision of India and Eurasia (Clift *et al*., 2001), with 90% of the water originating from the Himalayan and Karakoram glaciers and draining an area of ~950,000 km^2 (Lückge *et al*., 2012). The Indus Fan is the second largest submarine fan in the world, second to only the Ganges- and Brahmaputra-fed Bengal Fan, and holds an estimated 5 $\times 10^6$ km^3 of sediment (Naini & Kolla, 1982; Clift, 2002).

International Ocean Discovery Program (IODP) Expedition 355 targeted a portion of the Indus Fan deposited in the Laxmi Basin, located in the eastern Arabian Sea (Figure 1) and running parallel to the west coast of India. Sediment was cored at Sites U1456 and U1457, situated between the Laxmi Ridge to the west and Panikkar Ridge (consisting of Raman and Panikkar Seamounts and Wadia Guyot) to the east (Figure 2). Laxmi Basin and its fan sediments provide a unique opportunity to better understand the links between changing monsoonal intensity and tectonics through reconstructing the history of erosion and weathering in the Western Himalaya and Karakoram.

In order to improve the chronostratigraphic framework that is key to examining the evolution of the Himalayas and climate from the late Miocene to Holocene, we undertook new biostratigraphic, paleomagnetic and geochemical analyses. Here we present updated chronostratigraphic frameworks for Site U1456 using new magnetostratigraphic data and Site

U1457 that includes updated and additional biostratigraphic, paleomagnetic and geochemical results.

2. Regional setting

The Expedition 355 sites were located to sample sediments transported from the Indus Suture Zone and western Himalayan since the Paleogene. Site U1456 (16°37.28'N, 68°50.22'E) is located in the Laxmi Basin, ~475 km west of the Indian coastline and ~820 km south of the modern Indus River mouth (Figures 1 and 2) (Pandey *et al*., 2016). Five holes were cored at this site recovering a total of 1010.67 m of core with ~70% recovery across all holes using a combination of piston and rotary coring techniques and reaching a maximum depth of 1109.4 m below seafloor (mbsf) in Hole U1456E (Pandey *et al*., 2016). Site U1457 (17°9.95'N, 67°55.80'E) is located ~115 km northwest of Site U1456 on the margin of Laxmi Ridge (Figures 1, 2) (Pandey *et al*., 2016). Three holes were cored at Site U1457 with a total of 710.91 m of sediment recovered (~80% overall recovery) using piston and rotary coring techniques with a maximum penetration depth of 1108.6 mbsf reached in Hole U1457C (Pandey *et al*., 2016). Site U1457 also recovered ~8 m of igneous basement rock that will help to determine whether basement is rifted continental crust from the Indian continent or of truly oceanic crustal affinity (Pandey *et al*., 2016).

3. Methods

Age models for each site were constructed during the expedition using a combination of calcareous microfossil biostratigraphy and magnetostratigraphy (Pandey *et al*., 2016). Magnetic inclination plotted against depth was used to determine zones of normal and reverse polarity that were then correlated to the geomagnetic polarity timescale using constraints provided by calcareous microfossil bioevents (i.e., calcareous nannofossil and planktonic foraminifer first and

last occurrences). Ages for events are from the Gradstein *et al*. (2012) geological time scale. Details for shipboard methods and results are given in Pandey *et al*. (2016). Here we update the age models using new biostratigraphic, paleomagnetic and strontium isotope stratigraphies.

3.a. Depth scales

Multiple holes were cored at each site, with a depth scale assigned for each hole in meters core depth below seafloor, method A (CSF-A). In order to place samples from different holes onto a common depth scale, a core composite depth below seafloor (CCSF) was constructed during the expedition (Pandey *et al*., 2016). This process, known as stratigraphic correlation, uses unique features in physical property data (e.g., magnetic susceptibility, natural gamma radiation, etc.) and core images to create stratigraphic ties between adjacent holes to construct a complete stratigraphic section. Although the composite depth scale is somewhat expanded (up to ~10%) relative to the actual stratigraphy, the composite depth scale provides a means to constrain chronostratigraphic events between holes. Here, we report depths using the composite depth scale constructed during the expedition (Site U1456) (Pandey *et al*., 2016) or refined post-cruise (Site U1457) (Lyle *et al*., 2018). Several holes at each of the two sites were not included in the original composite depth scales and required special treatment. For Site U1456, a composite depth scale was constructed for Holes U1456A and U1456C. To place samples from Holes U1456D and U1456E on the composite depth scale, we added a constant offset of 8.79 m to the CSF-A sample depths for both holes to create a composite depth scale (m CCSF). For Site U1457, a composite depth scale was created for Holes U1457A and U1457B. Samples from Hole U1457C were placed on the composite depth scale for Site U1457 by adding a constant offset of 5.15 m to CSF-A depths to the CSF-A sample depths.

3.b. Calcareous nannofossils

Shipboard samples were prepared from core catchers at ~9.5 m intervals from all holes at each site using standard smear slide techniques (e.g., Bown & Young, 1998). Strewn slides were prepared when sediment was predominantly sand. We analyzed 245 samples at Site U1456 and 156 samples at Site U1457 using a Zeiss Axiophot microscope and cross-polarized (XPL), plane-transmitted (PL), or phase contrast (PC) light at 400–1600× magnification. An additional 221 post-cruise samples were analyzed at intervals of two per section (every ~75 cm) from Site U1457 between ~2–8 Ma. Analysis was performed on a Zeiss Photoscope II microscope that was equipped with oil immersion objectives under XPL, PL and PC light at magnifications of 400–1600×.

We used the same semi-quantitative counting technique and taxonomic concepts for shipboard and post-cruise samples for continuity, with calibrated ages of bioevents from Gradstein *et al*. (2012). Samples were assigned to the zonation schemes of Martini (1971) and Okada & Bukry (1980). The relative abundance of individual calcareous nannofossil species or taxa groups was estimated visually at 1000× magnification as:

VA = very abundant (>100 specimens per field of view [FOV]).

A = abundant (10–100 specimens per FOV).

C = common (1–10 specimens per FOV).

F = few (1 specimen per 2–10 FOV).

R = rare (<1 specimen per 10 FOV).

Biostratigraphy relies on the identification of bioevents, primarily last occurrences (extinctions or tops) of a species and the first occurrences (originations or bases) of a species. Analysis of higher resolution samples allowed us to refine the position of some shipboard bioevents and identify additional bioevents during post-cruise analysis. Here we report datums as

the midpoint depth between the sample in which the highest (lowest) specimen was observed and the next examined sample above (below).

3.c. Foraminifers

Shipboard samples were prepared from core catchers at ~9.5 m intervals from all holes at each site using water or weak Calgon/hydrogen peroxide (H_2O_2) solution to disaggregate the sample, which was then washed over a 63 µm sieve. Any lithified material was crushed, heated in Calgon/H_2O_2 and then sieved. All samples were dried on filter paper at low temperature and sieved over a 150 µm sieve, with the 63–150 µm size fraction retained for additional observation if necessary. The 150 µm size fraction was analyzed using a Zeiss Discovery V8 microscope and all age-diagnostic species were separated and mounted onto faunal slides with a total of 178 samples analyzed at Site U1456 and 134 samples at Site U1457. Due to the paucity of foraminifers throughout much of the cored interval, no systematic foraminifer biostratigraphic analyses were performed post-cruise.

3.d. Paleomagnetism

The magnetostratigraphies of Sites U1456 and U1457 are based on discrete samples taken and analyzed on the ship (Pandey *et al*., 2016), and supplemented by additional post-cruise samples analyzed in the Scripps Paleomagnetic Laboratory. Paleomagnetic measurements were analyzed with version 4.0 of the PmagPy software package of Tauxe *et al*. (2016) available at http://github.com/PmagPy/PmagPy and all measurement data and interpretations are available in the MagIC database (upon acceptance of this article). Step-wise demagnetization of discrete samples produced a wide variety of behavior (examples shown in Figure 3). The behavior shown in Figures 3a,b shows a quasi-linear decay to the origin, after removal of a soft, usually steeply dipping, coring-induced remanence after demagnetization to 15 or 20 mT. Such behavior was

classified as Type I in Pandey *et al*. (2016). We have re-interpreted all shipboard and shore-based data by fitting a line through at least four consecutive measurements. Here we used a threshold value of 15° for the maximum angle of deviation (MAD) and the angle between the best-fit line and the origin (deviation angle, or DANG; Paterson *et al*., 2014), rejecting data that exceeded these bounds. All other behaviors (Types II, III and IV in Figure 3) fail our criteria.

Type II behavior (Figure 3c) fails the criteria for Type I in that the data do not go to the origin. The deviation angle exceeds the threshold value, and the polarity is uncertain. On the equal area projection, data are initially spread along a great circle suggesting that the characteristic magnetization is upward directed but is never reached. It is also possible that the characteristic magnetization is downward directed and is being deflected by the acquisition of a laboratory remanence.

The demagnetization data in Figure 3d,e (Type III) illustrate the acquisition of a gyromagnetic remanence (GRM) by trending toward the origin, but then veering strongly away from the origin, growing in magnetization (Figure 3e). On the equal area projection (inset to Figure 3e) the directions spread out along a great circle trending toward the specimen's Y-axis. This fact suggests acquisition of a laboratory remagnetization starting at about 40 or 50 mT, perpendicular to the last axis demagnetized (in this case, the specimen's Z axis) characteristic of a GRM. GRM is frequently associated with the authigenic (diagenetic or biogenic) iron sulfide greigite (Fe_3S_4). We calculated a GRM-index (Fu *et al*., 2008), which is the remanence after demagnetization to 60 mT minus the minimum value, normalized by the vector difference sum of the portion of demagnetization data prior to the minimum value minus the minimum value. This index quantifies the tendency to gain remanence after the 40 or 50 mT demagnetization step. GRM ranges from 0 to above 1, and the specimen shown in Figure 3e has a value of 0.47.

Interpretation of GRM associated with the occurrence of greigite is not straightforward, as many studies have shown that it can grow significantly during diagenesis after initial shallow burial (e.g., Sagnotti *et al*., 2005). The systematic use of the GRM index throughout all cores allowed us to log the potential occurrence of greigite and to easily identify stratigraphic intervals that may have experienced a diagenetic remagnetization.

The final type of data (Type IV), shown in Figure 3f, show no stability at all. This type of demagnetization behavior is also ignored.

In order to assess the reliability of the Type I data, we plot the inclinations as histograms in Supplementary Figure S1 for the two sites (online Supplementary Material available at http://journals.cambridge.org/geo). Inclinations within about five degrees of zero cannot be interpreted as polarity and inclinations steeper than about 55^{o} are likely to be a drill string remanence. Despite the low latitude of the drill site and the difficulty in identifying characteristic directions, there are two modes of negative and positive inclinations. These we interpret as reverse and normal polarities, respectively.

We transformed the composite depths (CCSF in meters) to ages using the revised tie points listed in Tables 1 and 2 and assuming linear sedimentation rates within each sedimentary unit. The composite depths *versus* inferred ages for each paleomagnetic sampling level are plotted in Supplementary Figure S2 for the two sites. The age tie points used for calibration purposes are plotted as blue stars. The updated magnetostratigraphies for Sites U1456 and U1457 are shown in Figures 4 and 5 respectively.

3.e. Strontium isotope ages

Benthic and planktonic foraminifers were picked from the >150 μm and 63–150 μm size fractions for isotopic analysis from seven samples from Cores U1457C-46R through 58R.

Foraminifers were chosen for analysis because they are considered typically less susceptible to diagenesis than bulk carbonate (e.g., Hess *et al*., 1986). Sufficient material (at least 400 µg) for Sr-isotope analysis was only found in 4 samples from the >150 µm size fraction. Only one sample had sufficient planktonic forms for analysis. A majority of the specimens were broken, without ornamentation and with abraded surfaces suggesting possible reworking.

Samples were dissolved in 100 µL 8 M ultrapure HNO_3, loaded directly onto separation columns containing 125 µL of Eichrom's Sr specific resin, washed with 2 mL of 8 M ultra-pure nitric acid, and then collected in 1 mL 0.005 M ultra-pure nitric acid. A measured blank using this method (8 pg Sr) constitutes <<0.1% of the sample loaded. Isotopic analysis of the prepared samples was carried out using the Neptune Plus multi-collector inductively coupled plasma mass spectrometer (MC-ICPMS) at the University of South Carolina following methods outlined in Scher *et al*. (2014). Instrumental mass fractionation was corrected by normalizing to $^{86}Sr/^{88}Sr$ = 0.1194 using an exponential law. Replicate analysis of SRM 987 yielded 0.710306 ± 0.000012 (2SD, n = 13). $^{87}Sr/^{86}Sr$ data were normalized to SRM 987, which has a reported $^{87}Sr/^{86}Sr$ value of 0.710248 (McArthur, 1994). Sr isotope values were converted to age estimates using the Strontium Isotope Stratigraphy Look-Up Table Version 5: Fit 26 03 13 (McArthur *et al*., 2012). An error estimate of ±1.0 million years is assigned to the Sr ages as a conservative estimate following previous work (John *et al*., 2011). The error estimate includes uncertainty in the seawater Sr isotope calibration curve, measured value, and rate of change with time of seawater Sr. The Sr ratios *versus* inferred age for the data from Hole U1457C are shown in Supplementary Figure S3 and listed in Table 2.

4. Results

4.a. Biostratigraphy

Biostratigraphic datums for Sites U1456 and U1457 are listed in Tables 1 and 2, respectively and more biostratigraphic detail provided in Supplementary Tables S1 to S4. Across both sites there are abundant and well preserved planktonic foraminifers in sediment younger than ~1 Ma, which consists predominantly of hemipelagic deposits and thin, graded, coarser-grained beds interpreted as turbidites. In these coarser-grained intervals, foraminifers are generally absent or reworked from older sediment (Pandey *et al*., 2016). Due to the scarcity of foraminifers in sediments older that ~1 Ma, post-cruise analyses resulted in limited updates to the placement of foraminifer bioevents. In addition, foraminifers were utilized for geochemical analysis, with results from Sr-isotope dating reported here (see Section 4.c below). For Site U1457, post-cruise biostratigraphic analysis revised the top of *Globigerinoides ruber* pink (calibrated at 0.12 Ma) to 3.70 m CCSF. Additionally, the base of *Globorotalia truncatulinoides* (calibrated at 1.93 Ma) is placed at a revised depth of 400.75 m CCSF at Site U1457. Foraminifer bioevent positions in all holes are given in Supplementary Tables S1 (U1456) and S2 (U1457). Tables 1 and 2 include only the datum position used for the age model.

At both Sites U1456 and U1457, calcareous nannofossils are generally common to very abundant in ooze/chalk and nannofossil-rich clay lithologies, displaying moderate preservation and minimal reworking. Select taxa are illustrated in Figure 6. In the coarser-grained lithologies, there is reduced nannofossil abundance and common reworking of Cretaceous and Paleogene forms that hindered the identification of marker taxa as in-situ assemblages were sparse. Post-cruise analysis of calcareous nannofossils focused on the interval older than ~2 Ma at Site U1457.

Higher resolution sampling has allowed us to refine the position of some bioevents and add additional bioevents that were not used for construction of the shipboard age model due to

their paucity in the examined samples. Positions of nannofossil datums in all holes are given in Supplementary Tables S3 (U1456) and S4 (U1457), with those used to define the age model included in Tables 1 and 2. Top *Discoaster pentaradiatus* (2.39 Ma) is placed at 419.54 m CCSF, which is consistent with the revised depth of the base of *G. truncatulinoides* (1.93 Ma) at 400.75 m CCSF. The increased sampling resolution allowed for a more accurate placement of the top of *Discoaster surculus* as only sparse numbers of specimens were identified shipboard. The top of *D. surculus* (2.49 Ma) is identified at 423.63 m CCSF. The top of the genus *Sphenolithus* is recorded at 515.27 m CCSF and calibrated to 3.54 Ma.

We did not use the base of *Discoaster tamalis* (4.13 Ma) when constructing the shipboard age model due to its sparse presence; however, a more reliable base was identified post-cruise at 539.40 m CCSF. The top of *D. quinqueramus* (5.59 Ma) was identified deeper at 539.40 m CCSF during post-cruise analysis, with the sporadic occurrences above considered reworked (Supplementary Table S5). *Nicklithus amplificus* has a relatively short range calibrated to between 6.91 Ma and 5.94 Ma. We record its base at 628.94 m CCSF and its top at 610.21 m CCSF. The base *Amaurolithus* spp. (7.42 Ma in Gradstein *et al*., 2012) occurs at 644.91 m CCSF.

4.b. Paleomagnetism

Many of the chron boundaries have been revised slightly based on post-cruise analyses and their positions are listed in Tables 1 and 2, with the most important adjustments made in the upper Miocene section. We identified 10 magnetic polarity reversals in Site U1456 that we correlate to the geomagnetic polarity timescale (GPTS) of Gradstein *et al*. (2012) within the constraints provided by biostratigraphy. We also identified 11 magnetic polarity reversals for Site U1457. Based on the new results from the calcareous nannofossils, we made a significant

revision to the magnetostratigraphic interpretations for these reversals at Site U1457 with the revised magnetostratigraphy used here shown in Figure 5. Details of the correlation of reversals to the GPTS are discussed in Section 5.a below. All magnetic data are in the MagIC database (http://earthref.org/MagIC) and will be available upon acceptance of this article.

4.c. Strontium isotope ages

Four samples analyzed from Site U1457 yield ages of 7.70 to 5.08 Ma (Supplementary Figure S3; Table 2) that are in reasonably good agreement with the biostratigraphic and paleomagnetic datums. Planktonic and benthic foraminifer specimens from Sample U1457C-47R-1, 6–10 cm (633.31 m CCSF) were measured in separate runs and yielded significantly different ages of 6.60 Ma and 6.00 Ma, respectively. Diagenetic alteration or inclusion of Sr from clay during analysis would most likely increase the measured $^{87}Sr/^{86}Sr$ and result in a younger age than expected, which could explain the difference between the benthic and planktonic foraminifer ages from the same sample. This could also explain the young age for Sample U1457C-46R-2, 100–104 cm (625.94 m CCSF).

5. Discussion

5.a. Age models

All datums used for the revised age models are compiled in Table 1 (Site U1456) and Table 2 (Site U1457). Both sites record similar sedimentation histories from the late Miocene to present, which we divide into sediment packages (called units) that have a distinct origin (mass transport deposit [MTD]) or are bounded by unconformities. The age and composition of the sediment recovered below the MTD is different between the two sites, with Site U1457 recording a significantly longer hiatus between deposition of the lowermost sediment package and the overlying MTD.

5.a.1. Site U1456

The section recovered at Site U1456 spans the upper Miocene to Holocene (units 3–6) with a short interval of lower to middle Miocene (unit 1) below a large MTD (unit 2) (Figure 7; Table 1). Unit 1 is dated as early to middle Miocene based on the presence of the calcareous nannofossil *Sphenolithus heteromorphus* (event 42 on Figure 7) at 1111.49 m CCSF.

The base of unit 2 is an unconformity (U1 on Figure 7) defined by a distinct change in sediment composition at 1110.46 m CCSF. Unit 2 is composed of a mixture of lithologies that show a variety of sedimentary structures including microfaults, folds, and inclined to vertical bedding (Pandey *et al*., 2016) that indicate deposition as a MTD (identified as the Nataraja Slide (Calvès *et al*., 2015)) and an interruption to hemipelagic and siliciclastic sedimentation at the site. The base of *Catinaster coalitus* (event 40) at 10.89 Ma occurs at 995.54 m CCSF and is recorded within unit 2. The top of unit 2 is intermixed with the resumption of in-situ deposition, tentatively identified in Core U1456D-38R (~817 m CCSF), yielding a total MTD thickness of at least 295 m. The timing of the mass transport event is constrained by the presence of *Catinaster coalitus* (event 40) at 995.54 m CCSF. The presence of this taxon within the MTD indicates that the event happened sometime after the evolution of *C. coalitus* at 10.89 Ma.

Two biostratigraphic events in the bottom of Core U1456D-37R constrain the age of in-situ deposition (unit 3) overlying the MTD to the late Miocene. The bases of the nannofossil *Discoaster hamatus* (10.55 Ma; event 39) and planktonic foraminifer *Neogloboquadrina acostaensis* (9.83 Ma; event 38) are found at 816.04 m CCSF and 817.72 m CCSF, respectively. Above this is a sequence of biostratigraphic events that includes the top of *C. coalitus* (9.69 Ma; event 37) at 771.58 m CCSF and the top of *D. hamatus* (9.53 Ma; event 36) at 760.47 m CCSF. We identify another unconformity (U2) at ~737.47 m CCSF from a clustering of biostratigraphic

events at that depth, including the tops of *Discoaster bollii* (9.21 Ma; event 35) and *Minylitha convallis* (8.68 Ma; event 31), and base of *Discoaster berggrenii* (8.29 Ma; event 30). This sequence of datums allows us to tie two magnetic polarity reversals above and below unconformity U2 to the GPTS (Gradstein *et al*., 2012). The magnetic reversal (event 34) at 745.00 m CCSF in unit 3 is correlated to the top of Chron C4Ar (9.11 Ma), and the magnetic polarity reversal (event 32) at 730.28 m CCSF near the base of unit 4 is tied to the top of Chron C4An (8.77 Ma).

Above unconformity U2, the upper Miocene unit 4 consists of ~250 m of sediment deposited between ~8.7 Ma and 5.6 Ma. A series of 3 magnetic polarity reversals (events 28, 27, and 25) are correlated to the GPTS based on several biostratigraphic datums. The top of *Discoaster loeblichii* (7.53 Ma; event 29) is identified at 604.68 m CCSF, which allows correlation of the magnetic reversal at 605.11 m CCSF (event 28) to the top of Chron C4n (7.53 Ma). The base of *Nicklithus amplificus* (6.91 Ma; event 26) at 554.01 m CCSF and the base of *Pulleniatina primalis* (6.60 Ma; event 24) at 527.12 m CCSF constrain the magnetic reversals at 585.21 m CCSF (event 27) and 553.04 m CCSF (event 25) to the tops of Chrons C3Bn (7.14 Ma) and C3Ar (6.73 Ma), respectively.

An interval of chalk was deposited in the late Miocene between ~6.6 Ma and 5.6 Ma with the age constrained by the base of *P. primalis* (6.60 Ma; event 24) at 527.12 m CCSF, the top *of N. amplificus* (5.94 Ma; event 23) at 523.39 m CCSF, and the base of *Globorotalia tumida* (5.57 Ma; event 21) at 513.42 m CCSF. The top of *Discoaster quinqueramus* (5.59 Ma; event 22) is recorded at 475.10 m CCSF, above which there is a noticeable change in the nannofossil assemblage that suggests the presence of a hiatus (U3 on Figure 7) that encompasses the Miocene/Pliocene boundary. The absences of *Ceratolithus acutus* (total range 5.35–5.04 Ma),

Amaurolithus primus (top at 4.50 Ma), and *Amaurolithus tricorniculatus* (top at 3.92 Ma) in the sediment above unconformity U3 indicate an age <3.92 Ma for the base of unit 5 at ~475 m CCSF. This allows the magnetic polarity reversal at 474.46 m CCSF (event 20) to be tied to the top of Chron C2Ar (3.596 Ma). Several biostratigraphic events constrain deposition of unit 5 to the late Pliocene to earliest Pleistocene, including the top of *Sphaeroidinellopsis seminulina* (3.375 Ma; event 19) at 423.47 m CCSF and the top of *Discoaster surculus* (2.49 Ma; event 18) at 362.28 m CCSF. The top of unit 5 is marked by another unconformity, identified by the presence of the tops of *Discoaster pentaradiatus* (2.39 Ma; event 17) and *Discoaster brouweri* (1.93 Ma; event 17) in the same sample at 354.63 m CCSF.

Several nannofossil datums are identified in close proximity near the base of unit 6, just above unconformity U4, including the base of *Gephyrocapsa* spp. >4 µm (1.73 Ma; event 14) at 344.83 m CCSF, base of *Gephyrocapsa* spp. >5.5 µm (1.62 Ma; event 13) at 341.10 m CCSF), and top of *Calcidiscus macintyrei* (1.60 Ma; event 12) at 342.24 m CCSF. This sequence of events allows the magnetic reversal at 347.58 m CCSF (event 15) to be correlated to the top of Chron C2n (1.778 Ma). The age of an interval of rapid sedimentation in the lower part of unit 6 is constrained by the aforementioned nannofossil datums (events 14–12), as well as the top of *N. acostaensis* (1.58 Ma; event 11) at 329.41 m CCSF. The next biostratigraphic event above this is the base of *Reticulofenestra asanoi* (1.14 Ma; event 10), identified at 146.38 m CCSF. Magnetic reversals at 124.56 m CCSF (event 9) and 111.00 m CCSF (event 8) are correlated to the tops of Subchrons C1r.2r (1.072 Ma) and C1r.1n (0.988 Ma), respectively.

The age model for sedimentation during the last ~1 million years at Site U1456 is well-constrained with 7 biostratigraphic and magnetic reversal events (Figure 7; Table 1). The top of *R. asanoi* (0.91 Ma; event 7) and the *Pulleniatina* coiling change to dominantly dextral forms

(0.80 Ma; event 6) at 98.60 m CCSF and 104.36 m CCSF, respectively, fit well with the magnetic reversal correlated to the Matuyama/Brunhes boundary (C1r; 0.781 Ma) at 93.17 m CCSF (event 5). Other biostratigraphic events include the top of *Globorotalia tosaensis* (0.61 Ma; event 4) at 62.10 m CCSF, the top of *Pseudoemiliania lacunosa* (0.44 Ma; event 3) at 41.93 m CCSF, the base of *Emiliania huxleyi* (0.29 Ma; event 2) at 30.56 m CCSF, and the top of *Globigerinoides ruber* pink (0.12 Ma; event 1) at 9.60 m CCSF. An oxygen isotope stratigraphy for this site has also been developed for the last 1.2 million years by Kim *et al*. (2018).

5.a.2. Site U1457

The succession recovered at Site U1457 is very similar to that cored at Site U1456, and consists of upper Miocene to Holocene sediments (units 3–6) separated by unconformities and overlying an upper Miocene MTD (unit 2) (Table 2; Figure 8). Unlike at Site U1456, the sediment below the MTD (unit 1) is significantly older (early Paleocene) (Table 2) and consists of ~30 m of marine sediment with no apparent input from the Indus Fan. The lower Paleocene section is hydrothermally altered and overlies basaltic basement (Pandey *et al*., 2016). It contains an early Paleocene assemblage that includes *Coccolithus pelagicus*, *Cruciplacolithus primus*, *Cruciplacolithus tenuis*, and *Prinsius* spp. The age of unit 1 is younger than 63.25 Ma based on the presence of the nannofossil *Ellipsolithus macellus* (event 51 on Table 2 and Figure 8) at 1084.45 m CCSF. The absence of *Fasciculithus* spp. (event 50 on Table 2) further constrains the age to older than 62.13 Ma.

The top of unit 1 is marked by an abrupt lithologic change between Cores U1457C-92R and 93R (1067.35 m CCSF). The range of lithologies in unit 2 (MTD) at Site U1457 is similar to those of unit 2 at Site U1456, although the total thickness of the MTD at Site U1457 is significantly less (~190 m). As at Site U1456, the age of the transported deposit is constrained by

the presence of *Catinaster coalitus* (base at 10.89 Ma; event 49), as well as *Discoaster bellus* (base at 10.40 Ma; event 48), which are both present within the MTD at 1003.10 m CCSF. Another event, the base of *N. acostaensis* (9.83 Ma; event 47), is identified near the top of the MTD at 889.66 m CCSF, somewhat below the first downhole appearance of tilted bedding in Core U1457C-71R at ~870 m CCSF. This event is identified just above obviously deformed bedding at Site U1456, so its presence below tilted bedding at Site U1457 could help to further constrain the timing of MTD emplacement. The presence of these taxa within the MTD provide a maximum age of 10.89 Ma for the timing of the event, whereas sediment in unit 3 overlying the MTD provides a minimum age of 9.83 Ma.

The resumption of background sedimentation at Site U1457 is indicated by a succession of biostratigraphic events and one paleomagnetic reversal. The top of *C. coalitus* (9.69 Ma; event 45) is identified at 860.57 m CCSF and the top of *Discoaster bollii* (9.21 Ma; event 44) is found at 851.06 m CCSF. These events help to correlate the magnetic polarity reversal at 865.19 m CCSF (event 46) with the top of Chron C5n. The concurrence of two nannofossil datums, the top of *Minylitha convallis* (8.68 Ma; event 43) and the base of *Discoaster quinqueramus* (8.12 Ma event 42), at 839.24 m CCSF indicates an unconformity (U2) at the top of unit 3.

The lower part of unit 4 (between ~839 and 675 m CCSF) lacks age control; however, the overlying hemipelagic succession between 675 and 610 m CCSF is well dated with a sequence of biostratigraphic events, Sr-isotope ages, and magnetic polarity reversals. The revised placement of the bases of *Amaurolithus* spp. (7.42 Ma; event 38) and *Nicklithus amplificus* (6.91 Ma; event 35) are identified at 644.91 m CCSF and 628.94 m CCSF, respectively. The base of *Pulleniatina primalis* (6.60 Ma; event 33) is found at 618.43 m CCSF, and top of *N. amplificus* (5.94 Ma; event 30) is found at 610.21 m CCSF. These biostratigraphic events help to constrain a

sequence of four magnetic polarity reversals. The reversals at 675.05 m CCSF (event 41) and 663.92 m CCSF (event 39) are correlated with the tops of Chrons C4r (8.11 Ma) and C4n (7.53 Ma), respectively. The events at 643.60 m CCSF (event 36) and 624.83 m CCSF (event 32) are correlated with the tops of Subchrons C3Br.2r (7.29 Ma) and C3An.1r (6.25 Ma), respectively. Sr-isotopes ages from near the base of the unit (events 40 and 37) correlate well with the other chronostratigraphic tie points (Figure 8). Events 31 and 34 are Sr-isotope ages from benthic and planktonic foraminifers picked from the same sample but that yield significantly different ages, with the age from the benthic foraminifer (event 31) appearing too young. This is also the case for the Sr-isotope age at 625.94 m CCSF (event 27), although both of these ages are within error (±1 million years) of the overall line of correlation.

The top of unit 4 is marked by an unconformity (U3) that spans the Miocene/Pliocene boundary. The length of the hiatus is well constrained at this site (~1.5 million years), with the identification of two nannofossil events at the same depth (539.40 m CCSF): the top of *D. quinqueramus* (5.59 Ma; event 28) and the base of *Discoaster tamalis* (4.13 Ma; event 26). The top of *Globoquadrina dehiscens* (5.92 Ma; event 29) may be reworked up-section, as it is found at 519.87 m CCSF, above unconformity U3 (Figure 8).

Unit 5 is dated to between ~4.1 and 2.3 Ma. The tops of *Sphenolithus* spp. (3.54 Ma; event 24) and *Dentoglobigerina altispira* (3.30 Ma; event 23) are identified at 515.27 m CCSF and 485.27 m CCSF, respectively. These datums help to correlate the magnetic polarity reversal at 484.56 m CCSF (event 25) with the top of Chron C2Ar (3.596 Ma). The bases of *Discoaster surculus* (2.49 Ma; event 21) and *Discoaster pentaradiatus* (2.39 Ma; event 20) are found in close proximity to each other at 423.63 m CCSF and 419.54 m CCSF, respectively. These data

constrain the magnetic polarity reversal at 422.16 m CCSF (event 22), allowing correlation with the top of Chron C2An (2.58 Ma).

A short unconformity (U4) marks the top of unit 5 and is identified by the concurrence of the tops of *Globoturborotalita woodi* (2.30 Ma; event 19) and *Discoaster brouweri* (1.93 Ma; event 17) at 402.62 m CCSF. The base of *Globorotalia truncatulinoides* (1.93 Ma; event 16) is also found near this depth at 400.75 m CCSF. These data help to correlate the magnetic reversal at 403.02 m CCSF (event 15) with the top of Chron C2n (1.778 Ma). The age of the lower part of unit 6 is constrained by the bases of *Gephyrocapsa* spp. >4 μm (1.73 Ma; event 14) and *Gephyrocapsa* spp. >5.5 μm (1.62 Ma; event 13) at 388.72 m CCSF and 365.23 m CCSF, respectively. The top of the foraminifer *Neogloboquadrina acostaensis* (1.58 Ma; event 12) is present at 211.64 m CCSF, although this event may be reworked up-section here, as it is found near the base of the sequence at Site U1456 (event 11 on Figure 7).

A series of biostratigraphic events and magnetic polarity reversals constrains the age model for the top 95.69 m CCSF of the site. The tops of *Globoturborotalita obliquus* (1.30 Ma; event 11) and *Gephyrocapsa* spp. >5.5 μm (1.24 Ma; event 10), as well as the base of *Reticulofenestra asanoi* (1.14 Ma; event 9) are identified at 95.69 m CCSF, 89.33 m CCSF, and 80.04 m CCSF, respectively. These events help to correlate magnetic polarity reversals at 76.20 m CCSF (event 8) and 66.98 m CCSF (event 7) to the tops of Subchrons C1r.2r (1.072 Ma) and C1r.1n (0.988 Ma), respectively. The tops of *R. asanoi* (0.91 Ma; event 6) and *Globorotalia tosaensis* (0.61 Ma; event 4) at 54.86 m CCSF and 31.53 m CCSF, respectively, constrain the magnetic polarity reversal at 47.15 m CCSF to the Matuyama/Brunhes boundary (top of Chron C1r; 0.781 Ma). The remainder of the stratigraphy is constrained by the top of *Pseudoemiliania lacunosa* (0.44 Ma; event 3) at 21.47 m CCSF, the base of *Emiliania huxleyi* (0.29 Ma; event 2)

at 25.87 m CCSF, and the top of *Globigerinoides ruber* pink (0.12 Ma; event 1) at 3.70 m CCSF. We note that the sequence of events for *P. lacunosa* and *E. huxleyi* appear to be reversed; however, this is likely due to uncertainty induced by looking only at samples every ~10 m, as well as the difficulty of identifying the base of *E. huxleyi* using a transmitted light microscope instead of a scanning electron microscope.

5.b. Sedimentary succession

The sedimentary successions at both sites are similar, with 4 units of sediment (units 3–6) overlying a MTD (unit 2). Emplacement of the MTD eroded different amounts of sediment at each site, as indicated by the very different ages of sediment underlying the MTD: early to middle Miocene (13.53–17.71 Ma) at Site U1456 and early Paleocene (62.13–63.25 Ma) at Site U1457. The sedimentary sequence at Site U1456 is thicker (estimated at ~1490 m based on seismic reflection profiles) as the site is located in the middle of the Laxmi Basin (Figure 2), whereas Site U1457 is located on the flank of Laxmi Ridge and has only ~1090 m of sedimentary fill overlying the basaltic basement (Pandey *et al*., 2016). At Site U1457, much of the Cenozoic sediments that were emplaced were removed by the MTD and only ~30 m of lower Paleocene marine sediment that lacks Indus-derived material (unit 1 on Figure 8) remains between the base of the MTD and basement. With a significantly thicker sedimentary succession at Site U1456, the MTD removed only Miocene-aged material, with upper lower to middle Miocene sediment present below the MTD. At Site U1456, the Miocene sediment in unit 1 is composed of interbedded gray silty claystone and silty sandstone, and likely represents a mixture of Indus Fan and hemipelagic deposition (Pandey *et al*., 2016).

The MTD (unit 2) varies in thickness from ~300 m at Site U1456 to ~190 m at Site U1457. The MTD is dominated by calcarenite, calcilutite, breccia and limestone that show

deformation structures throughout the deposit including microfaults, tilted bedding and slickensides (Pandey *et al*., 2016). Clasts of vesicular volcanic rock may derive from Deccan Plateau basalt and some of the limestone indicates deposition in shallow water, suggesting that the MTD is of shelf origin (Pandey *et al*., 2016). Calvès *et al*. (2015) identified a potential source area for the MTD on the West India continental margin offshore of the Saurashtra platform using seismic profiles and bathymetric maps. They named the MTD the Nataraja Slide and estimated a total volume of ~19 × 10^3 km^3, making it the second largest known submarine landslide. Shipboard biostratigraphy indicates that much of the sediment within the MTD is of Paleogene age, although there are intervals that also contain early to middle Miocene taxa (Pandey *et al*., 2016). The presence of the nannofossil *Catinaster coalitus* (total range 10.89–9.69 Ma) within the MTD at both sites constrains the timing of emplacement, which must have happened after the origination of *C. coalitus* at 10.89 Ma. Furthermore, the planktonic foraminifer *Neogloboquadrina acostaensis* (base at 9.83 Ma) is found in sediment immediately above obviously deformed strata at Site U1456 and just below obviously deformed strata at Site U1457, suggesting that the event occurred after 9.83 Ma. At both sites, *C. coalitus* is present in undeformed sediment above the MTD. While we cannot completely rule out reworking, we interpret that emplacement happened before the extinction of *C. coalitus* at 9.69 Ma, providing a narrow interval between ~9.69 and 9.83 Ma for MTD emplacement. The age of this event also constrains the length of the hiatus in unconformity U1 to between 3.8 and 8.0 million years at Site U1456 and ~52.5 to 53.5 million years at Site U1457.

At both sites, sediment above the MTD (unit 3) is primarily mudstone with sparse interbedded, graded sand beds that are interpreted as distal turbidites (Pandey *et al*., 2016). A similar sequence of biostratigraphic events is found in unit 3 at both sites that indicates a late

Miocene age. The sedimentation rate in unit 3 is higher at Site U1456 (10 cm/kyr) compared with Site U1457 (~6 cm/kyr). Unit 3 is separated from the overlying unit 4 by a disconformity (U2 on Figures 7 and 8) in the upper Miocene constrained to between 8.12 Ma and 9.21 Ma. At Site U1456, the hiatus is identified by the tops of *Minylitha convallis* (8.68 Ma) and *Discoaster bollii* (9.21 Ma), as well as the base of *Discoaster berggrenii* (8.29 Ma) at the same horizon, indicating a hiatus of at least 0.9 My. The last occurrence of *D. bollii* is found slightly deeper than the last occurrence of *M. convallis* at Site U1457 (851.06 m CCSF and 839.24 m CCSF, respectively), which suggests deposition continued at this site slightly longer after 9.21 Ma relative to Site U1456. At Site U1457, the top of *Discoaster quinqueramus* (8.12 Ma) is found at the same horizon as *M. convallis* (top at 8.68 Ma), indicating a hiatus of at least 0.56 My.

Unit 4 is also dominated by mudstone; however, thin sand beds are more frequent and intervals of hemipelagic chalk are also present in the upper part of unit 4 at both sites. The terrigenous sediment is interpreted as distal turbidity current deposits, with similar sedimentation rates at both sites (~9–10 cm/kyr). Siliciclastic-dominated deposition was interrupted in the late Miocene by deposition of hemipelagic chalk between ~8 and 6 Ma, which correlates to a climate transition marked by a change from C3- to C4-dominated terrestrial vegetation in the region (e.g., Quade *et al*., 1989; Cerling *et al*., 1997; Strömberg, 2011). Resumption of siliciclastic input occurred at roughly 6 Ma at both sites, with renewed deposition of sand and mud.

A hiatus of ~1.4 to 1.6 million years that spans the Miocene/Pliocene boundary (U3 on Figures 7 and 8) separates unit 4 from unit 5 at both sites. At Site U1457, the presence of *D. quinqueramus* (top at 5.59 Ma) and *Discoaster tamalis* (base at 4.13 Ma) at the same horizon (539.40 m CCSF), indicates a minimum hiatus duration of 1.46 million years. The disconformity is better constrained at Site U1457 than at Site U1456 where *D. tamalis* was not identified.

Sediment in unit 5 is similar to that of unit 4 and is dominantly siliciclastic, albeit with thin intervals of hemipelagic chalk. Sediment appears to be somewhat coarser-grained at Site U1457 relative to Site U1456 (Pandey *et al*., 2016), although poor recovery at Site U1457 hampers quantifying this observation. Sedimentation rates were similar at both sites, between ~8 and 10 cm/kyr.

Another short hiatus (unconformity U4) separates unit 5 from unit 6 and encompasses part of the early Pleistocene. It is identified by the tops of *Discoaster brouweri* (1.93 Ma) and *Discoaster pentaradiatus* (2.39 Ma) at the same horizon (354.63 m CCSF) at Site U1456. At Site U1457, the hiatus appears to be of slightly shorter duration and is indicated by the tops of *Globoturborotalita woodi* (2.3 Ma) and *D. brouweri* (1.93 Ma) at the same horizon (402.62 m CCSF). Furthermore, the last occurrence of *D. brouweri* occurs within a normal polarity zone at both Sites U1456 and U1457, whereas its extinction at 1.93 Ma is correlated with a reversed polarity interval at the top of Chron C2r (Gradstein *et al*., 2012). Taken together, these lines of evidence suggest a hiatus of ~0.45 million year duration in the early Pleistocene.

The lower part of unit 6 consists of a thick section (>200 m) of siliciclastic sediment deposited very rapidly in the early Pleistocene. This sediment is very coarse-grained at Site U1456. Recovery of this interval at Site U1457 was much poorer due to use of the rotary core barrel coring assembly, so it is difficult to determine the dominant grain size. Regardless, sedimentation rates over this interval were at least 40 cm/kyr at Site U1456 and 60 cm/kyr at Site U1457. These deposits are interpreted as a sheet-type lobe in a mid- or lower fan setting (Pandey *et al*., 2016). Sedimentation at both sites since ~1.2 Ma was dominantly hemipelagic with the sediment comprised of deep-sea calcareous ooze interbedded with clay, silt and sand, whereby

the sand layers comprise thin turbidite sequences likely deposited in a distal basin setting (Pandey *et al*., 2016).

5.c. Regional comparison

Previous drilling in the Arabian Sea during Deep Sea Drilling Project (DSDP) Leg 23 and Ocean Drilling Program (ODP) Leg 117 (Figure 1) provided age control for distal Indus Fan sediments. At Site 219 on the Laccadive Ridge and Site 223 on the Murray Ridge to the southeast and west of our drill sites, respectively, the oldest sediment recovered was late Paleocene in age (Whitmarsh *et al*., 1974). This cross-basin comparison aligns with sediments at Site U1457, where a ~30 m thick section of lower Paleocene sediment was recovered directly below the MTD and overlying the basaltic basement (Pandey *et al*., 2016).

Comparison of biostratigraphic events across the Arabian Sea from the Laxmi Basin to the western-most edge of the Indus Fan indicates the rarity or absence of several Miocene nannofossil biomarkers including the genera *Amaurolithus* and *Ceratolithus*, as well as a few species of *Discoaster* (e.g., *D. surculus*, *D. asymmetricus* and *D. tamalis*) at both Sites U1456 and U1457 as well as at Sites 721, 722 and 731 (Prell *et al*., 1989). Genera belonging to the family Ceratolithaceae (e.g., *Amaurolithus* and *Ceratolithus*) are considered warm water, open ocean dwellers (Wade & Bown, 2006) but are noticeably rare to absent in the Arabian Sea. This scarcity in the fan setting might be a result of dilution due to high rates of terrigenous sediment input, or, in the wider Arabian Sea, by exclusion from higher productivity environments.

The hiatus encompassing the Miocene/Pliocene boundary at Sites U1456 and U1457 is recorded at several other sites within the Arabian Sea, from the southern-most and western-most edge of the Indus Fan (DSDP Sites 221 and 224 and ODP Sites 720, 721, 722 and possibly Site

731). Other sites drilled in the Arabian Sea (including DSDP Sites 219, 220, 222 and 223) recovered the Miocene/Pliocene boundary.

5.d. Taxonomy and age calibrations

The family Ceratolithaceae includes the distinctive and biostratigraphically important Neogene genera *Amaurolithus*, *Ceratolithus*, *Nicklithus*, *Orthorhabdus* and *Triquetrorhabdulus*. The ornate nannolith genera *Amaurolithus*, *Ceratolithus* and *Nicklithus* are useful late Miocene through Pliocene biostratigraphic markers for low latitude, open ocean settings.

Amaurolithus primus is the first representative of the genus *Amaurolithus*, which evolved from *Triquetrorhabdulus rugosus* in the late Miocene (Raffi *et al*., 1998). This event is dated to 7.42 Ma in the eastern Mediterranean using astronomical tuning (Raffi *et al*., 2003), but is known to occur slightly later (7.36 Ma) in the Atlantic at ODP Sites 925 and 926 (Backman & Raffi, 1997; Shackleton & Crowhurst, 1997). In the eastern Equatorial Pacific (ODP Leg 138), the base of *Amaurolithus* was dated to ~7.25 Ma at Site 844 (Shackleton *et al*., 1995). The position of this event falls within the middle of Subchron C3Br.2r based on the magnetostratigraphy of Schneider (1995), equivalent to ~7.3 Ma on the GPTS2012. At ODP Site 710 in the equatorial Indian Ocean, this event falls within Subchron C3.Br.1r (Rio *et al*., 1990), which is equivalent to ~7.23 Ma on the GPTS2012. Thus, the first appearance of this genus is diachronous between the Mediterranean, South Atlantic, Pacific and Indian Oceans, and is closer to 7.3 or 7.2 Ma in the Indian Ocean. While we plot the age as 7.42 Ma in Figure 8 (as given in GPTS2012), we suggest that this event occurs 100 or 200 kyr later at this site, which better aligns with the magnetostratigraphic interpretation for polarity reversal events above and below this datum (see red circle and arrow for event 38 in Figure 8).

The genus *Nicklithus* was once included within *Amaurolithus*; however, phylogenetic evidence presented by Raffi *et al*. (1998) suggested that it evolved independently and proposed a new genus. Both the evolution and extinction of *Nicklithus amplificus* are stratigraphically significant bioevents in the late Miocene (range reported as 6.91 Ma to 5.94 Ma in Gradstein *et al*., 2012). The evolution of *N. amplificus* is astronomically tuned at 6.91 Ma in the South Atlantic at ODP Sites 925 and 926 (Backman & Raffi, 1997; Shackleton & Crowhurst, 1997). Its first appearance is known to occur later in the eastern Mediterranean (6.68 Ma; Raffi *et al*., 2003). Raffi *et al.* (1995) examined the occurrences of Miocene bioevents in the equatorial Indian (ODP Leg 115) and Pacific (ODP Leg 138) Oceans. They reported that the first occurrence of *N. amplificus* occurs very near the Chron C3Ar/C3An boundary (~6.73 Ma) at sites in both oceans, including Sites 844 and 845 (Raffi & Flores, 1995; Schneider, 1995) and Site 710 (Rio *et al*., 1990). At Site U1456, the base of *N. amplificus* is found within 1 m of a magnetic polarity reversal, which we interpret to be the top of Chron C3Ar (6.73 Ma), supporting the younger age of ~6.7 Ma for the evolution of *N. amplificus* in the Indian Ocean (see red circle and arrow for event 26 in Figure 7 and event 35 in Figure 8).

5.e. Microfossil reworking

The abundance of reworked Cretaceous and Paleogene calcareous nannofossils recorded throughout the stratigraphy at Sites U1456 and U1457 were similarly recorded at Sites 222 and 731 in the western Arabian Sea (Whitmarsh *et al*., 1974; Prell *et al*., 1989). Reworked forms appear to have undergone significant diagenesis as well as dissolution and breakage that is likely due to the distance travelled post-deposition. The source of the Cretaceous reworking is not immediately clear but could originate from Cretaceous limestone outcrops in Western Pakistan

and/or eroded from the Himalayas and transported by the Indus River into the fan sediments (Whitmarsh *et al*., 1974).

6. Conclusions

IODP Expedition 355 to the Arabian Sea cored Sites U1456 and U1457 in the Laxmi Basin. The integration of new and shipboard biostratigraphic, paleomagnetic and geochemical data has allowed us to revise the age models, which are critical to examining the relationship between Himalayan uplift, erosion, and climate through the Cenozoic. The stratigraphy at both sites is similar, and includes four units of Neogene and Quaternary sediment separated by unconformities that overlay a MTD emplaced in the late Miocene. Below the MTD, the age and composition of the sediments are very different between the two sites.

- Unit 1 underlies the MTD. At Site U1456, unit 1 consists of a mixture of terrigenous (likely sourced from the Indus River) and hemipelagic sediment of early to middle Miocene age. At Site U1457, unit 1 is of early Paleocene age and consists of 30 m of hydrothermally altered marine mud that directly overlies the basaltic basement.
- Unit 2 is the MTD that is composed of a wide variety of mixed lithologies, including calcilutite, calcarenite, limestone, and mudstone with a variety of deformation features consistent with emplacement during a mass transport event. Biostratigraphy indicates that the MTD was emplaced between ~9.83 and 9.69 Ma.
- Unit 3 represents a return to in situ deposition above the MTD and is composed of nannofossil-rich mudstone with thin graded sandstone beds interpreted as turbidites of the Indus Fan. The sedimentation rate for unit 3 was ~10 cm/kyr at Site U1456 and ~6 cm/kyr at Site U1457. The top of this unit is marked by a hiatus (unconformity U2) at both sites between ~9.21 and 8.12 Ma.

- Unit 4 includes a sequence of interbedded coarser-grained sand and mud deposited at ~9–10 cm/kyr. Turbidite deposition was interrupted between ~8 Ma and 6 Ma in the late Miocene by hemipelagic chalk deposition. Turbidite deposition resumed in the late Miocene at ~6 Ma, with sedimentation rates again ~10 cm/kyr. The top of unit 3 is a longer hiatus (1.4–1.6 My) that encompasses the Miocene/Pliocene boundary.
- Turbidite deposition continued in unit 5 at a rate of ~8–10 cm/kyr. This unit was deposited between ~4.1 and 2.4 Ma. The top of unit 5 is a short (~0.45 My) hiatus in the lower Pleistocene.
- Unit 6 consists of a thick (~200 m) sequence of coarse-grained sediment deposited very rapidly (~40–45 cm/kyr at Site U1456 and ~60 cm/kyr at Site U1457) between ~1.9 and 1.2 Ma. Hemipelagic deposition has dominated the region since ~1.2 Ma. Sedimentation rates were still high (~7–12 cm/kyr), but much slower than deposition during the early Pleistocene.

These revised age models will enable tighter constraint of tectonic and climate interaction as a result of Himalayan uplift.

Acknowledgements

This research used samples and data provided by the International Ocean Discovery Program (IODP). Many thanks go to the operational and technical staff as well as the shipboard science party for an enjoyable and successful expedition. This work was partially supported by USSSP PEA funding to CMR, DKK, and LT, and NSF Grant EAR1547263 to LT.

Declaration of Interest

The authors have no conflicts of interest to declare.

References

BACKMAN, J., & RAFFI, I. 1997. Calibration of Miocene nannofossil events to orbitally tuned cyclostratigraphies from Ceara Rise. *Proceedings of the Ocean Drilling Program, Scientific Results*, **154**, 83–99.

BOWN, P. R., & YOUNG, J. R. 1998. Techniques. In P. R. Bown (Ed.), *Calcareous Nannofossil Biostratigraphy* (First, pp. 16–28). Cambridge: Chapman & Hall.

BRIGGS, J. C. 2003. The biogeographic and tectonic history of India. *J Biogeography*, **30**(3), 381–388.

CALVÈS, G., HUUSE, M., CLIFT, P. D., & BRUSSET, S. 2015. Giant fossil mass wasting off the coast of West India: The Nataraja submarine slide. *Earth and Planetary Science Letters*, **432**, 265–272.

CERLING, T. E., HARRIS, J. M., MACFADDEN, B. J., LEAKEY, M. G., QUADE, J., EISENMANN, V., & EHIERINGER, J. R. 1997. Global vegetation change through the Miocene/Pliocene boundary. *Nature*, **389**, 153–158.

CLIFT, P. D. 2002. A brief history of the Indus River. *Geological Society, London, Special Publications*, **195**(1), 237–258.

CLIFT, P. D., LEE, J. I., HILDEBRAND, P., SHIMIZU, N., LAYNE, G. D., BLUSZTAJN, J., BLUM, J. D., GARZANTI, E., & KHAN, A. A. 2002. Nd and Pb isotope variability in the Indus River System: implications for provenance and crustal heterogeneity in th Western Himalaya. *Earth and Planetary Science Letters*, **200**, 91–106.

CLIFT, P. D., SHIMIZU, N., LAYNE, G. D., BLUSZTAJN, J. S., GAEDICKE, C., SCHLÜTER, H. U., CLARK, M. K., & AMJAD, S. 2001. Development of the Indus Fan and its significance for the

erosional history of the Western Himalaya and Karakoram. *Bulletin of the Geological Society of America*, **113**(8), 1039–1051.

CLIFT, P., SHIMIZU, N., LAYNE, G., GAEDICKE, C., SCHL TER, H. U., CLARK, M., & AMJAD, S. 2000. Fifty-five million years of Tibetan evolution recorded in the Indus Fan. *Eos*, **81**(25), 277–281.

FU, Y., VON DOBENECK, T., FRANKE, C., HESLOP, D., & KASTEN, S. 2008. Rock magnetic identification and geochemical process models of greigite formation in Quaternary marine sediments from the Gulf of Mexico (IODP Hole U1319A). *Earth and Planetary Science Letters*, **275**(3–4), 233–245.

GRADSTEIN, F., OGG, J., SCHMITZ, M., & OGG, G. 2012. *The Geologic Time Scale 2012*. (F. Gradstein, J. Ogg, M. Schmitz, & G. Ogg, Eds.). Amsterdam: Elsevier.

HESS, J., BENDER, M. L., & SCHILLING, J. 1986. Evolution of the ratio of strontium-87 to strontium-86 in seawater from Cretaceous to Present. *Science*, **231**(4741), 979–984.

JOHN, C. M., KARNER, G. D., BROWNING, E., LECKIE, R. M., MATEO, Z., CARSON, B., & LOWERY, C. 2011. Timing and magnitude of Miocene eustasy derived from the mixed siliciclastic-carbonate stratigraphic record of the northeastern Australian margin. *Earth and Planetary Science Letters*, **304**(3–4), 455–467.

KIM, J. E., KHIM, B. K., IKEHARA, M., & LEE, J. 2018. Orbital-scale denitrification changes in the Eastern Arabian Sea during the last 800 kyrs. *Scientific Reports*, **8**(1), 1–8.

KOLLA, V., & COUMES, K. 1987. Morphology, internal structure, seismic stratigraphy, and sedimentation of Indus Fan. *AAPG Bulletin*, **71**(6), 650–677.

LÜCKGE, A., DEPLAZES, G., SCHULZ, H., SCHEEDER, G., SUCKOW, A., KASTEN, S., & HAUG, G. H. 2012. Impact of indus River discharge on productivity and preservation of organic carbon in

the Arabian Sea over the Twentieth century. *Geology*, **40**(5), 399–402.

LYLE, M. W., SARASWAT, R., & SCIENTISTS, I. E. 355. 2018. Data report: Revised Pleistocene sediment splice for Site U1457, IODP Expedition 355. *Proceedings of the International Ocean Discovery Program*, **355**.

MARTINI, E. 1971. Standard Tertiary and Quaternary calcareous nannoplankton zonation. *Proceedings of the Second Planktonic Conference, Roma 1970*, 739–785.

MATTHEWS, K. J., DIETMAR MÜLLER, R., & SANDWELL, D. T. 2016. Oceanic microplate formation records the onset of India-Eurasia collision. *Earth and Planetary Science Letters*, **433**, 204–214.

MCARTHUR, J. M. 1994. Recent trends in strontium isotope stratigraphy. *Terra Review*, **6**(4), 331–358.

MCARTHUR, J. M., HOWARTH, R. J., & SHIELDS, G. A. 2012. Strontium isotope stratigraphy. In *The Geologic Time Scale 2012* (pp. 127–144). Elsevier.

NAINI, B. R., & KOLLA, V. 1982. Acoustic character and thickness of sediments of the Indus Fan and the continental margin of western India. *Marine Geology*, **47**(3–4), 181–195.

OKADA, H., & BUKRY, D. 1980. Supplementary modification and introduction of code numbers to the low-latitude coccolith biostratigraphic zonation (Bukry, 1973; 1975). *Marine Micropaleontology*, **5**, 321–325.

PANDEY, D. K., CLIFT, P. D., KULHANEK, D. K., ANDÒ, S., BENDLE, J. A. P., BRATENKOV, S., GRIFFITH, E. M., GURUMURTHY, G. P., HAHN, A., IWAI, M., KHIM, B.-K., KUMAR, A., KUMAR, A. G., LIDDY, H. M., LU, H., LYLE, M. W., MISHRA, R., RADHAKRISHNA, T., ROUTLEDGE, C. M., SARASWAT, R., SAXENA, R., SCARDIA, G., SHARMA, G. K., SINGH, A. D., STEINKE, S., SUZUKI, K., TAUXE, L., TIWARI, M., XU, Z., & YU, Z. 2016. Arabian Sea

Monsoon. *Proceedings of the International Ocean Discovery Program*, **355**.

PATERSON, G. A., TAUXE, L., BIGGIN, A. J., SHAAR, R., & JONESTRASK, L. C. 2014. On improving the selection of Thellier-type paleointensity data. *Geochemistry, Geophysics, Geosystems*, **15**, 1180–1192.

PRELL, W. L., NIITSUMA, N., EMEIS, K.-C., AL-SULAIMAN, Z. K., AL-TOBBAH, A. N. K., ANDERSON, D. M., BARNES, R. O., BILAK, R. A., BLOEMENDAL, J., BRAY, C. J., BUSCH, W. H., CLEMENS, S. C., DE MENOCAL, P., KRISSEK, L. A., KROON, D., MURRAY, D. M., NIGRINI, C. A., PEDERSEN, T. F., RICKEN, W., SHIMMIELD, G. B., SPAULDING, S. A., TAKAYAMA, T., TEN HAVEN, H. LO, & WEEDON, G. P. 1989. Oman margin/Neogene package. *Proceedings of the Ocean Drilling Program, Initial Reports*, **117**, 1–1235.

QUADE, J., CERLING, T. E., & BOWMAN, J. R. 1989. Development of Asian monsoon revealed by marked ecological shift during the latest Miocene in northern Pakistan. *Nature*, **342**, 163–166.

RAFFI, I., BACKMAN, J., & RIO, D. 1998. Evolutionary trends of tropical calcareous nanofossils in the late Neogene. *Marine Micropaleontology*, **35**, 17–41.

RAFFI, I., & FLORES, J. A. 1995. Pleistocene through Miocene calcareous nannofossils from eastern equatorial Pacific Ocean (Leg 138). *Proceedings of the Ocean Drilling Program, Scientific Results*, **138**, 233–282.

RAFFI, I., MOZZATO, C., FORNACIARI, E., HILGEN, F. J., & RIO, D. 2003. Late Miocene calcareous nannofossil biotratigraphy and astrobiochronology for the Mediterranean region. *Micropaleontology*, **49**(1), 1–26.

RAFFI, I., RIO, D., D'ATRI, A., FORNACIARI, E., & ROCCHETTI, S. 1995. Quantitative distribution patterns and biomagnetostratigraphy of middle and late Miocene calcareous nannofossils

from Equatorial Indian and Pacific Oceans (Legs 115, 130, and 138). *Proceedings of the Ocean Drilling Program, Scientific Results*, **138**, 479–502.

RIO, D., FORNACIARI, E., & RAFFI, I. 1990. Late Oligocene through early Pleistocene calcareous nannofossils from western equatorial Indian Ocean (Leg 115). *Proc., Scientific Results, ODP, Leg 115, Mascarene Plateau*, **115**(Leg 115), 175–235.

RYAN, W. B. F., CARBOTTE, S. M., COPLAN, J. O., HARA, S. O., MELKONIAN, A., ARKO, R., WEISSEL, R. A., FERRINI, V., GOODWILLIE, A., NITSCHE, F., BONCZKOWSKI, J., & ZEMSKY, R. 2009. Global Multi-Resolution Topography synthesis. *Geochemistry, Geophysics, Geosystems*, **10**(3), 1–9.

SAGNOTTI, L., ROBERTS, A. P., WEAVER, R., VEROSUB, K. L., FLORINDO, F., PIKE, C. R., CLAYTON, T., & WILSON, G. S. 2005. Apparent magnetic polarity reversals due to remagnetization resulting from late diagenetic growth of greigite from siderite. *Geophysical Journal International*, **160**, 89–100.

SCHER, H. D., GRIFFITH, E. M., & BUCKLEY JR, W. P. 2014. Accuracy and precision of 88Sr/86Sr and 87Sr/86Sr measurements by MC-ICPMS compromised by high barium concentrations. *Geochemistry, Geophysics, Geosystems*, **15**, 499–508.

SCHNEIDER, D. A. 1995. Paleomagnetism of Some Leg 138 Sediments: Detailing Miocene. *Proceedings of the Ocean Drilling Program, 138 Scientific Results*, **138**, 59–72.

SHACKLETON, N. J., BALDAUF, J. G., FLORES, J.-A., IWAI, M., MOORE JR., T. C., RAFFI, I., & VINCENT, E. 1995. Biostratigraphic Summary for Leg 138. *Proceedings of the Ocean Drilling Program, 138 Scientific Results*, **138**, 517–536.

SHACKLETON, N. J., & CROWHURST, S. 1997. Sediment fluxes based on an orbitally tuned time scale 5 Ma to 14 Ma, Site 926. *Proceedings of the Ocean Drilling Program, Scientific*

Results, **154**, 69–82.

STRÖMBERG, C. A. E. 2011. Evolution of grasses and grassland ecosystems. *Annual Review of Earth and Planetary Sciences*, **39**(1), 517–544.

TAUXE, L., SHAAR, R., JONESTRASK, L. C., SWANSON-HYSELL, N. L., MINNETT, R., KOPPERS, A. A. P., CONSTABLE, C. G., JARBOE, N., GAASTRA, K., & FAIRCHILD, L. 2016. PmagPy: Software package for paleomagnetic data analysis and a bridge to theMagnetics Information Consortium (MagIC) Database. *Geochemistry Geophysics Geosystems*, **17**, 2450–2463.

WADE, B. S., & BOWN, P. R. 2006. Calcareous nannofossils in extreme environments: The Messinian Salinity Crisis, Polemi Basin, Cyprus. *Palaeogeography, Palaeoclimatology, Palaeoecology*, **233**(3–4), 271–286.

WHITMARSH, R. B., WESER, O. E., ALI, S., BOUDREAUX, J. E., FLEISHER, R. L., JIPA, D., KIDD, R. B., MALLIK, T. K., MATTER, A., NIGRINI, C., SIDDIQUIE, H. N., STOFFERS, P., HAMILTON, N., & HUNZIKER, J. 1974. Arabian Sea. *Initial Reports of the Deep Sea Drilling Project*, **23**, 1–1173.

Figure and Table Captions

Figure 1. Map of Expedition 355 drill sites and surrounding land masses. Bathymetric map of the Arabian Sea and surrounding landmasses from GeoMapApp after Ryan *et al*. (2009). Yellow circles: Expedition 355 sites; white lines: major branches of the Indus River and its tributaries; red stars: earlier scientific drilling sites that have sampled the Indus Fan; pink line: approximate extent of the fan after Kolla and Coumes (1987); black box outlines Figure 2 close-up. [Figure modified from Pandey *et al*. (2016).]

Figure 2. Close-up of Expedition 355 drill sites and other bathymetric features. Bathymetric map of Laxmi Basin and surround area, showing the location of Expedition 355 sites in relation to other major bathymetric features, especially Laxmi Ridge. Yellow circles: Expedition 355 sites; black lines are contours in meters below sea level. Bathymetric data are from GeoMapApp after Ryan *et al*. (2009). [Figure modified from Pandey *et al*. (2016).]

Figure 3. Examples of behavior of paleomagnetic specimens during alternating field demagnetization. (a-f) Vector end-point diagrams. Red circles are x,y pairs (in vertically oriented coordinate system where x and y are in the horizontal plane, but are unoriented with respect to geographic north) and the blue squares are x, z pairs. In these plots x is parallel to the natural remnant magnetization (NRM) direction and z is taken as positive down, as per paleomagnetic practice. The NRM is the untreated initial measurement. Subsequent treatment steps in alternating fields of up to 100 mT are labeled and the bounds of interpretation are indicated by

the green squares. (e) Remanence decay versus alternating field treatment. Insets to c and e are equal area projections. The line from the center to the edge is the azimuth of the NRM remanence vector. [Figure modified from Pandey *et al*. (2016).]

Figure 4. Revised magnetostratigraphic data and interpretations for Site U1456. (a) Inclinations versus composite depth (CCSF m). (b) GRM index as described in the text. (c) Same as (a) but plotted against inferred age. (d) Geomagnetic polarity time scale of Gradstein *et al*. (2012).

Figure 5. Revised magnetostratigraphic data and interpretations for Site U1457. (a) Inclinations versus composite depth (CCSF m). (b) GRM index as described in the text. (c) Same as (a) but plotted against inferred age. (d) Geomagnetic polarity time scale of Gradstein *et al*. (2012).

Figure 6. Photomicrographs of selected calcareous nannofossils from Site U1457. A 5 µm scale bar is shown next to the first image. (1–4) *Ceratolithus cristatus*. (5) *Reticulofenestra pseudoumbilicus*. (6) *R. pseudoumbilicus* (5–7 µm). (7, 8) *Helicosphaera carteri*. (9) *Pontosphaera japaonica*. (10) *Reticulofenestra bisecta* (reworked). (11) *Calcidiscus leptoporus*. (12) *Sphenolithus abies*. (13, 14) *Discoaster brouweri*. (15, 16) *Discoaster surculus*. (17) *Discoaster asymmetricus*. (18) *Discoaster tamalis*. (19) *Discoaster triradiatus*. (20) *Discoaster bergenii*. (21, 22) *Discoaster berggrenii*. Images 1–6, 8, 10, 12, 21 from U1457C-45R-4, 7 cm. Images 7, 9, 17, 18 from U1457C-35R-3, 32 cm. Images 11, 13–16, 19, 20, 22 from U1457C-49R-2, 27 cm.

Figure 7. Chronostratigraphic framework for Site U1456. Blue triangles are calcareous

nannofossil events (up are tops, down are bases); green triangles are foraminifera events (up are tops, down are bases); orange circle is change in foraminifer coiling direction; and red diamonds are paleomagnetic chron boundaries. Black lines represent error bars (both age and depth). Number correlates to chronostratigraphic event, refer to Table 1.

Figure 8. Chronostratigraphic framework for Site U1457. Symbols as in Figure 3, pink squares are Strontium isotope values. Number correlates to chronostratigraphic event, refer to Table 2.

Table 1. Biostratigraphic datums and magnetic polarity tie points for Site U1456 Holes A–E. CN = calcareous nannofossil; PF = planktonic foraminifer; MR = magnetic reversal; T = top event; B = base event/; Bc = base common. All paleomagnetic chron boundaries are the tops.

Table 2. Biostratigraphic datums and magnetic polarity tie points for Site U1457 Holes A–C. CN = calcareous nannofossil; PF = planktonic foraminifer; MR = magnetic reversal; T = top event; B = base event; Bc = base common. All paleomagnetic chron boundaries are the tops.

Table 1

Datum Label	Datum Type	Event	Age (Ma)	Sample ID	Depth (m CSF-A)	Depth (m CCSF)[1]	Sample ID (error range)	Depth (m CSF-A)	Depth (m CCSF)	Midpoint Depth (m CCSF)[2]
1	PF	**T** *Globigerinoides ruber* pink	0.12	U1456A-2H-CC, 13 - 18 cm	10.35	11.87	U1456C-1H-CC, 14 - 19 cm	7.33	7.33	9.6
2	CN	**B** *Emiliania huxleyi*	0.29	U1456A-3H-CC, 19 - 24 cm	23.34	25.29	U1456A-4H-CC, 27 - 32 cm	32.86	35.82	30.555
3	CN	**T** *Pseudoemiliania lacunosa*	0.44	U1456A-5H-CC, 9 - 14 cm	42.25	46.25	U1456C-5H-CC, 14 - 19 cm	35.84	37.61	41.93
4	PF	T *Globorotalia tosaensis*	0.61	U1456C-8H-5, 85 - 87 cm	63.15	65.97	U1456C-7H-CC, 0 - 5 cm	55.42	58.23	62.1
5	MR	C1r	0.781	U1456A-10H-4, 40 cm	85.4	91.55	U1456A-10H-6, 63 cm	88.63	94.78	93.165
6	PF	*Pulleniatina* coiling change	0.8	U1456A-10H-CC, 17 - 22 cm	89.61	95.76	U1456A-12H-CC, 54 - 59 cm	106.23	112.95	104.355
7	CN	**T** *Reticulofenestra asanoi*	0.91	U1456C-13H-CC, 55 - 60 cm	95.64	101.44	U1456A-10H-CC, 17 - 22 cm	89.61	95.76	98.6
8	MR	C1r.1n	0.988	U1456C-14H-6, 90 cm	104.7	110.5	U1456A-12H-5, 75 cm	105.35	111.5	111
9	MR	C1r.2r	1.072	U1456A-13H-6, 47 cm	116.94	124.04	U1456C-16H-2, 93 cm	117.73	125.07	124.555
10	CN	**B** *Reticulofenestra asanoi*	1.14	U1456C-18H-CC, 10 - 15 cm	136.97	144.93	U1456C-19F-CC, 0 - 5 cm	139.86	147.82	146.375
11	PF	**T** *Neogloboquadrina acostaensis*	1.58	U1456A-58F-CC, 24 - 29 cm	330.77	342.5	U1456D-52F-CC, 0 - 5 cm	304.58	316.31	329.405
12	CN	**T** *Calcidiscus macintyrei*	1.6	U1456A-58F-CC, 24 - 29 cm	330.77	342.5	U1456A-58F-2, 86 cm	330.25	341.98	342.24
13	CN	**B** *Gephyrocapsa* spp. >5.5 µm	1.62	U1456A-58F-1, 74 cm	329.14	340.87	U1456A-58F-2, 20 cm	329.59	341.32	341.095
14	CN	**B** *Gephyrocapsa* spp. >4 µm	1.73	U1456A-58F-CC, 24 - 29 cm	330.77	342.5	U1456A-59F-2, 83 cm	335.43	347.16	344.83
15	MR	C2n	1.778	U1456A-59F-1, 60 cm	333.7	345.43	U1456A-59F-2, 50 cm	335.1	349.72	347.575
		Unconformity 4 (U4)								354.63
16	CN	**T** *Discoaster brouweri*	1.93	U1456A-61F-CC, 0 - 5 cm	345.84	357.57	U1456A-60F-CC, 0 - 5 cm	339.96	351.69	354.63
17	CN	**T** *Discoaster pentaradiatus*	2.39	U1456A-61F-CC, 0 - 5 cm	345.84	357.57	U1456A-60F-CC, 0 - 5 cm	339.96	351.69	354.63
18	CN	**T** *Discoaster surculus*	2.49	U1456A-63F-1, 116 cm	353.06	364.79	U1456A-62F-CC, 9 - 14 cm	348.04	359.77	362.28
19	PF	**T** *Sphaeroidinellopsis seminulina*	3.375	U1456A-73X-CC, 45 - 50 cm	417.21	428.94	U1456A-72X-CC, 24–29 cm	406.26	417.99	423.465

20	MR	C2Ar	3.596	U1456D-2R-3, 83 cm	462.17	470.96	U1456D-3R-1, 67 cm	469.17	477.96	474.46
21	PF	**B** *Globorotalia tumida*	5.57	U1456D-6R-CC, 10 - 15 cm	497.86	506.65	U1456D-7R-CC, 18 - 23 cm	511.39	520.18	513.415
		Unconformity 3 (U3)								475.1
22	CN	**T** *Discoaster quinqueramus*	5.59	U1456D-3R-CC, 15 - 20 cm	470.26	479.05	U1456D-2R-CC, 15 - 20 cm	462.36	471.15	475.1
23	CN	**T** *Nicklithus amplificus*	5.94	U1456D-8R-1, 81 cm	517.81	526.6	U1456D-7R-CC, 18 - 23 cm	511.39	520.18	523.39
24	PF	**B** *Pulleniatina primalis*	6.6	U1456D-7R-CC, 18 - 23 cm	511.39	520.18	U1456D-8R-CC, 19 - 24 cm	525.26	534.05	527.115
25	MR	C3Ar	6.73	U1456D-10R-4, 118 cm	541.83	550.62	U1456D-11R-1, 57 cm	546.67	555.46	553.04
26	CN	**B** *Nicklithus amplificus*	6.91	U1456D-10R-CC, 12 - 17 cm	543.76	552.55	U1456D-11R-1, 58 cm	546.68	555.47	554.01
27	MR	C3Bn	7.14	U1456D-13R-2, 68 cm	567.18	575.97	U1456D-15R-1, 76 cm	585.66	594.45	585.21
28	MR	C4n	7.53	U1456D-16R-1, 70 cm	595.3	604.09	U1456D-16R-3, 24 cm	597.33	606.12	605.105
29	CN	**T** *Discoaster loeblichii*	7.53	U1456D-16R-CC, 15 - 20 cm	603.9	612.69	U1456D-15R-CC, 15 - 20 cm	587.87	596.66	604.675
30	CN	**B** *Discoaster berggrenii*	8.29	U1456D-29R-CC, 7 - 12 cm	726.55	735.34	U1456D-30R-1, 41 cm	730.81	739.6	737.47
31	CN	T *Minylitha convallis*	8.68	U1456D-30R-1, 41 cm	730.81	739.6	U1456D-29R-CC, 7 - 12 cm	726.55	735.34	737.47
32	MR	C4An	8.77	U1456D-28R13, 73 cm	711.7	720.49	U1456D-30R-1, 87 cm	731.27	740.06	730.275
33	PF	**B** *Globigerinoides extremus*	8.93	U1456D-8R-CC, 19 - 24 cm	525.26	534.05	U1456D-9R-5, 97 - 100 cm	533.56	542.35	538.2
		Unconformity 2 (U2)								737.47
34	MR	C4Ar	9.11	U1456D-30R-4, 43 cm	735.33	744.12	U1456D-30R-5, 68 cm	737.08	745.87	744.995
35	CN	**T** *Discoaster bollii*	9.21	U1456D-30R-1, 41 cm	730.81	739.6	U1456D-29R-CC, 7 - 12 cm	726.55	735.34	737.47
36	CN	**T** *Discoaster hamatus*	9.53	U1456D-32R-3, 85 cm	753.65	762.44	U1456D-31R-CC, 22 - 27 cm	749.7	758.49	760.465
37	CN	**T** *Catinaster coalitus*	9.69	U1456D-33R-4, 144 cm	765.25	774.04	U1456D-33R-1, 83 cm	760.33	769.12	771.58
38	PF	**B** *Neogloboquadrina acostaensis*	9.83	U1456D-37R-CC, 23 - 28 cm	804.51	813.3	U1456D-38R-CC, 12 - 17 cm	813.34	822.13	817.715
39	CN	**B** *Discoaster hamatus*	10.55	U1456D-37R-CC, 23 - 28 cm	804.51	813.3	U1456D-38R-2, 48 cm	809.98	818.77	816.035
40	CN	**B** *Catinaster coalitus*	10.89	U1456D-57R-7, 80 cm	986.65	995.44	U1456D-57R-CC, 12 - 17 cm	986.84	995.63	995.535
		Unconformity 1 (U1)		U1456E-19R-2, 19 cm	1101.67	1110.46				1110.46
41	CN	**T** *Sphenolithus heteromorphus*	15.62	U1456E-19R-4, 46 cm	1103.73	1112.52	U1456E-19R-2, 19 cm	1101.67	1110.46	1111.49

[1]CCSF created by adding constant offset of 8.79 m to Holes U1456D and U1456E CSF-A depth scale.					
[2]Midpoint depth for biostratigraphic datums is the midpoint between the sample in which the event is identified, and the overlying (underlying) sample for tops (bases). Midpoint depth for					
a magnetic reversal is the midpoint between the last point of stable polarity and first point of newly stable polarity					

859

Table 2

Datum Label	Datum Type	Event	GPTS2012 Age (Ma)	Indian Ocean calibration (Ma)	Age error (My)	Sample ID	Depth (m CSF-A)	Depth (m CCSF)[1]	Sample ID (error range)	Depth (m CSF-A)	Depth (m CCSF)	Midpoint Depth (m CCSF)[2]
1	PF	**T** *Globigerinoides ruber* pink	0.12			U1457A-1H-2, 9–11 cm	1.03	4.23	U1457B-1H-CC, 14–19 cm	3.17	3.17	3.7
2	CN	**B** *Emiliania huxleyi*	0.29			U1457A-2H-CC, 12 - 17 cm	14.02	18.91	U1457A-3H-CC, 11–16 cm	27.07	32.83	25.87
3	CN	**T** *Pseudoemiliania lacunosa*	0.44			U1457B-3H-CC, 10 - 15 cm	21.64	26.58	U1457B-2H-CC, 0–5 cm	12.49	16.36	21.47
4	PF	**T** *Globorotalia tosaensis*	0.61			U1457B-4H-CC, 20 - 25 cm	31.14	36.48	U1457B-3H-CC, 10–15 cm	21.64	26.58	31.53
5	MR	C1r	0.781			U1457A-5H-2, 65 cm	39.35	46.21	U1457A-5H-3, 103 cm	41.23	48.09	47.15
6	CN	**T** *Reticulofenestra asanoi*	0.91			U1457B-6H-CC, 0 - 5 cm	50.32	57.29	U1457A-5H-CC, 13–18 cm	45.56	52.42	54.855
7	MR	C1r.1n	0.988			U1457A-6H-6, 60 cm	54.8	61.42	U1457A-7H-3, 122 cm	65.68	72.54	66.98
8	MR	C1r.2r	1.072			U1457A-8H-2, 137 cm	68.57	74.95	U1457A-8H-4, 87 cm	71.07	77.45	76.2
9	CN	**B** *Reticulofenestra asanoi*	1.14			U1457A-8H-5, 38 cm	72.08	78.46	U1457A-8H-CC, 14–19 cm	75.24	81.62	80.04
10	CN	**T** *Gephyrocapsa* spp. >5.5 µm	1.24			U1457A-9H-CC, 44 - 49 cm	83.78	90.62	U1457B-9H-CC, 30–35 cm	79.39	88.04	89.33
11	PF	**T** *Globoturborotalita obliquus*	1.3			U1457A-10H-CC, 44 - 49 cm	94.36	100.75	U1457A-9H-CC, 44–49 cm	83.78	90.62	95.685
12	PF	**T** *Neogloboquadrina acostaensis*	1.58			U1457C-4R-CC, 0 - 5 cm	211	216.15	U1457C-3R-1, 68–73 cm	201.98	207.13	211.64
13	CN	**B** *Gephyrocapsa* spp. >5.5 µm	1.62			U1457C-18R-CC, 14 - 19 cm	356.6	361.75	U1457C-19R-CC, 0–5 cm	363.55	368.7	365.225
14	C	**B**	1.			U1457C-	376.	381.	U1457C-	39	39	388.71

	N	*Gephyrocapsa* spp. >4 µm	73			21R-1, 13 - 18 cm	03	18	22R-CC, 15–20 cm	1.1	6.25	5
15	MR	C2n	1.778			U1457C-23R-2, 56 cm	397.24	402.39	U1457C-23R-3, 34 cm	398.5	403.65	403.02
16	PF	B *Globorotalia truncatulinoides*	1.93			U1457C-23R-1, 18–20 cm	395.48	400.63	U1457C-23R-1, 42–44 cm	395.72	400.87	400.75
17	CN	**T** *Discoaster brouweri*	1.93			U1457C-23R-CC, 0 - 5 cm	403.83	408.98	U1457C-22R-CC, 15–20 cm	391.1	396.25	402.615
		Unconformity 4 (U4)										402.62
18	PF	**T** *Globigerinoides extremus*	1.98			U1457C-19R-CC, 0 - 5 cm	363.55	368.7	U1457C-18R-CC, 14–19 cm	356.6	361.75	365.225
19	PF	**T** *Globoturborotalita woodi*	2.3			U1457C-23R-CC, 0 - 5 cm	403.83	408.98	U1457C-22R-CC, 15–20 cm	391.1	396.25	402.615
20	CN	**T** *Discoaster pentaradiatus*	2.39			U1457C-25R-1, 65 cm	415.35	420.5	U1457C-24R-CC, 0–5 cm	413.42	418.57	419.535
21	CN	**T** *Discoaster surculus*	2.49			U1457C-25R-3, 120 cm	418.82	423.97	U1457C-25R-3, 52 cm	418.14	423.29	423.63
22	MR	C2An	2.58			U1457C-25R-1, 98 cm	415.68	420.83	U1457C-25R-3, 72 cm	418.34	423.49	422.16
23	PF	**T** *Dentoglobigerina altispira*	3.3			U1457C-32R-CC, 13 - 18 cm	484.43	489.58	U1457C-31R-CC, 20–25 cm	475.8	480.95	485.265
24	CN	**T** *Sphenolithus* spp.	3.54			U1457C-35R-1, 60 cm	512.3	517.45	U1457C-34R-CC, 12–17 cm	507.94	513.09	515.27
25	MR	C2Ar	3.596			U1457C-31R-2, 106 cm	475.76	480.91	U1457C-32R-1, 45 cm	483.05	488.2	484.555
26	CN	**B** *Discoaster tamalis*	4.13			U1457C-37R-3, 39 cm	534	539.15	U1457C-37R-CC, 20–25 cm	534.5	539.65	539.4
		Unconformity 3 (U3)										539.4
27	Sr	Sr = 0.709034 ± 0.000008	5.08		1	U1457C-46R-2, 100 - 104 cm	620.79	625.94				625.94
28	CN	**T** *Discoaster quinqueramus*	5.59			U1457C-37R-CC, 20 - 25 cm	534.5	539.65	U1457C-37R-3, 39 cm	534	539.15	539.4
29	PF	**T** *Globoquadrina dehiscens*	5.92			U1457C-35R-CC, 0 - 5 cm	521.49	526.64	U1457C-34R-CC, 12–17 cm	507.94	513.09	519.865
30	CN	**T** *Nicklithus amplificus*	5.94			U1457C-44R-5, 64	605.21	610.36	U1457C-44R-5, 33	604.	610.	610.205

						cm			cm	9	05	
31	Sr	Sr = 0.708992 ± 0.000008 (benthic)	6.00		1	U1457C-47R-1, 6 - 10 cm	628.16	633.31				633.31
32	MR	C3An.1r	6.25			U1457C-46R-1 68 cm	619.08	624.23	U1457C-46R-2, 48 cm	620.27	625.42	624.825
33	PF	**B** *Pulleniatina primalis*	6.6			U1457C-45R-2, 24 cm	610.35	615.5	U1457C-45R-CC, 0–7 cm	616.21	621.36	618.43
34	Sr	Sr = 0.708964 ± 0.000008 (planktonic)	6.6		1	U1457C-47R-1, 6 - 10 cm	628.16	633.31				633.31
35	CN	**B** *Nicklithus amplificus*	6.91	6.7		U1457C-46R-4, 40 cm	623.19	628.34	U1457C-46R-5, 69 cm	624.38	629.53	628.935
36	MR	C3Br.2r	7.29			U1457C-48R-1, 9 cm	637.89	643.04	U1457C-48R-2, 22 cm	639.01	644.16	643.6
37	Sr	Sr = 0.708943 ± 0.000006	7.3		1	U1457C-49R-2, 85 - 89 cm	649.85	655				655
38	CN	**B** *Amaurolithus* spp.	7.42	7.2–7.3		U1457C-48R-2, 60 cm	639.9	645.05	U1457C-48R-CC, 0–5 cm	639.61	644.76	644.905
39	MR	C4n	7.53			U1457C-50R-1, 57 cm	657.77	662.92	U1457C-50R-2, 112 cm	659.77	664.92	663.92
40	Sr	Sr = 0.708936 ± 0.000006	7.7		1	U1457C-50R-4, 64 - 68 cm	662.3	667.45				667.45
41	MR	C4r	8.11			U1457C-51R-2, 92 cm	669.32	674.47	U1457C-51R-3, 57 cm	670.47	675.62	675.045
42	CN	**B** *Discoaster quinqueramus*	8.12			U1457C-67R-CC, 0 - 5 cm	827.7	832.85	U1457C-68R-CC, 9–14 cm	840.47	845.62	839.235
		Unconformity 2 (U2)										839.24
43	CN	T *Minylitha convallis*	8.68			U1457C-68R-CC, 9 - 14 cm	840.47	845.62	U1457C-67R-CC, 0–5 cm	827.7	832.85	839.235
44	CN	**T** *Discoaster bollii*	9.21			U1457C-69R-CC, 25 - 30 cm	851.35	856.5	U1457C-68R-CC, 9–14 cm	840.47	845.62	851.06
45	CN	**T** *Catinaster coalitus*	9.69			U1457C-70R-CC, 18 - 23 cm	859.49	864.64	U1457C-69R-CC, 25–30 cm	851.35	856.5	860.57
46	MR	C5n	9.79			U1457C-70R-6, 35 cm	859.03	864.18	U1457C-71R-1, 15 cm	861.05	866.2	865.19
47	PF	**B** *Neogloboquadri*	9.83			U1457C-72R-CC, 23	879.87	885.02	U1457C-73R-CC,	889.	894.	889.66

		na acostaensis				- 28 cm			0–5 cm	15	3	
48	C N	**B** *Discoaster bellus*	10.4			U1457C-84R-CC, 10 - 15 cm	995.93	1001.08	U1457C-85R-CC, 0–5 cm	999.96	1005.11	1003.095
49	C N	**B** *Catinaster coalitus*	10.89			U1457C-84R-CC, 10 - 15 cm	995.93	1001.08	U1457C-85R-CC, 0–5 cm	999.96	1005.11	1003.095
		Unconformity 1 (U1)				U1457C-93R-1, 0 cm	1062.2	1067.35				1067.35
50	C N	Absence of *Fasciculithus* spp.	62.13			U1457C-93R-1, 128 cm	1063.48	1068.63	U1457C-93R-1, 0 cm	1062.2	1067.35	1067.99
51	C N	**B** *Ellipsolithus macellus*	63.25			U1457C-94R-CC, 18 - 23 cm	1073.69	1078.84	U1457C-95R-CC, 16–21 cm	1084.91	1090.06	1084.45
[1]CCSF created by adding constant offset of 5.15 m to Hole U1457C CSF-A depth scale.												
[2]Midpoint depth for biostratigraphic datums is the midpoint between the sample in which the event is identified, and the overlying (underlying) sample for tops (bases). Midpoint depth for												
a magnetic reversal is the midpoint between the last point of stable polarity and first point of newly stable polarity. Sr isotope data are plotted at the sample depth from which the foraminifers were picked.												

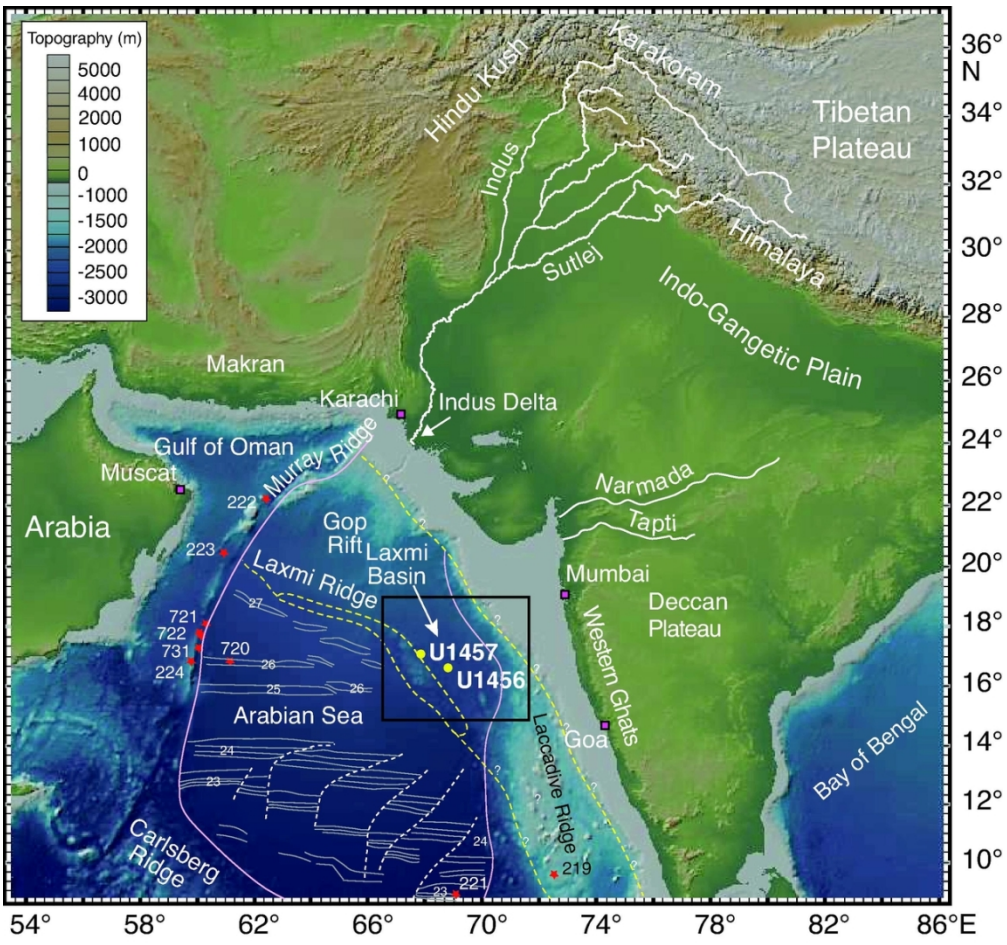

Map of Expedition 355 drill sites and surrounding land masses. Bathymetric map of the Arabian Sea and surrounding landmasses from GeoMapApp after Ryan et al. (2009). Yellow circles: Expedition 355 sites; white lines: major branches of the Indus River and its tributaries; red stars: earlier scientific drilling sites that have sampled the Indus Fan; pink line: approximate extent of the fan after Kolla and Coumes (1987); black box outlines Figure 2 close-up. [Figure modified from Pandey et al. (2016).]

107x101mm (300 x 300 DPI)

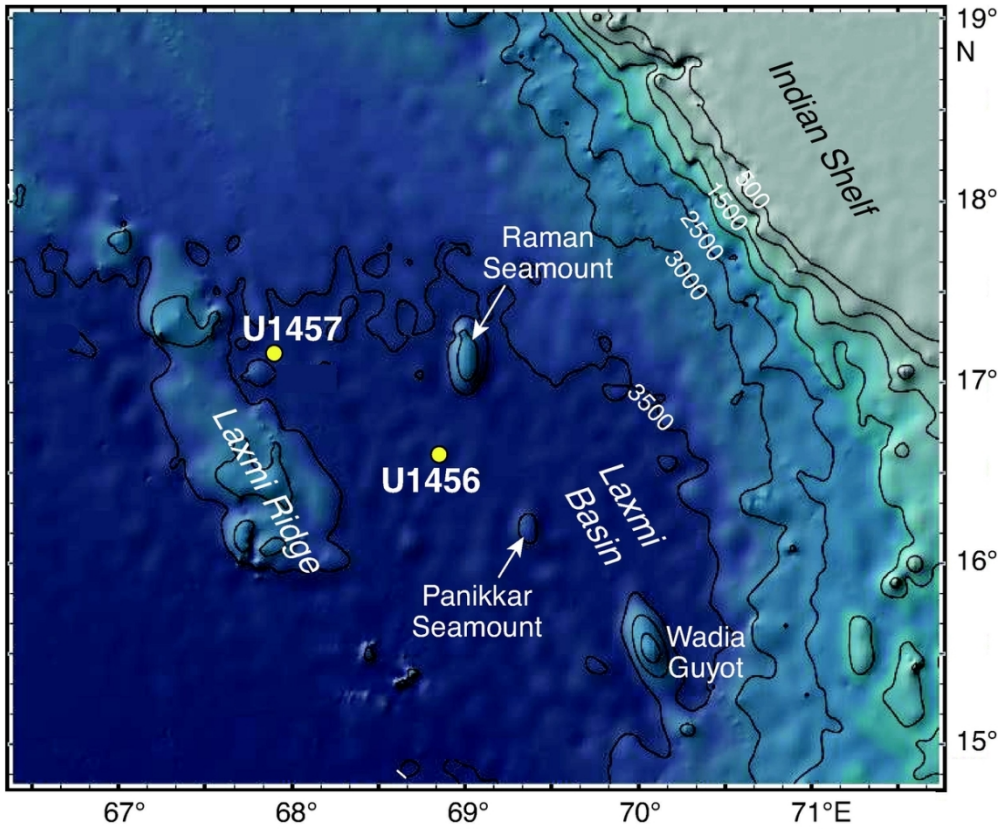

Close-up of Expedition 355 drill sites and other bathymetric features. Bathymetric map of Laxmi Basin and surround area, showing the location of Expedition 355 sites in relation to other major bathymetric features, especially Laxmi Ridge. Yellow circles: Expedition 355 sites; black lines are contours in meters below sea level. Bathymetric data are from GeoMapApp after Ryan et al. (2009). [Figure modified from Pandey et al. (2016).]

105x87mm (300 x 300 DPI)

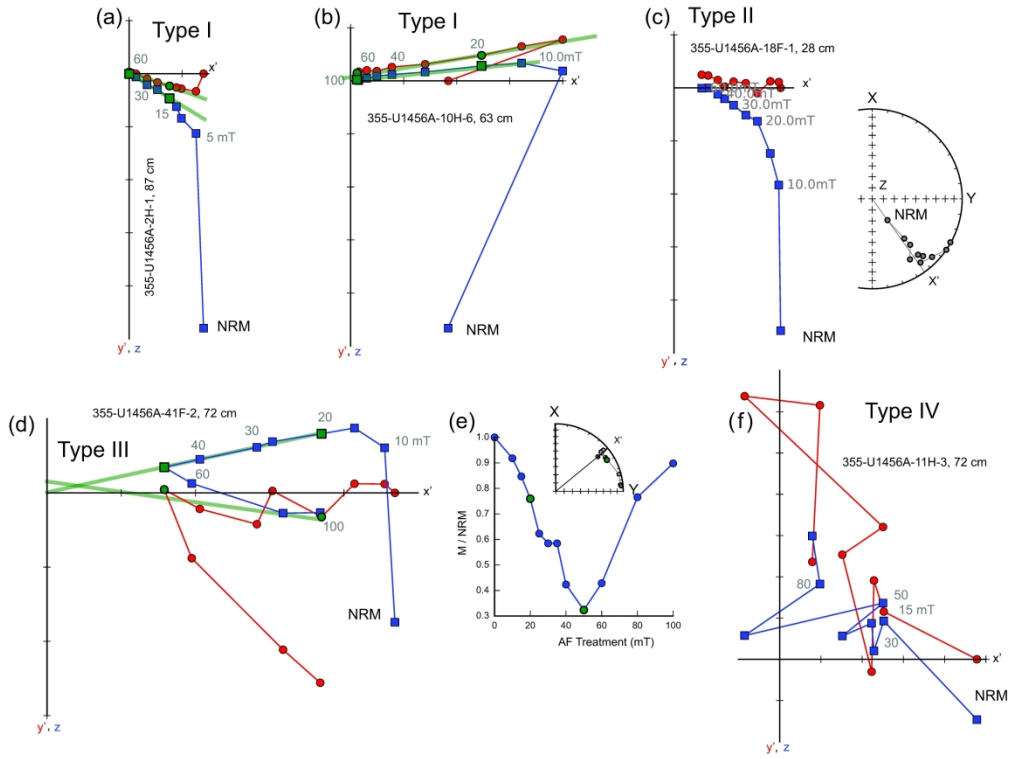

Examples of behavior of paleomagnetic specimens during alternating field demagnetization. (a-f) Vector end-point diagrams. Red circles are x,y pairs (in vertically oriented coordinate system where x and y are in the horizontal plane, but are unoriented with respect to geographic north) and the blue squares are x, z pairs. In these plots x is parallel to the natural remnant magnetization (NRM) direction and z is taken as positive down, as per paleomagnetic practice. The NRM is the untreated initial measurement. Subsequent treatment steps in alternating fields of up to 100 mT are labeled and the bounds of interpretation are indicated by the green squares. (e) Remanence decay versus alternating field treatment. Insets to c and e are equal area projections. The line from the center to the edge is the azimuth of the NRM remanence vector. [Figure modified from Pandey et al. (2016).]

289x217mm (300 x 300 DPI)

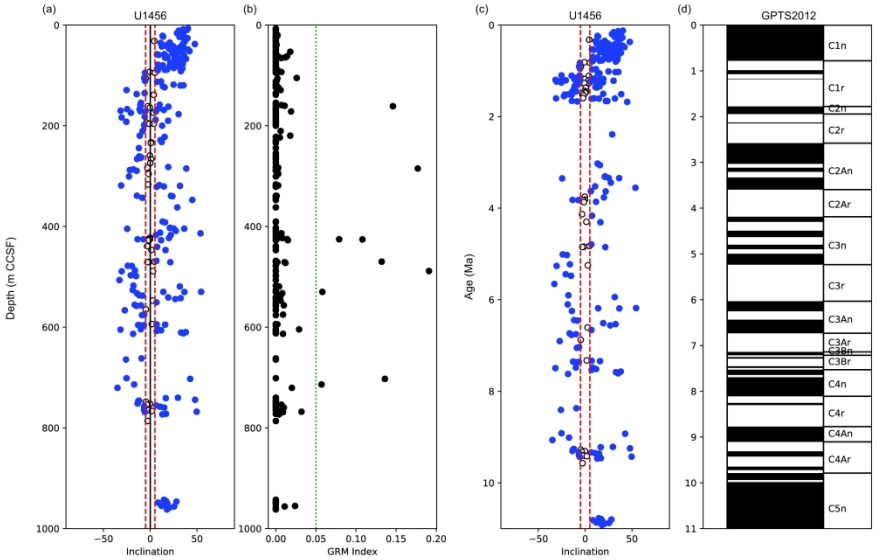

Revised magnetostratigraphic data and interpretations for Site U1456. (a) Inclinations versus composite depth (CCSF m). (b) GRM index as described in the text. (c) Same as (a) but plotted against inferred age. (d) Geomagnetic polarity time scale of Gradstein et al. (2012).

381x254mm (300 x 300 DPI)

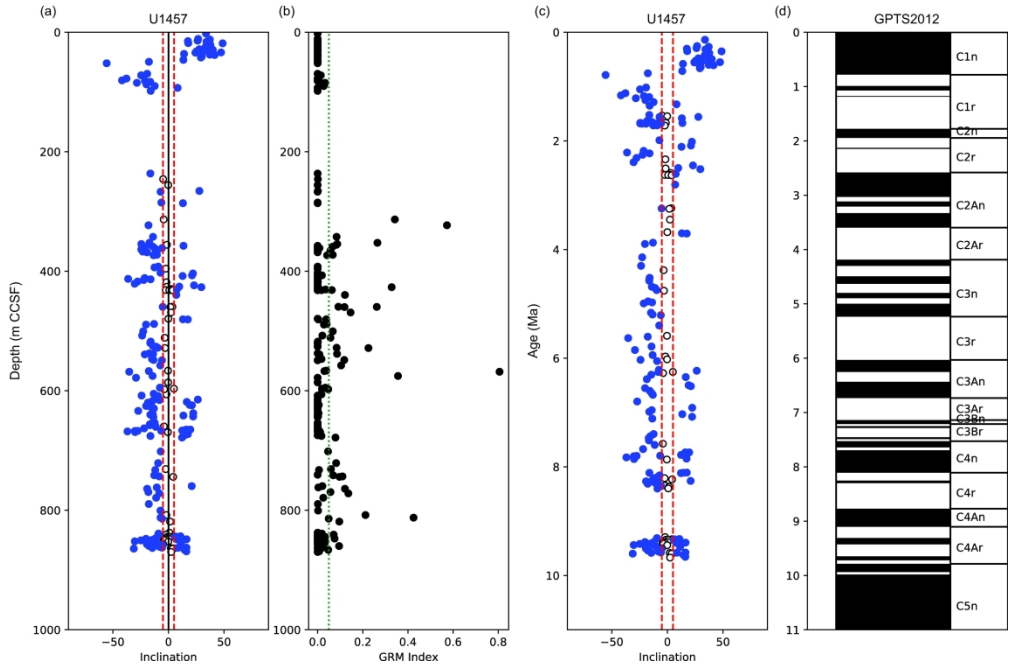

Revised magnetostratigraphic data and interpretations for Site U1457. (a) Inclinations versus composite depth (CCSF m). (b) GRM index as described in the text. (c) Same as (a) but plotted against inferred age. (d) Geomagnetic polarity time scale of Gradstein et al. (2012).

320x210mm (300 x 300 DPI)

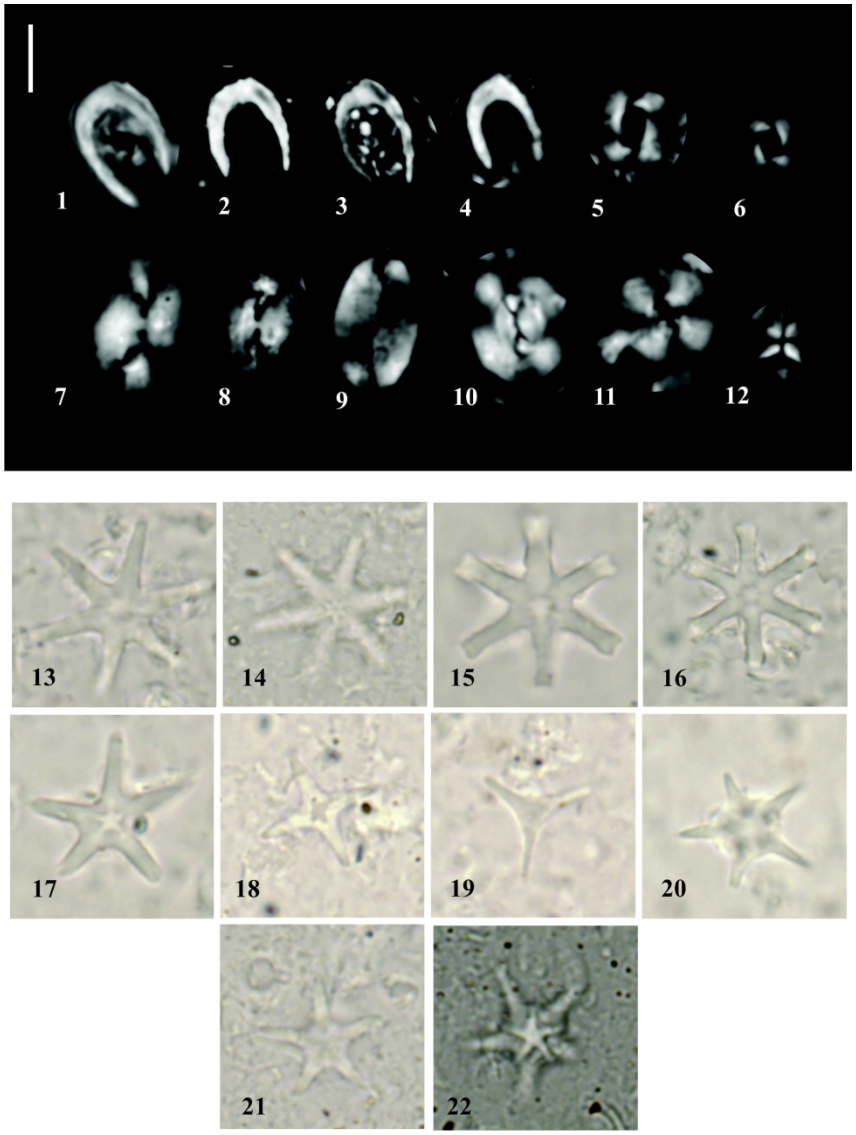

Photomicrographs of selected calcareous nannofossils from Site U1457. A 5 µm scale bar is shown next to the first image. (1–4) Ceratolithus cristatus. (5) Reticulofenestra pseudoumbilicus. (6) R. pseudoumbilicus (5–7 µm). (7, 8) Helicosphaera carteri. (9) Pontosphaera japaonica. (10) Reticulofenestra bisecta (reworked). (11) Calcidiscus leptoporus. (12) Sphenolithus abies. (13, 14) Discoaster brouweri. (15, 16) Discoaster surculus. (17) Discoaster asymmetricus. (18) Discoaster tamalis. (19) Discoaster triradiatus. (20) Discoaster bergenii. (21, 22) Discoaster berggrenii. Images 1–6, 8, 10, 12, 21 from U1457C-45R-4, 7 cm. Images 7, 9, 17, 18 from U1457C-35R-3, 32 cm. Images 11, 13–16, 19, 20, 22 from U1457C-49R-2, 27 cm.

201x284mm (300 x 300 DPI)

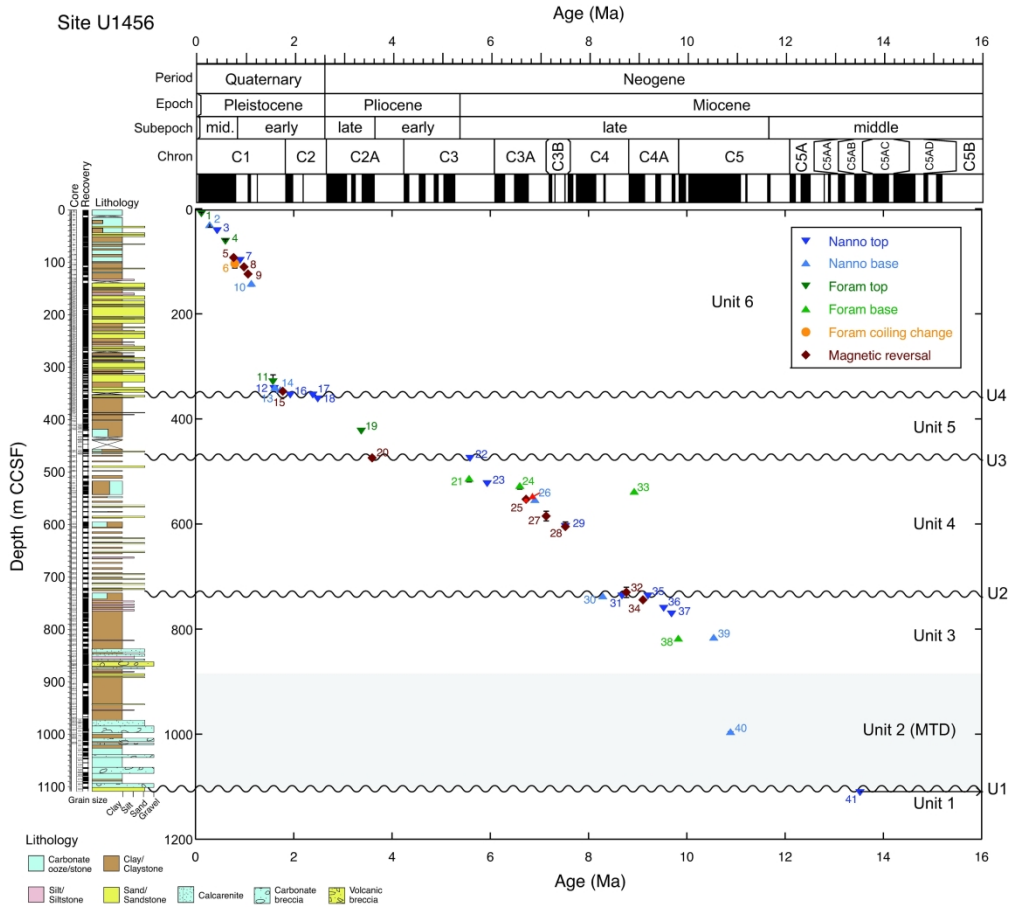

Chronostratigraphic framework for Site U1456. Blue triangles are calcareous nannofossil events (up are tops, down are bases); green triangles are foraminifera events (up are tops, down are bases); orange circle is change in foraminifer coiling direction; and red diamonds are paleomagnetic chron boundaries. Black lines represent error bars (both age and depth). Number correlates to chronostratigraphic event, refer to Table 1.

323x290mm (300 x 300 DPI)

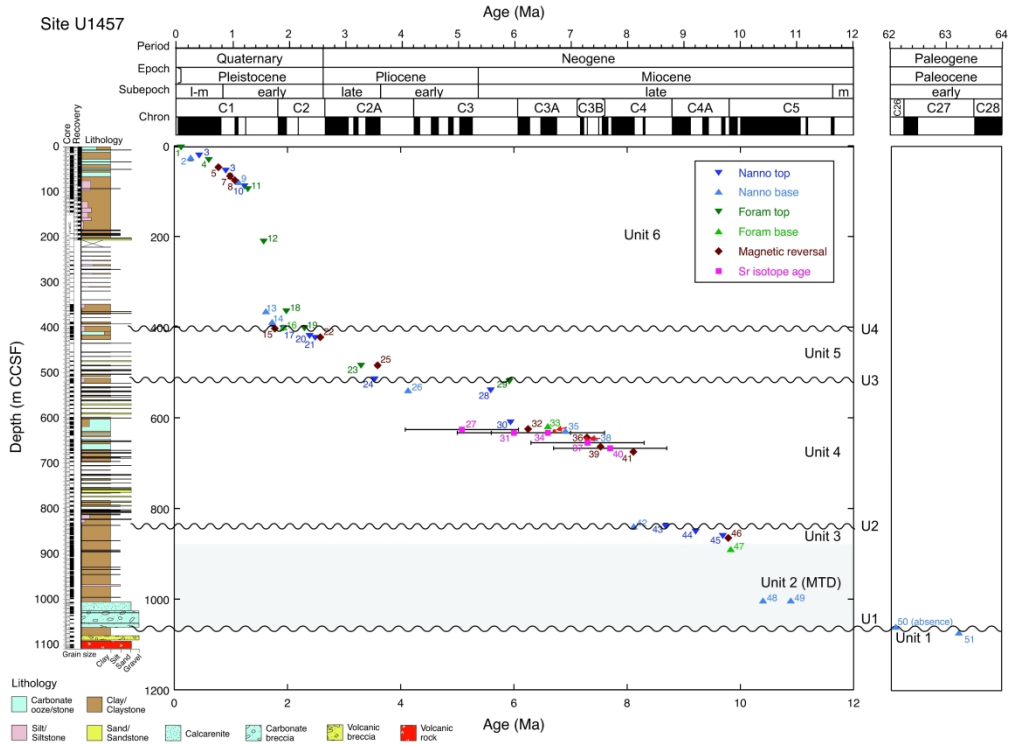

Chronostratigraphic framework for Site U1457. Symbols as in Figure 3, pink squares are Strontium isotope values. Number correlates to chronostratigraphic event, refer to Table 2.

373x276mm (300 x 300 DPI)

Geological Magazine

A revised chronostratigraphic framework for International Ocean Discovery Program Expedition 355 sites in Laxmi Basin, eastern Arabian Sea

Claire M. Routledge, Denise K. Kulhanek, Lisa Tauxe, Giancarlo Scardia, Arun D. Singh, Stephan Steinke, Elizabeth M. Griffith & Rajeev Saraswat

Supplementary material

This supplement includes a list of five tables (uploaded as separate excel files) and three figures.

Supplementary Table S1. Foraminifer datum levels in Holes U1456A, U1456C, and U1456D.

Supplementary Table S2. Foraminifer datum levels in Holes U1457A, U1457B, and U1457C.

Supplementary Table S3. Nannofossil datum levels in Holes U1456A, U1456C, and U1456D.

Supplementary Table S4. Nannofossil datum levels in Holes U1457A, U1457B, and U1457C.

Supplementary Table S5. Distribution of calcareous nannofossils for the 2–8 Ma interval in Hole U1457C (combined shipboard and post-cruise analyses).

Supplementary Figure S1. Histograms of inclinations for Sites (a) U1456 and (b) U1457.

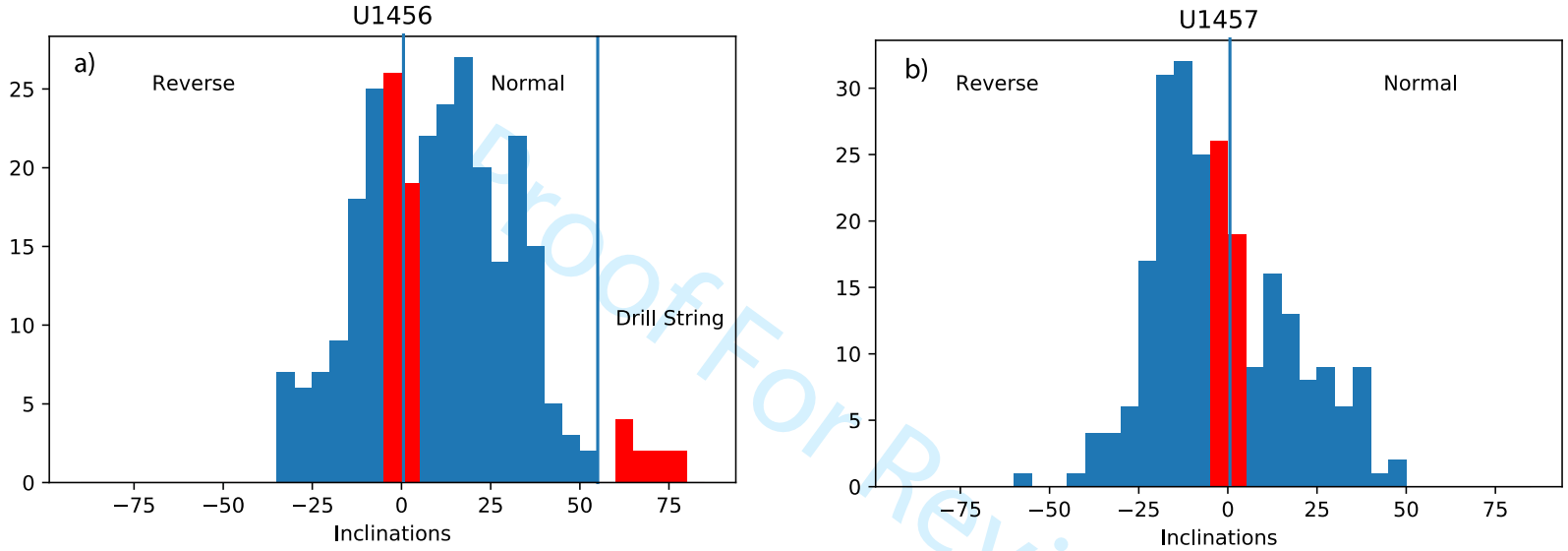

Supplementary Figure S2. Age model for conversion of composite depth (m CCSF) to age. Red dots are paleomagnetic sampling sites, blue stars are the age constraints from Tables 1 and 2 for Sites (a) U1456 and (b) U1457.

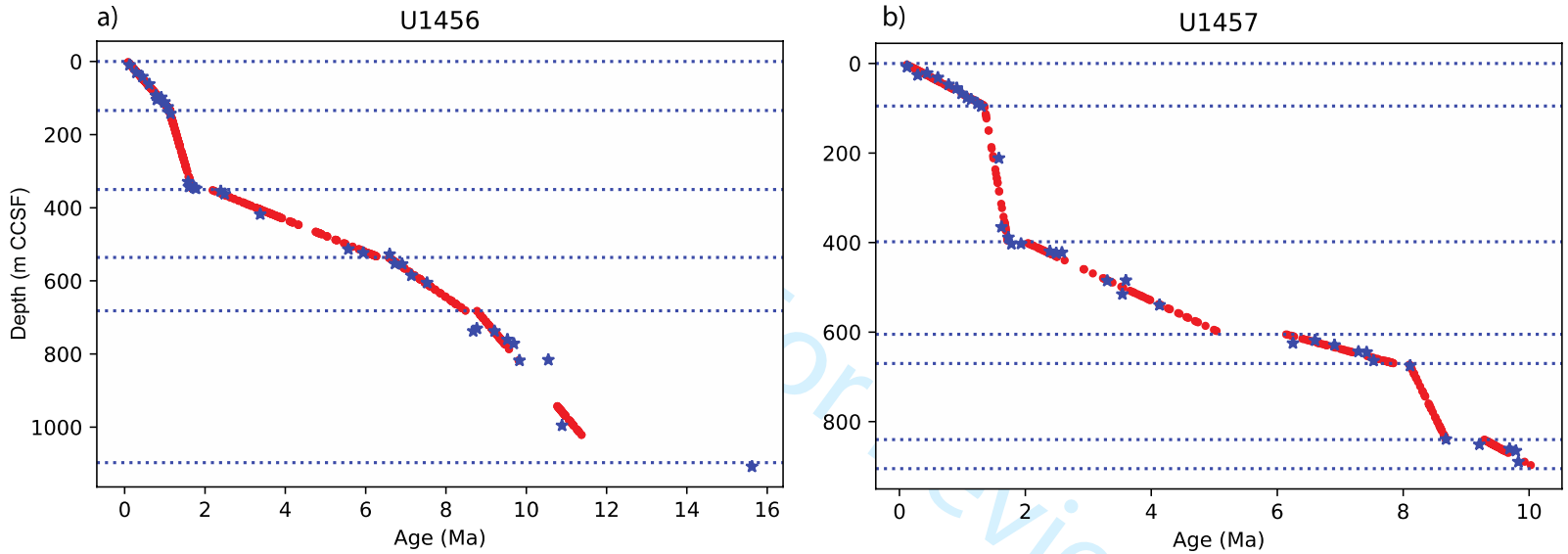

Supplementary Figure S3. Strontium isotope data with age estimates and errors on measurement and seawater strontium isotope curve from MacArthur et al. (2012)[1]. Gray lines are minimum and maximum ages for seawater strontium isotope curve from MacArthur et al. (2012). Error on carbonate strontium isotopes are plotted as twice the standard error.

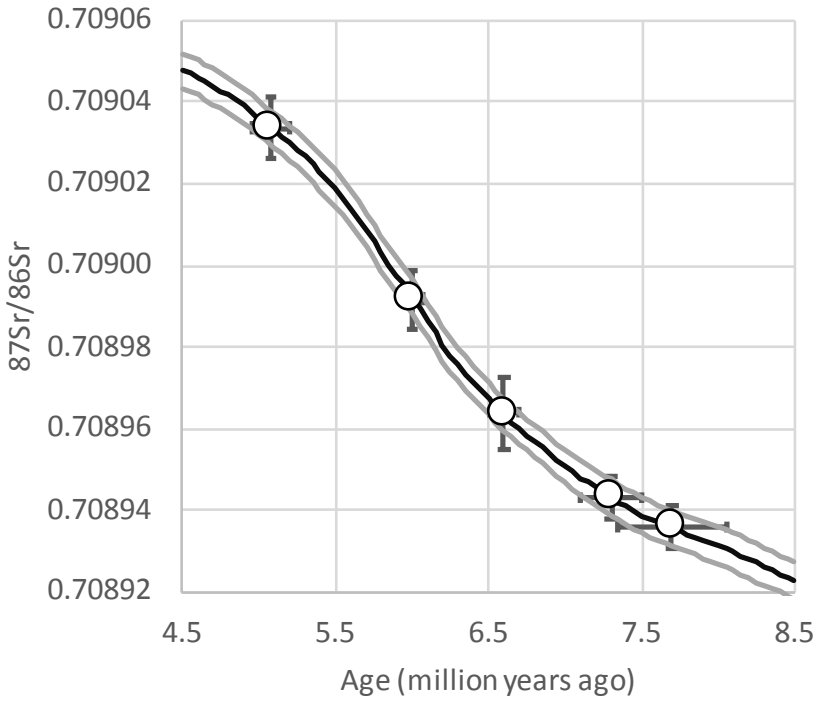

[1] McArthur, J. M., Howarth, R. J., & Shields, G. A. (2012). Strontium Isotope Stratigraphy. In *The Geologic Time Scale 2012* (pp. 127–144). Elsevier. https://doi.org/10.1016/B978-0-444-59425-9.00007-X

Supplementary Table S1. Foraminifer datum levels in Holes U1456A, U

Event	Age (Ma)	Datum Midpoint depth (m CCSF)
T *Globigerinoides ruber* pink	0.12	9.6
T *Globorotalia tosaensis*	0.61	62.1
Coiling change (random -> d) *Pulleniatina*	0.8	104.355
T *Neogloboquadrina acostaensis*	1.58	329.405
T *Sphaeroidinellopsis seminulina*	3.375	423.465
B *Globorotalia tumida*	5.57	513.415
B *Pulleniatina primalis*	6.6	527.115
B *Globigerinoides extremus*	8.93	538.2
B *Neogloboquadrina acostaensis*	9.83	817.715

[1]CCSF created by adding constant offset of 8.79 m to Hole U1456D CSF

[2]Sample in which fossil top or base identified.

[3]Sample error is next sample above (for top) or below (for base) where

1456C, and U1456D. Yellow shading indicates samples used to determine datum midpoint dept

U1456A / U1456D[1]				
Sample ID[2]	Depth (m CSF-A)	Depth (m CCSF)	Sample ID (error range)[3]	Depth (m CSF-A)
U1456A-2H-CC, 13–18 cm	10.35	11.87	U1456A-1H-CC, 17–22 cm	4.49
U1456A-9H-CC, 16–21 cm	80.28	85.91	U1456A-8H-CC, 15–20 cm	69.79
U1456A-10H-CC, 17–22 cm	89.61	95.76	U1456A-12H-CC, 54–59 cm	106.23
U1456A-58F-CC, 24–29 cm	330.77	342.5	U1456D-52F-CC, 0–5 cm	304.58
U1456A-73X-CC, 45–50 cm	417.21	428.94	U1456A-72X-CC, 24–29 cm	406.26
U1456D-6R-CC, 10–15 cm	497.86	506.65	U1456D-7R-CC, 18–23 cm	511.39
U1456D-7R-CC, 18–23 cm	511.39	520.18	U1456D-8R-CC, 19–24 cm	525.26
U1456D-8R-CC, 19–24 cm	525.26	534.05	U1456D-9R-5, 97–100 cm	533.56
U1456D-37R-CC, 23–28 cm	804.51	813.3	U1456D-38R-CC, 12–17 cm	813.34

-A depth scale.

e fossil was not found. Actual top or base lies somewhere in between the sample in which the fo

h used for age model.

	U1456C			
Depth (m CCSF)	Sample ID[2]	Depth (m CSF-A)	Depth (m CCSF)	Sample ID (error range)[3]
4.49	U1456C-3H-CC, 12–17 cm	17.7	18.68	U1456C-1H-CC, 14–19 cm
74.85	U1456C-8H-5, 85–87 cm	63.15	65.97	U1456C-7H-CC, 0–5 cm
112.95	U1456C-10H-4, 70–72 cm	72	75.79	U1456C-12H-4, 77–79 cm
316.31				
417.99	U1456C-38X-CC, 17–22 cm	409.05	417.84	Within drilled interval (U1456C
520.18				
534.05				
542.35				
822.13				

ɔssil was found and the next sample where it was not found (we use midpoint between these tv

Depth (m CSF-A)	Depth (m CCSF)
7.33	7.33
55.42	58.23
82.57	87.48
-371)	

NO).

Supplementary Table S2. Foraminifer datum levels in Holes U1457A, U1457B, and U1457C. Yellow sha

Event	Age (Ma)	Datum Midpoint depth (m CCSF)	Sample ID[2]
T *Globigerinoides ruber* pink	0.12	3.7	U1457A-1H-2, 9–11 cm
T *Globorotalia tosaensis*	0.61	31.53	U1457A-5H-CC, 13–18 cm
T *Globoturborotalita obliquus*	1.3	95.685	U1457A-10H-CC, 44–49 cm
T *Neogloboquadrina acostaensis*	1.58	211.64	U1457C-4R-CC, 0–5 cm
T *Globigerinoides extremus*	1.98	365.225	U1457C-19R-CC, 0–5 cm
T *Globoturborotalita woodi*	2.3	402.615	U1457C-23R-CC, 0–5 cm
B *Globorotalia truncatulinoides*	2.255	400.75	U1457C-23R-1, 18–20 cm
T *Dentoglobigerina altispira*	3.3	485.265	U1457C-32R-CC, 13–18 cm
T *Globoquadrina dehiscens*	5.92	519.865	U1457C-35R-CC, 0–5 cm
B *Pulleniatina primalis*	6.6	618.43	U1457C-45R-2, 24 cm
B *Neogloboquadrina acostaensis*	9.83	889.66	U1457C-72R-CC, 23–28 cm

[1]CCSF created by adding constant offset of 5.15 m to Hole U1457C CSF-A depth scale.

[2]Sample in which fossil top or base identified.

[3]Sample error is next sample above (for top) or below (for base) where fossil was not found. Actual to

ading indicates samples used to determine datum midpoint depth used for

U1457A / U1457C[1]				
Depth (m CSF-A)	Depth (m CCSF)	Sample ID (error range)[3]	Depth (m CSF-A)	Depth (m CCSF)
1.03	4.23	Seafloor	0	0
45.56	52.42	U1457A-4H-CC, 12–17 cm	36.59	42.75
94.36	100.75	U1457A-9H-CC, 44–49 cm	83.78	90.62
211	216.15	U1457C-3R-1, 68–73 cm	201.98	207.13
363.55	368.7	U1457C-18R-CC, 14–19 cm	356.6	361.75
403.83	408.98	U1457C-22R-CC, 15–20 cm	391.1	396.25
395.48	400.63	U1457C-23R-1, 42–44 cm	395.72	400.87
484.43	489.58	U1457C-31R-CC, 20–25 cm	475.8	480.95
521.49	526.64	U1457C-34R-CC, 12–17 cm	507.94	513.09
610.35	615.5	U1457C-45R-CC, 0–7 cm	616.21	621.36
879.87	885.02	U1457C-73R-CC, 0–5 cm	889.15	894.3

op or base lies somewhere in between the sample in which the fossil was fc

age model.

U1457B				
Sample ID[2]	Depth (m CSF-A)	Depth (m CCSF)	Sample ID (error range)[3]	Depth (m CSF-A)
U1457B-2H-CC, 0–5 cm	12.49	16.36	U1457B-1H-CC, 14–19 cm	3.17
U1457B-4H-CC, 20–25 cm	31.14	36.48	U1457B-3H-CC, 10–15 cm	21.64
U1457B-13H-CC, 36–41 cm	108.56	115.05	U1457B-12H-CC, 87–92 cm	99.1

ound and the next sample where it was not found (we use midpoint between these two).

Depth (m CCSF)
3.17
26.58
107.72

Supplementary Table S3. Nannofossil datum levels in Holes U1456A, U1456C, and U1456D. Ye

Event	Age (Ma)	Datum Midpoint depth (m CCSF)	Sample ID[2]
B *Emiliania huxleyi*	0.29	30.555	U1456A-3H-CC, 19–24 cm
T *Pseudoemiliania lacunosa*	0.44	41.93	U1456A-5H-CC, 9–14 cm
T *Reticulofenestra asanoi*	0.91	98.6	U1456A-11H-CC, 21–26 cm
B *Reticulofenestra asanoi*	1.14	146.375	
T *Calcidiscus macintyrei*	1.6	342.24	U1456A-58F-CC, 24–29 cm
B *Gephyrocapsa* spp. >5.5 µm	1.62	341.095	U1456A-58F-1, 74 cm
B *Gephyrocapsa* spp. >4 µm	1.73	344.83	U1456A-58F-CC, 24–29 cm
T *Discoaster brouweri*	1.93	354.63	U1456A-61F-CC, 0–5 cm
T *Discoaster pentaradiatus*	2.39	354.63	U1456A-61F-CC, 0–5 cm
T *Discoaster surculus*	2.49	362.28	U1456A-63F-1, 116 cm
T *Discoaster quinqueramus*	5.59	475.1	U1456D-3R-CC, 15–20 cm
T *Nicklithus amplificus*	5.94	523.39	U1456D-8R-1, 81 cm
B *Nicklithus amplificus*	6.91	554.01	U1456D-10R-CC, 12–17 cm
T *Discoaster loeblichii*	7.53	604.675	U1456D-16R-CC, 15–20 cm
B *Discoaster berggrenii*	8.29	737.47	U1456D-29R-CC, 7–12 cm
T Minylitha convallis	8.68	737.47	U1456D-30R-1, 41 cm
T *Discoaster bollii*	9.21	737.47	U1456D-30R-1, 41 cm
T *Discoaster hamatus*	9.53	760.465	U1456D-32R-3, 85 cm
T *Catinaster coalitus*	9.69	771.58	U1456D-33R-4, 144 cm
B *Discoaster hamatus*	10.55	816.035	U1456D-37R-CC, 23–28 cm
B *Catinaster coalitus*	10.89	995.535	U1456D-57R-7, 80 cm
T *Sphenolithus heteromorphus*	15.62	1111.49	U1456E-19R-4, 46 cm

[1]CCSF created by adding constant offset of 8.79 m to Holes U1456D and U1456E CSF-A depth

[2]Sample in which fossil top or base identified.

[3]Sample error is next sample above (for top) or below (for base) where fossil was not found. A

[4]Sample ID (error range) based on the position of the unconformity that separates MTD sedim

ellow shading indicates samples used to determine datum midpoint depth us

U1456A / U1456D[1]				
Depth (m CSF-A)	Depth (m CCSF)	Sample ID (error range)[3]	Depth (m CSF-A)	Depth (m CCSF)
23.34	25.29	U1456A-4H-CC, 27–32 cm	32.86	35.82
42.25	46.25	U1456A-4H-CC, 27–32 cm	32.86	35.82
99.24	105.62	U1456A-10H-CC, 17–22 cm	89.61	95.76
330.77	342.5	U1456A-58F-2, 86 cm	330.25	341.98
329.14	340.87	U1456A-58F-2, 20 cm	329.59	341.32
330.77	342.5	U1456A-59F-2, 83 cm	335.43	347.16
345.84	357.57	U1456A-60F-CC, 0–5 cm	339.96	351.69
345.84	357.57	U1456A-60F-CC, 0–5 cm	339.96	351.69
353.06	364.79	U1456A-62F-CC, 9–14 cm	348.04	359.77
470.26	479.05	U1456D-2R-CC, 15–20 cm	462.36	471.15
517.81	526.6	U1456D-7R-CC, 18–23 cm	511.39	520.18
543.76	552.55	U1456D-11R-1, 58 cm	546.68	555.47
603.9	612.69	U1456D-15R-CC, 15–20 cm	587.87	596.66
726.55	735.34	U1456D-30R-1, 41 cm	730.81	739.6
730.81	739.6	U1456D-29R-CC, 7–12 cm	726.55	735.34
730.81	739.6	U1456D-29R-CC, 7–12 cm	726.55	735.34
753.65	762.44	U1456D-31R-CC, 22–27 cm	749.7	758.49
765.25	774.04	U1456D-33R-1, 83 cm	760.33	769.12
804.51	813.3	U1456D-38R-2, 48 cm	809.98	818.77
986.65	995.44	U1456D-57R-CC, 12–17 cm	986.84	995.63
1103.73	1112.52	[4]U1456E-19R-2, 19 cm	1101.67	1110.46

scale.

Actual top or base lies somewhere in between the sample in which the fossil

nents from Indus Fan deposition

sed for age model.

U1456C				
Sample ID[2]	Depth (m CSF-A)	Depth (m CCSF)	Sample ID (error range)[3]	Depth (m CSF-A)
U1456C-1H-CC, 14–19 cm	7.33	7.33	U1456C-3H-CC, 12–17 cm	17.7
U1456C-6H-CC, 17–22 cm	46.77	48.72	U1456C-5H-CC, 14–19 cm	35.84
U1456C-13H-CC, 55–60 cm	95.64	101.44	U1456C-12H-CC, 14–19 cm	86.62
U1456C-18H-CC, 10–15 cm	136.97	144.93	U1456C-19F-CC, 0–5 cm	139.86

was found and the next sample where it was not found (we use midpoint between these two).

Depth (m CCSF)
18.68
37.61
91.53
147.82

.

Supplementary Table S4. Nannofossil datum levels in Holes U1457A, U1457B, and U1457C. Yel

Event	Age (Ma)	Datum Midpoint depth (m CCSF)	Sample ID[2]
B *Emiliania huxleyi*	0.29	25.87	U1457A-2H-CC, 12–17 cm
T *Pseudoemiliania lacunosa*	0.44	21.47	U1457A-5H-CC, 13–18 cm
T *Reticulofenestra asanoi*	0.91	54.855	U1457A-6H-CC, 13–18 cm
B *Reticulofenestra asanoi*	1.14	80.04	U1457A-8H-5, 38 cm
T *Gephyrocapsa* spp. >5.5 µm	1.24	89.33	U1457A-9H-CC, 44–49 cm
B *Gephyrocapsa* spp. >5.5 µm	1.62	365.225	U1457C-18R-CC, 14–19 cm
B *Gephyrocapsa* spp. >4 µm	1.73	388.715	U1457C-21R-1, 13–18 cm
T *Discoaster brouweri*	1.93	402.615	U1457C-23R-CC, 0–5 cm
T *Discoaster pentaradiatus*	2.39	419.535	U1457C-25R-1, 65 cm
T *Discoaster surculus*	2.49	423.63	U1457C-25R-3, 120 cm
T *Sphenolithus* spp.	3.54	515.27	U1457C-35R-1, 60 cm
B *Discoaster tamalis*	4.13	539.4	U1457C-37R-3, 39 cm
T *Discoaster quinqueramus*	5.59	539.4	U1457C-37R-CC, 20–25 cm
T *Nicklithus amplificus*	5.94	610.205	U1457C-44R-5, 64 cm
B *Nicklithus amplificus*	6.91	628.935	U1457C-46R-4, 40 cm
B *Amaurolithus* spp.	7.42	644.905	U1457C-48R-2, 60 cm
B *Discoaster quinqueramus*	8.12	839.235	U1457C-67R-CC, 0–5 cm
T *Minylitha convallis*	8.68	839.235	U1457C-68R-CC, 9–14 cm
T *Discoaster bollii*	9.21	851.06	U1457C-69R-CC, 25–30 cm
T *Catinaster coalitus*	9.69	860.57	U1457C-70R-CC, 18–23 cm
B *Discoaster bellus*	10.4	1003.095	U1457C-84R-CC, 10–15 cm
B *Catinaster coalitus*	10.89	1003.095	U1457C-84R-CC, 10–15 cm
Absence of *Fasciculithus* spp.	>62.13	1067.99	U1457C-93R-1, 128 cm
B *Ellipsolithus macellus*	63.25	1084.45	U1457C-94R-CC, 18–23 cm

[1]CCSF created by adding constant offset of 5.15 m to Hole U1457C CSF-A depth scale.

[2]Sample in which fossil top or base identified.

[3]Sample error is next sample above (for top) or below (for base) where fossil was not found. A

[4]Sample ID (error range) based on the position of the unconformity that separates MTD sedim

llow shading indicates samples used to determine datum midpoint depth u

U1457A / U1457C[1]				
Depth (m CSF-A)	Depth (m CCSF)	Sample ID (error range)[3]	Depth (m CSF-A)	Depth (m CCSF)
14.02	18.91	U1457A-3H-CC, 11–16 cm	27.07	32.83
45.56	52.42	U1457A-4H-CC, 12–17 cm	36.59	42.75
55.74	62.36	U1457A-5H-CC, 13–18 cm	45.56	52.42
72.08	78.46	U1457A-8H-CC, 14–19 cm	75.24	81.62
83.78	90.62	U1457A-8H-CC, 14–19 cm	75.24	81.62
356.6	361.75	U1457C-19R-CC, 0–5 cm	363.55	368.7
376.03	381.18	U1457C-22R-CC, 15–20 cm	391.1	396.25
403.83	408.98	U1457C-22R-CC, 15–20 cm	391.1	396.25
415.35	420.5	U1457C-24R-CC, 0–5 cm	413.42	418.57
418.82	423.97	U1457C-25R-3, 52 cm	418.14	423.29
512.3	517.45	U1457C-34R-CC, 12–17 cm	507.94	513.09
534	539.15	U1457C-37R-CC, 20–25 cm	534.5	539.65
534.5	539.65	U1457C-37R-3, 39 cm	534	539.15
605.21	610.36	U1457C-44R-5, 33 cm	604.9	610.05
623.19	628.34	U1457C-46R-5, 69 cm	624.38	629.53
639.9	645.05	U1457C-48R-CC, 0–5 cm	639.61	644.76
827.7	832.85	U1457C-68R-CC, 9–14 cm	840.47	845.62
840.47	845.62	U1457C-67R-CC, 0–5 cm	827.7	832.85
851.35	856.5	U1457C-68R-CC, 9–14 cm	840.47	845.62
859.49	864.64	U1457C-69R-CC, 25–30 cm	851.35	856.5
995.93	1001.08	U1457C-85R-CC, 0–5 cm	999.96	1005.11
995.93	1001.08	U1457C-85R-CC, 0–5 cm	999.96	1005.11
1063.48	1068.63	[4]U1457C-93R-1, 0 cm	1062.2	1067.35
1073.69	1078.84	U1457C-95R-CC, 16–21 cm	1084.91	1090.06

ctual top or base lies somewhere in between the sample in which the fossil

ents from Paleocene sediments.

ısed for age model.

U1457B				
Sample ID[2]	Depth (m CSF-A)	Depth (m CCSF)	Sample ID (error range)[3]	Depth (m CSF-A)
U1457B-1H-CC, 14–19 cm	3.17	3.17	U1457B-2H-CC, 0–5 cm	12.49
U1457B-3H-CC, 10–15 cm	21.64	26.58	U1457B-2H-CC, 0–5 cm	12.49
U1457B-6H-CC, 0–5 cm	50.32	57.29	U1457B-5H-CC, 0–5 cm	40.23
U1457B-7H-CC, 23–28 cm	59.35	66.91	U1457B-8H-CC, 35–40 cm	68.51
U1457B-10H-CC, 68–73 cm	87.7	96.93	U1457B-9H-CC, 30–35 cm	79.39

l was found and the next sample where it was not found (we use midpoint between these two

Depth (m CCSF)
16.36
16.36
46.03
76.6
88.04

ɔ).

Supplementary Table S5. Distribution of calcareous nannofossils for the 2–8 Ma interval in Hole U1457C (com

Sample	Top [cm]	Bottom [cm]	Top Depth [m]	Bottom Depth [m]	Preservation	Group Abundance	Amaurolithus delicatus	Amaurolithus primus	Amaurolithus tricorniculatus	Blackites spp.
U1457C-25R-1-W 65/65	65	65	415.35	415.35	M	V				
U1457C-25R-1W-120/121	120	121	415.9	415.91	G	A				
U1457C-25R-2W-61/62	61	62	416.73	416.74	G	A				
U1457C-25R-2W-120/121	120	121	417.32	417.33	G	A				
U1457C-25R-3-W 52/52	52	52	418.14	418.14	G	A				
U1457C-25R-3W-120/121	120	121	418.82	418.83	M	V				
U1457C-25R-4W-60/61	60	61	419.72	419.73	G	A				
U1457C-25R-4W-120/121	120	121	420.32	420.33	G	C				
U1457C-25R-5W-60/61	60	61	421.23	421.24	M	C				
U1457C-25R-5W-110/111	110	111	421.73	421.74	M	C				
U1457C-25R-CC	0	5	422.14	422.19	M	F				*
U1457C-26R-1W-60/61	60	61	425	425.01	M	C				
U1457C-26R-1W-120/121	120	121	425.6	425.61	M	A				
U1457C-26R-2W-49/50	49	50	426.39	426.4	M	C				
U1457C-26R-CC	0	5	426.8	426.85	P	F				
U1457C-27R-1W-34/35	34	35	434.44	434.45	M	A				
U1457C-27R-1-W 97/102	97	102	435.07	435.12	M	C				
U1457C-28R-1-W 0/5	0	5	443.8	443.85	M	F				
U1457C-29R-1W-86/87	86	87	454.36	454.37	M	A				
U1457C-29R-1-W 126/131	126	131	454.76	454.81	M	C				
U1457C-30R-1W-59/60	59	60	463.79	463.8	G	A				
U1457C-30R-1-W 82/87	82	87	464.02	464.07	M	C				
U1457C-31R-1W-60/61	60	61	473.5	473.51	G	C				
U1457C-31R-1W-120/121	120	121	474.1	474.11	M	C				
U1457C-31R-2W-40/41	40	41	474.8	474.81	G	C				
U1457C-31R-2W-100/101	100	101	475.4	475.41	M	C				
U1457C-31R-CC	0	5	475.8	475.85	M	C				
U1457C-32R-1-W 53/53	53	53	483.13	483.13	M	V				
U1457C-32R-2W-19/20	19	20	483.5	483.51	M	C				
U1457C-32R-2W-80/81	80	81	484.11	484.12	M	C				
U1457C-32R-CC	0	5	484.43	484.48	M	C				
U1457C-33R-1W-60/61	60	61	492.9	492.91	G	C				
U1457C-33R-1-W 108/110	108	110	493.38	493.4	M	C				
U1457C-33R-2W-120/121	120	121	495	495.01	G	C				
U1457C-33R-3W-61/61	61	61	495.91	495.91	G	A				
U1457C-33R-CC	0	5	496.28	496.33	M	C				
U1457C-34R-1W-60/61	60	61	502.6	502.61	M	C				
U1457C-34R-1W-133/134	133	134	503.33	503.34	M	C				

U1457C-34R-2W-31/31	31	31	503.81	503.81	G	A				
U1457C-34R-2W-115/115	115	115	504.65	504.65	M	C				
U1457C-34R-3W-60/61	60	61	505.6	505.61	G	A				
U1457C-34R-3W-120/121	120	121	506.2	506.21	G	A				
U1457C-34R-4W-50/51	50	51	507	507.01	G	A				
U1457C-34R-4W-120/121	120	121	507.7	507.71	G	A				
U1457C-34R-CC	0	5	507.94	507.99	G	A				
U1457C-35R-1W-60/61	60	61	512.3	512.31	G	A				
U1457C-35R-1W-119/120	119	120	512.89	512.9	G	A				
U1457C-35R-2W-60/61	60	61	513.8	513.81	M	A				
U1457C-35R-2W-120/121	120	121	514.4	514.41	G	A				
U1457C-35R-3-W 32/33	32	33	515.02	515.03	M	A				
U1457C-35R-3W-55/56	55	56	515.25	515.26	G	V				
U1457C-35R-3W-119/120	119	120	515.89	515.9	M	A				
U1457C-35R-4W-69/70	69	70	516.89	516.9	M	V				
U1457C-35R-4W-89/90	89	90	517.09	517.1	M	A				
U1457C-35R-4W-120/121	120	121	517.4	517.41	G	A				
U1457C-35R-5W-19/20	19	20	517.89	517.9	G	A				
U1457C-35R-5W-59/60	59	60	518.29	518.3	G	A				
U1457C-35R-5W-99/100	99	100	518.69	518.7	M	A				
U1457C-35R-5W-120/121	120	121	518.9	518.91	G	A				
U1457C-35R-6W-10/11	10	11	519.3	519.31	G	V				
U1457C-35R-6-W 29/29	29	29	519.49	519.49	M	A				
U1457C-35R-6W-89/90	89	90	520.09	520.1	G	V				
U1457C-35R-7W-29/30	29	30	520.99	521	M	V				
U1457C-35R-CC	0	5	521.49	521.54	M	A				
U1457C-36R-1W-60/61	60	61	522	522.01	M	C				
U1457C-36R-2W-40/41	40	41	523.3	523.31	M	C				
U1457C-36R-2A-80/85	80	85	523.7	523.75	G	C				
U1457C-37R-1W-59/60	59	60	531.7	531.71	M	C				
U1457C-37R-1W-120/121	120	121	532.3	532.31	M	C				
U1457C-37R-2W-52/53	52	53	533.12	533.13	M	A				
U1457C-37R-3W-39/40	39	40	534	534.01	M	V				
U1457C-37R-CC	0	5	534.5	534.55	M	F				
U1457C-38R-1W-68/69	68	69	541.48	541.49	M	C				
U1457C-38R-1W-120/121	120	121	542	542.01	M	C				
U1457C-38R-2W-60/61	60	61	542.9	542.91	M	A				
U1457C-38R-2W-123/124	123	124	543.5	543.51	M	C				
U1457C-38R-3W-53/54	53	54	544.33	544.34	M	C				
U1457C-38R-CC	0	5	544.66	544.71	P	C				
U1457C-39R-1W-81/82	81	82	551.31	551.32	M	C				
U1457C-39R-2W-120/121	120	121	553.2	553.21	G	A				
U1457C-39R-3W-30/31	30	31	553.8	553.81	P	C				
U1457C-39R-3W-80/81	80	81	554.3	554.31	P	C				
U1457C-39R-CC	0	5	555.03	555.08	M	C				
U1457C-40R-1W-37/38	37	38	560.57	560.58	M	C				
U1457C-40R-1W-90/91	90	91	561.1	561.11	M	A				
U1457C-40R-2W-32/33	32	33	561.83	561.84	G	A				
U1457C-40R-2W-92/93	92	93	562.43	562.44	G	A				
U1457C-40R-3W-72/73	72	73	563.43	563.44	M	A				

U1457C-40R-CC	0	5	563.73	563.78	M	C				
U1457C-41R-1W-52/53	52	53	570.42	570.43	M	C				
U1457C-41R-1W-120/121	120	121	571.1	571.11	G	A				
U1457C-41R-2W-36/37	36	37	571.66	571.67	G	A				
U1457C-41R-2W-79/80	79	89	572.09	572.1	G	C				
U1457C-41R-3W-38/39	38	39	572.7	572.71	G	C				
U1457C-41R-CC	0	5	573.26	573.31	M	A				
U1457C-42R-1W-24/25	24	25	579.84	579.85	M	C				
U1457C-42R-1W-122/123	122	123	580.82	580.83	M	C				
U1457C-42R-CC	0	5	581.18	581.23	M	A				
U1457C-43R-1W-90/91	90	91	590.2	590.21	M	C				
U1457C-43R-2W-40/41	40	41	591.11	591.12	M	C				
U1457C-43R-3W-60/61	60	61	592.31	592.32	M	A				
U1457C-43R-CC	0	5	592.58	592.63	M	C				
U1457C-44R-1W-30/31	30	31	599.3	599.31	M	A		R		
U1457C-44R-1W-80/81	80	81	599.8	599.81	M	C				
U1457C-44R-2W-60/61	60	61	600.82	600.83	M	A	R			*
U1457C-44R-2W-121/122	121	122	601.43	601.44	P	C				
U1457C-44R-3W-60/61	60	61	602.32	602.33	G	A				
U1457C-44R-3W-120/121	120	121	602.92	602.93	G	V	R			
U1457C-44R-4W-30/31	30	31	603.45	603.46	M	V	R			
U1457C-44R-4-W 93/93	93	93	604.08	604.08	M	V				
U1457C-44R-5-W 33/33	33	33	604.9	604.9	G	V		R		
U1457C-44R-5W-64/65	64	65	605.21	605.22	M	V	R			
U1457C-44R-CC	0	5	605.65	605.7	M	V		R		
U1457C-45R-1W-61/62	61	62	609.31	609.32	G	V				
U1457C-45R-1W-119/120	119	120	609.89	609.9	G	V				
U1457C-45R-2-W 24/26	24	26	610.35	610.37	M	V				
U1457C-45R-2W-120/121	120	121	611.31	611.32	M	V		R		
U1457C-45R-3W-60/61	60	61	612.21	612.22	M	V				
U1457C-45R-3W-113/114	113	114	612.74	612.75	M	V			R	
U1457C-45R-4-W 7/7	7	7	613.18	613.18	M	V	R	R	R	
U1457C-45R-4W-59/60	59	60	613.7	613.71	M	V				
U1457C-45R-5W-35/36	35	36	614.75	614.76	M	V				
U1457C-45R-6W-60/61	60	61	615.85	615.86	M	V				
U1457C-45R-CC	0	7	616.21	616.28	G	A				
U1457C-46R-1W-60/61	60	61	619	619.01	M	V				
U1457C-46R-1W-115/116	115	116	619.55	619.56	G	V				
U1457C-46R-2-W 45/45	45	45	620.24	620.24	M	V			R	
U1457C-46R-2W-120/121	120	121	620.99	621	M	V				
U1457C-46R-3W-70/71	70	71	621.99	622	M	V				
U1457C-46R-3W-120/121	120	121	622.49	622.5	M	V				
U1457C-46R-4-W 40/40	40	40	623.19	623.19	M	V				
U1457C-46R-5W-69/70	69	70	624.38	624.39	G	V				
U1457C-46R-CC	0	5	624.53	624.58	M	V		R		
U1457C-47R-1-W 40/42	40	42	628.5	628.52	M	V				
U1457C-47R-1W-122/123	122	123	629.32	629.33	G	V				
U1457C-47R-2W-13/14	13	14	629.73	629.74	G	V				
U1457C-47R-2W-120/121	120	121	630.8	630.81	G	C				
U1457C-47R-3W-60/61	60	61	631.7	631.71	G	A				

U1457C-47R-3W-121/122	121	122	632.31	632.32	G	V				
U1457C-47R-4-W 13/13	13	13	632.73	632.73	M	A				
U1457C-47R-4W-123/124	123	124	633.83	633.84	M	V				
U1457C-47R-5W-60/61	60	61	634.7	634.71	M	V				
U1457C-47R-5W-120/121	120	121	635.3	635.31	M	V	R	R		
U1457C-47R-6W-71/73	71	73	636.31	636.33	M	V				
U1457C-47R-7W-28/29	28	29	637.38	637.39	G	V		R		
U1457C-47R-CC	0	5	638.02	638.07	M	A		1?		
U1457C-48R-1W-62/62	62	62	638.42	638.42	G	V		R		
U1457C-48R-2W-30/31	30	31	639.09	639.1	M	V				
U1457C-48R-2W-60/61	60	61	639.39	639.4	G	V	1	1?		
U1457C-48R-CC	0	5	639.61	639.66	M	A				
U1457C-49R-1W-60/61	60	61	648.1	648.11	M	C	1?			
U1457C-49R-1W-126/127	126	127	648.76	648.77	M	V				
U1457C-49R-2W-27/27	27	27	649.27	649.27	M	V		2?		
U1457C-49R-2W-82/83	82	83	649.82	649.83	M	V				
U1457C-49R-3W-45/46	45	46	650.95	650.96	P	V				
U1457C-49R-3W-100/101	100	101	651.5	651.51	G	C				
U1457C-49R-4W-59/60	59	60	652.59	652.6	G	C				
U1457C-49R-4W-120/121	120	121	653.2	653.21	G	C				
U1457C-49R-5W-20/21	20	21	653.7	653.71	P	A				
U1457C-49R-5W-100/101	100	101	654.5	654.51	M	A				
U1457C-49R-6W-60/61	60	61	655.21	655.22	M	A				
U1457C-49R-CC	0	5	655.85	655.9	M	F				
U1457C-50R-1W-48/48	48	48	657.68	657.68	P	V				
U1457C-50R-1W-98/99	98	99	658.18	658.19	G	V				
U1457C-50R-2W-59/60	59	60	659.24	659.25	M	V				
U1457C-50R-2W-120/121	120	121	659.85	659.86	M	V				
U1457C-50R-3W-60/61	60	61	660.76	660.77	M	V				
U1457C-50R-3W-130/131	130	131	661.46	661.47	M	V				
U1457C-50R-4W-49/49	49	49	662.15	662.15	M	V				
U1457C-50R-4W-124/125	124	125	662.9	662.91	P	V				
U1457C-50R-5W-20/21	20	21	663.38	663.39	M	V				
U1457C-50R-5W-80/81	80	81	663.98	663.99	P	V				
U1457C-50R-CC	0	5	664.38	664.43	M	A				
U1457C-51R-1W-60/61	60	61	667.5	667.51	G	V				
U1457C-51R-1W-100/101	100	101	667.9	667.91	M	V				
U1457C-51R-2W-27/28	27	28	668.67	668.68	G	V				
U1457C-51R-2W-94/95	94	95	669.34	669.35	G	V				
U1457C-51R-3W-60/61	60	61	670.5	670.51	G	V				
U1457C-51R-3W-119/120	119	120	671.09	671.1	G	A				
U1457C-51R-4W-60/61	60	61	672	672.01	G	C				
U1457C-51R-4W-120/121	120	121	672.6	672.61	G	C				
U1457C-51R-CC	0	5	673.67	673.72	M	F				
U1457C-52R-1W-60/61	60	61	677.2	677.21	G	C				
U1457C-52R-1W-120/121	120	121	677.8	677.81	G	C				
U1457C-52R-2W-60/61	60	61	678.61	678.62	M	C				
U1457C-52R-2W-120/121	120	121	679.21	679.22	M	A				
U1457C-52R-CC	0	5	679.67	679.72	M	F				
U1457C-53R-1W-60/61	60	61	686.9	686.91	M	C				

U1457C-53R-2W-60/61	60	61	688.3	688.31	M	C				
U1457C-53R-3W-60/61	60	61	689.76	689.77	G	C				
U1457C-53R-3W-120/121	120	121	690.36	690.37	M	A				
U1457C-53R-CC	0	5	690.69	690.74	M	C				
U1457C-54R-1W-30/31	30	31	696.3	696.31	M	C				
U1457C-54R-1W-74/75	74	75	696.74	696.75	M	C				
U1457C-54R-2W-60/61	60	61	697.64	697.65	M	A				
U1457C-54R-2W-120/121	120	121	698.24	698.25	M	C				
U1457C-54R-CC	0	5	698.41	698.46	M	C				
U1457C-55R-1W-30/31	30	31	706	706.01	M	C				
U1457C-55R-1W-110/111	110	111	706.8	706.81	M	C				
U1457C-55R-CC	0	5	707.08	707.13	G	A				
U1457C-56R-1W-58/59	58	59	715.98	715.99	M	C				
U1457C-56R-1W-90/91	90	91	716.3	716.31	M	C				
U1457C-56R-1-W 115/120	115	120	716.55	716.6	M	C				
U1457C-57R-1W-70/71	70	71	725.8	725.81	M	C				
U1457C-57R-1W-123/124	123	124	726.33	726.34	M	C				
U1457C-57R-2W-20/21	20	21	726.8	726.81	P	F				
U1457C-57R-2W-58/59	58	59	727.18	727.19	M	C				
U1457C-57R-3W-20/21	20	21	727.8	727.81	G	A				
U1457C-57R-CC	0	5	728.27	728.32	M	V				
U1457C-58R-1W-30/31	30	31	735.1	735.11	M	C				
U1457C-58R-1W-80/81	80	81	735.6	735.61	M	C				
U1457C-58R-2W-62/63	62	63	736.61	736.62	P	C				
U1457C-58R-2W-120/121	120	121	737.19	737.2	P	C				
U1457C-58R-3W-30/31	30	31	737.68	737.69	M	C				
U1457C-58R-4W-46/48	46	48	739.9	739.92	M	A				
U1457C-58R-CC	0	8	739.13	739.21	M	A				
U1457C-59R-1W-39/40	39	40	744.89	744.9	M	C				
U1457C-59R-1-W 136/141	136	141	745.86	745.91	M	R				
U1457C-60R-1W-60/61	60	61	754.8	754.81	M	C				
U1457C-60R-1W-120/121	120	121	755.4	755.41	M	C				
U1457C-60R-2W-53/54	53	54	756.23	756.24	M	C				
U1457C-60R-2W-104/105	104	105	756.74	756.75	M	C				
U1457C-60R-3W-45/46	45	46	757.65	757.66	M	C				
U1457C-60R-3W-87/88	87	88	758.07	758.08	M	F				
U1457C-60R-4W-50/51	50	51	758.9	758.91	M	C				
U1457C-60R-CC	0	5	759.29	759.34	M	C				
U1457C-61R-1W-60/61	60	61	764.5	764.51	M	F				
U1457C-61R-1W-120/121	120	121	765.1	765.11	M	C				
U1457C-61R-2W-62/63	62	63	765.99	766	M	C				
U1457C-61R-3W-30/31	30	31	766.52	766.53	M	F				
U1457C-61R-CC	0	5	767.03	767.08	M	F				
U1457C-62R-1W-31/32	31	32	773.91	773.92	M	C				
U1457C-62R-1W-75/76	75	76	774.35	774.36	M					
U1457C-62R-2W-3/4	3	4	774.72	774.73	M	C				
U1457C-62R-CC	0	5	775.7	775.75	M	C				
U1457C-63R-1W-32/33	32	33	783.9	783.91	M	F				
U1457C-63R-1W-107/108	107	108	784.5	784.51	M	C				
U1457C-63R-2W-62/63	62	63	785.32	785.33	M	C				

U1457C-63R-3W-40/41	40	41	786.13	786.14	M	C				
U1457C-63R-CC	0	5	786.92	786.97	M	F				
U1457C-64R-1W-77/78	77	78	793.6	793.61	M	C				
U1457C-64R-1W-120/121	120	121	794.2	794.21	M	C				
U1457C-64R-2W-31/32	31	32	794.81	794.82	M	C				
U1457C-64R-2W-75/76	75	76	795.25	795.26	M	C				
U1457C-64R-3W-37/38	37	38	795.8	795.81	M	C				
U1457C-64R-3W-70/71	70	71	796.2	796.21	M	C				
U1457C-64R-CC	0	5	796.47	796.52	M	F				
U1457C-65R-1W-53/54	53	54	803.23	803.24	M	C				
U1457C-65R-1W-112/113	112	113	803.9	803.91	M	C				
U1457C-65R-2W-58/59	58	59	804.7	804.71	M	C				
U1457C-65R-2W-120/121	120	121	805.32	805.33	M	F				
U1457C-65R-3W-60/61	60	61	806.18	806.19	M	C				
U1457C-65R-3W-110/111	110	111	806.68	806.69	M	C				
U1457C-65R-4W-60/61	60	61	806.18	806.19	M	C				
U1457C-65R-4W-119/120	119	120	808.03	808.04	M	C				
U1457C-65R-5W-41/42	41	42	808.51	808.52	P	C				
U1457C-65R-5W-70/71	70	71	808.91	808.92	M	C				
U1457C-65R-6W-40/41	40	41	809.69	809.7	P	C				
U1457C-65R-CC	0	5	810.16	810.21	M	F				
U1457C-66R-1W-50/51	50	51	812.9	812.91	M	C				
U1457C-66R-1W-100/101	100	101	813.4	813.41	M	C				
U1457C-66R-2W-57/58	57	58	814.18	814.19	M	C				
U1457C-66R-2W-108/109	108	109	814.69	814.7	M	C				
U1457C-66R-3W-62/63	62	63	815.59	815.6	M	C				
U1457C-66R-CC	0	5	815.94	815.99	M	F				
U1457C-67R-1W-34/35	34	35	822.7	822.71	M	C				
U1457C-67R-1W-120/121	120	121	823.3	823.31	P	C				
U1457C-67R-2W-60/61	60	61	824.07	824.08	M	F				
U1457C-67R-2W-120/121	120	121	824.67	824.68	M	C				
U1457C-67R-3W-60/61	60	61	825.35	825.36	M	C				
U1457C-67R-3W-120/121	120	121	825.95	825.96	M	C				
U1457C-67R-4W-60/61	60	61	826.7	826.71	M	C				
U1457C-67R-4W-104/105	104	105	827.14	827.15	G	C				
U1457C-67R-5W-30/31	30	31	827.52	827.53	P	C				
U1457C-67R-CC	0	5	827.7	827.75	M	C				

bined shipboard and post-cruise analyses).

Braarudosphaera bigelowii	Calcidiscus leptoporus	Calcidiscus macintyrei	Calcidiscus tropicus	Campylosphaera dela	Catinaster coalitus	Ceratolithus cristatus	Chiasmolithus nitidus	Chiasmolithus spp.	Clausicoccus fenestratus	Clausicoccus subdistichus	Coccolithus formosus	Coccolithus miopelagicus	Coccolithus pelagicus	Coronocyclus nitescens	Cruciplacolithus edwardsii	Cruciplacolithus frequens	Cruciplacolithus intermedius	Cruciplacolithus primus	Cruciplacolithus tenuis	Cryptococcolithus mediaperforatu	Cyclagelosphaera spp.	Cyclicargolithus abisectus	Cyclicargolithus floridanus
	C	F	F										C										
	C	R	F			R							F										
	F	R	R										C										*
	F		R			F							C										
	F	R	R								*		F									*	
	F	F	C			R							C										
	F	R	F			R							F										*
		R	R										F										
R	R									*											*	*	*
R													R								*		*
	R			*									F										*
													F								*		*
R	R												F								*		
													F								*		*
	R			*									F									*	*
	R												R								*	*	*
	R												F										*
			R										R										
R													R										*
R	R	R	R										R										*
R	R												R								*	*	*
R													R										
	R	R											R										*
R	R		R										R								*		*
R											*		R										*
													F										
	R	F	F										F										*
		R	R										R										*
			R										R										*
										*			F								*	*	*
													R								*		*
R																		*			*		
R	R		R								*		R										*
	F		F																				
	R							*		*			R								*		*
R	R	R	R																		*	*	*
	R	F	R								*		R								*		*

R	F	F	F								*		F							*	*	*
	R	F	C										R							*		
			F										R									
	F	R	R										R									
	F	F	F										R									
	F	R																				
	F	F	R										F									
	F	F	F			R							R									
	F	F	F																			*
	F	F	F			R																
	F	C	F			R																
	C	F	C			F																
	C	C	F			R							F									
R	C	F	C			F							R									
	F	F	C			F														*		
	F	F	C			F																
R	R		F																			
	F	F	C			F																*
	C	F	F			R							R									
	C	R	R			R																
	C	F	R			R							R									
	C	F	F			F																
		F	C										R									*
	C		F			F								*								
	C		C			F					*		R	*								
													F							*		
R			R								*		R							*		*
R	F		R																	*	*	*
	F		R										R							*	*	*
	F												R								*	*
			R								*		F									*
	C		F			F							F									
	C		F			F																*
													R			*						*
			R								*		F							*	*	*
	R										*		R								*	*
R	R												R							*		*
	F		R										R								*	*
	F		R								*		R									*
		R						*					R							*		*
	R		R										R									*
	R		R										R							*		*
	R												F							*		*
													R						R	*		*
													F									
													R		*					*		*
	R												R							*		*
R	R										*		R							*		*
	R												R							*		*
	R		R										F							*		*

			R										F				*	*	*		*		*
													F								*		*
	R		R										R								*		*
			R										R							R	*		*
	R												R							R	*		
	R												R								*		*
	F	F	R										F										*
	R												R							R	*		*
	R												F							R	*		*
									*				F								*		*
R	R												R								*		*
R	R		F										F								*	*	*
	F		R								*		R								*		*
	F												F		*			*			*	*	*
	R		R			R							R							R	*		
	F												F								*	*	*
R	R																				*		*
	R												F								*		
R	F												R							R	*		*
	C		C			R							R										
	C		F			R														R			
	F		R										F									*	*
	F	F	F										F										
	C		C			R							F							R			
	F	F	R										F										
	C		F			F																	
R	C		F			F																	
	F	F	C			R							R										
	F		F																				
	C		F			F																	
	C		F			R														R			
	F	C																		F			
	C		F			F																	
	C		C			F																	
	F		F										R										
	F		F										F										
	F					R							F										
	C		F										F										
	F												F										
	F												F										
	F		F										F										
	F		F										F										
	F												F										
	C		R																				
	F												F										
		R											F										
	F		F																				
	F		F										R										
	R		R										R									*	
R	R																						

	F		R										R									
		F											F									
	F		F										R									
	C		C										R									
	F		F										R									
	R		R																			
	R		F										R						F			
	R		F																R			
	F		R										F									
	C		F																R			
	F	F	F										R						R			
	C		F										F									
	F		R										F									
	F		R										F									
	F												F									
	F		R										C						R			
													R				*			*		*
R													R							*	*	*
	R												R							*		*
R	R												F									*
R													F						R	*		*
R													F							*		*
				*			*				*		R									*
	F												F									
	C		F										C						R			
	F		F										C									
	C												C									
	C		R										C									
	C		R										C						R			
	F												C									*
	F												F									
	F												C									
	F		R										C								*	
	R											*	F						R			
	F		R										C						R			*
	C												C									
	C		R										C									
	C		F		*								C						R		*	*
	C		F										C									
	F		R						*				F						R	*		*
R	F												F					*		*		*
R	R		R								*		R							*		*
	F												F									*
									*				R							*	*	*
													R							*		*
													R					*		*	*	*
	R									*			R							*		*
	R								*				R									
													R							*		*

R	R		R										R							*		*
	F		F										F									
	R												R								*	*
	R		R										R									*
	R		F										R							*		*
	F																			*		*
	R		R																			*
	R	R	F					*					R									
			R																	*		*
			R										R									*
	F		F										F						F			
R	R											*	R					*		*	*	*
			R										R							*		*
									*				F						R			*
R	R		R										R								*	*
	R																					*
																						*
													R							*		
	F		F										R							*		
	C	F	C										C						C			*
	R												R							*		*
	F												R							*		*
																				*		*
	R		F										F									
R	F		F																	*		*
			F										C									*
	F	R											C						F			
													R	*						*		*
R																						
													R							*		*
	R																			*		*
													R							*		*
													R									*
	R																			*		*
	R												R							*		*
													F	*						*		*
R	R												F									
	R												R									*
	R												R							*		*
													R							*		*
R	R												R							*		*
	R												R									*
	R												R								*	*
R													R							*		*
													R									*
		R											F									*
R	R												R							*		*
																				*		*
										*										*		*

R													R										*
													F										*
R													R										*
R													F										*
	F												R										*
R													R								*		*
													R								*		*
	F																				*	*	*
													R										*
													F								*		*
	R												R								*		*
R													F								*	*	*
	R												R	*							*		*
	R		R										R								*		*
													R								*	*	*
	R												R								*		*
R													R								*		*
R	R												R								*		*
	R												R								*		*
													R								*		*
	R								*				F						*			*	*
													R								*		*
R													R								*		*
R	R												F								*	*	*
	R												R								*		*
	R												R										*
									*		*		R				*			R			
	R		R										R								*	*	*
R													R								*		*
	R												R										*
R													R								*	*	*
																					*	*	*
													R								*		*
													R								*		*
R													R										*
													R								*		*
	R	R											R							R			*

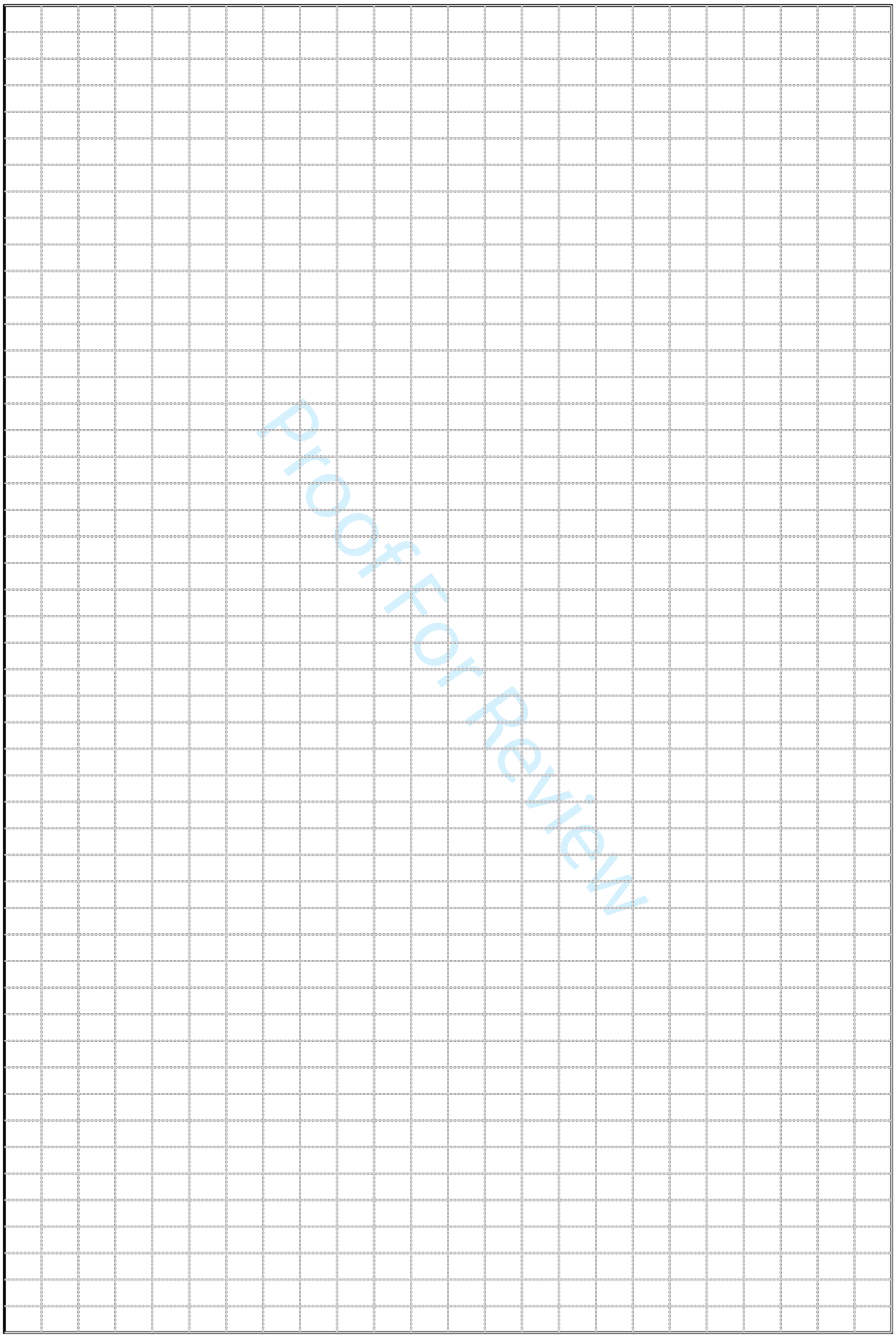
Proof For Review

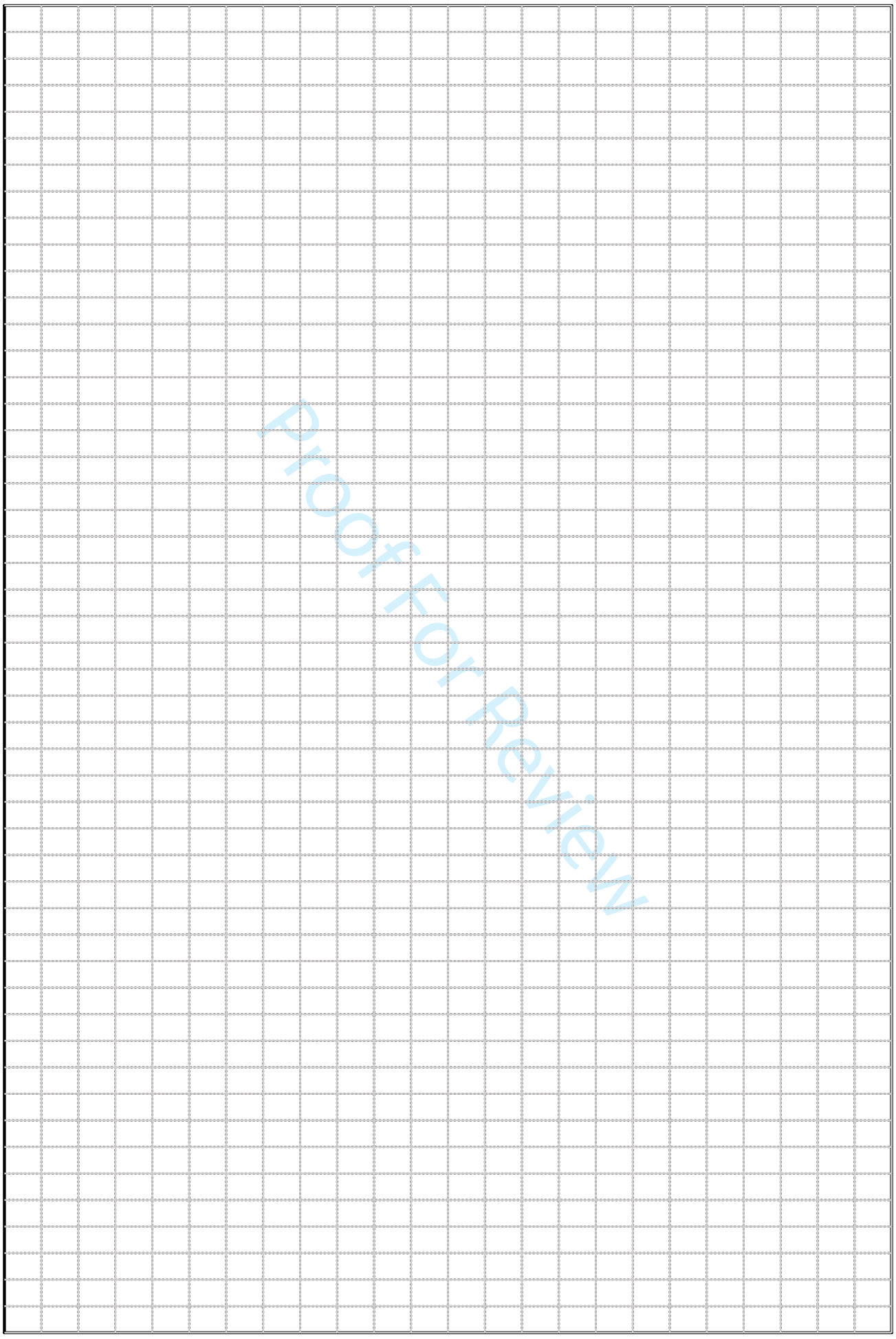
Proof For Review

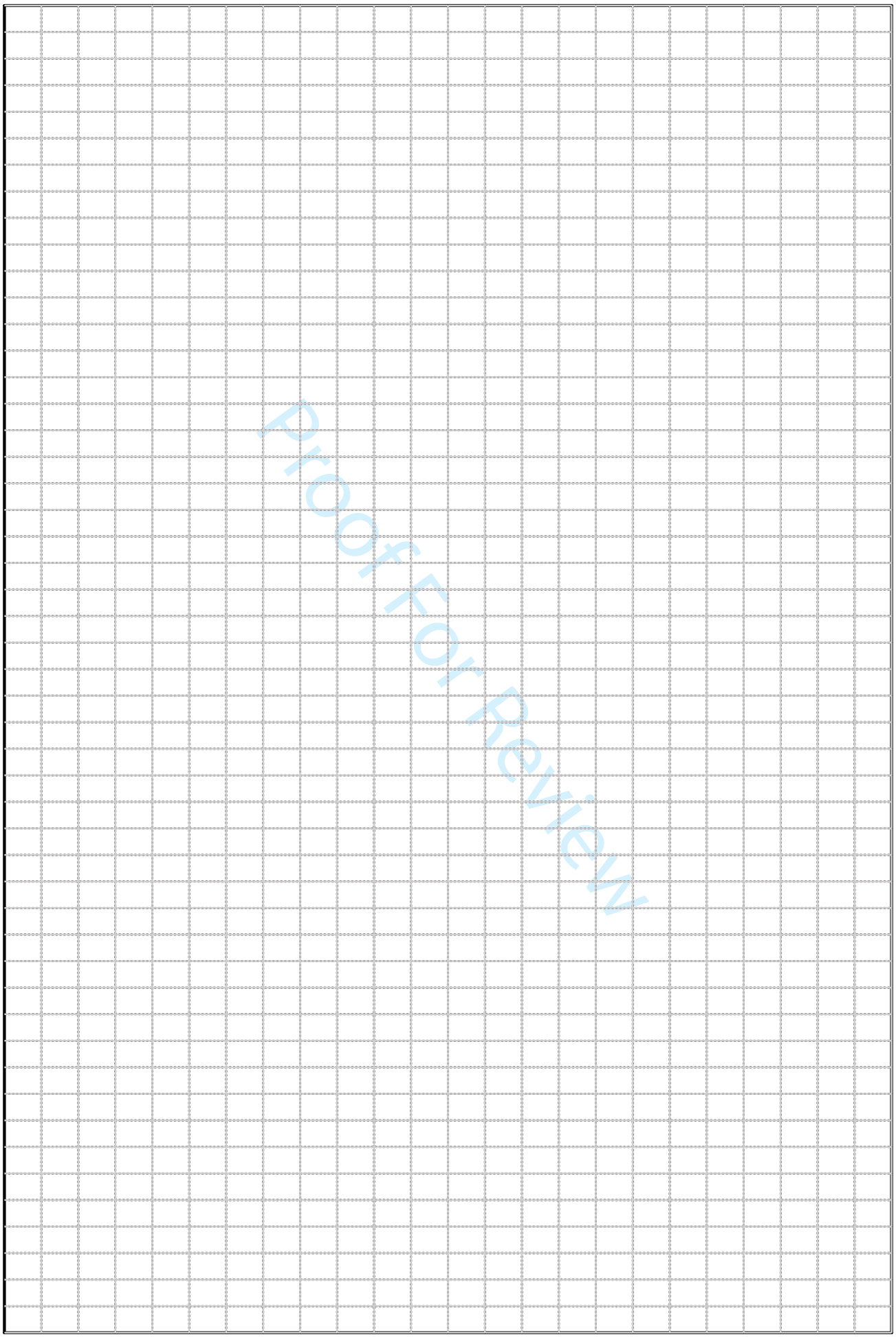
Proof For Review

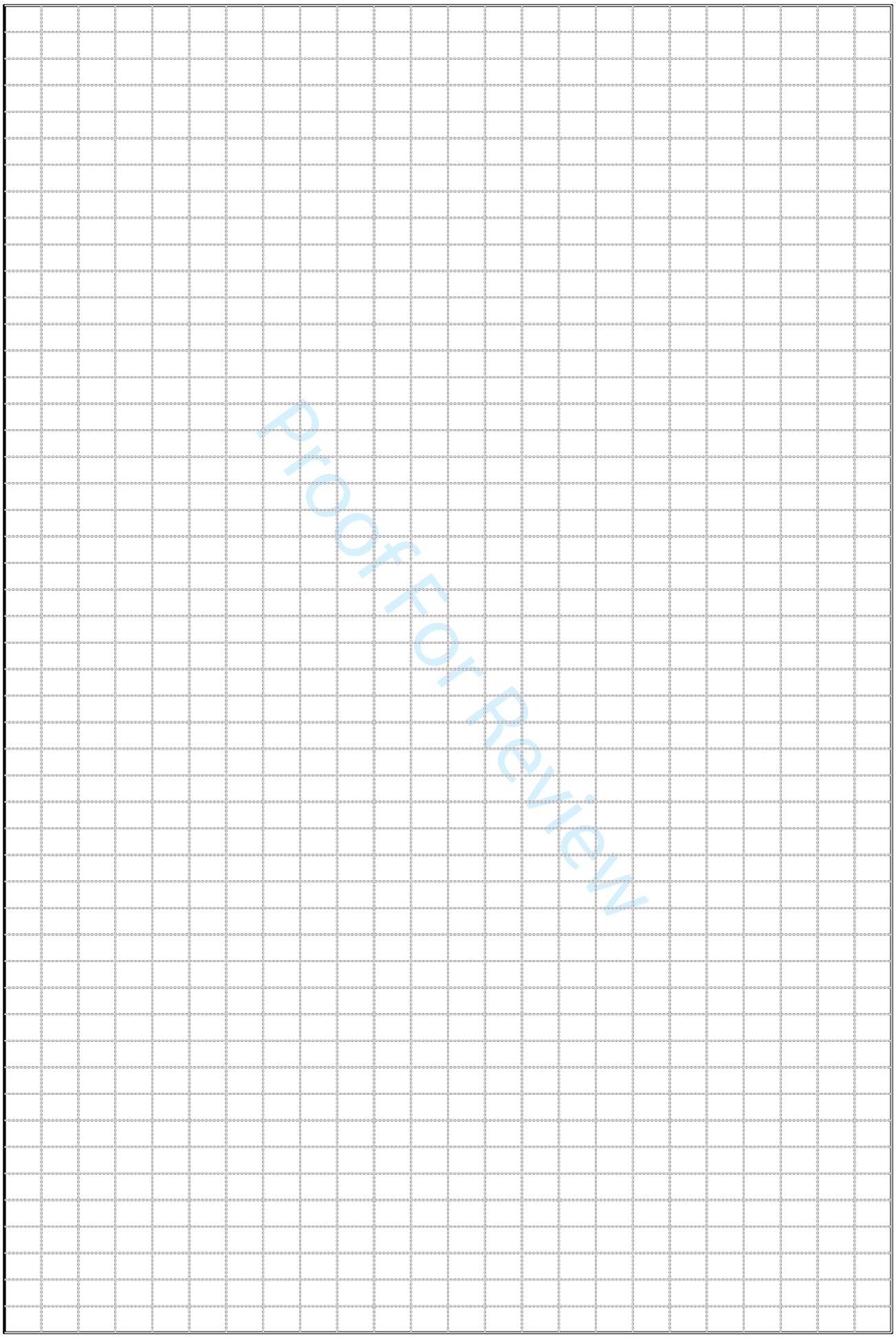
Proof For Review

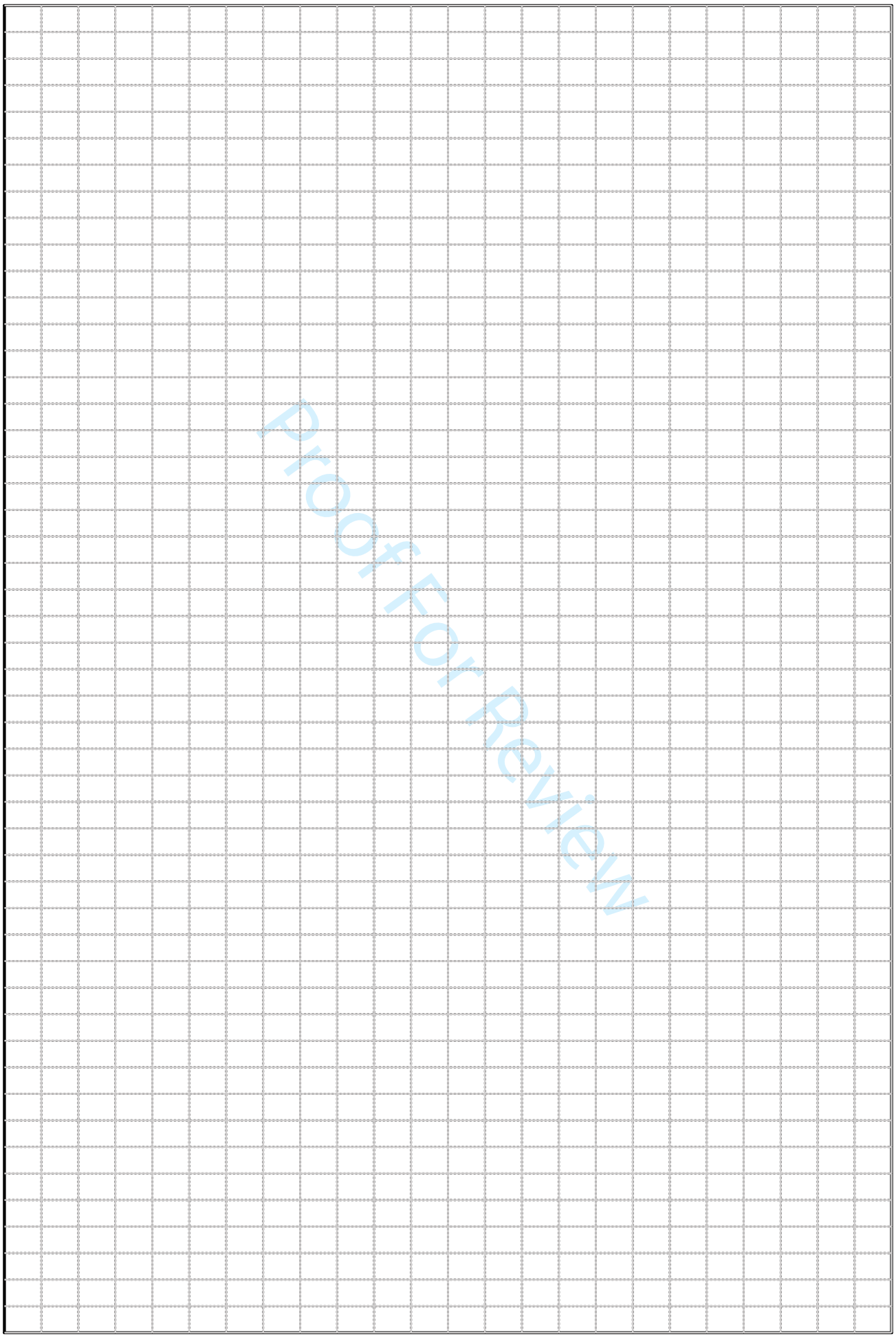

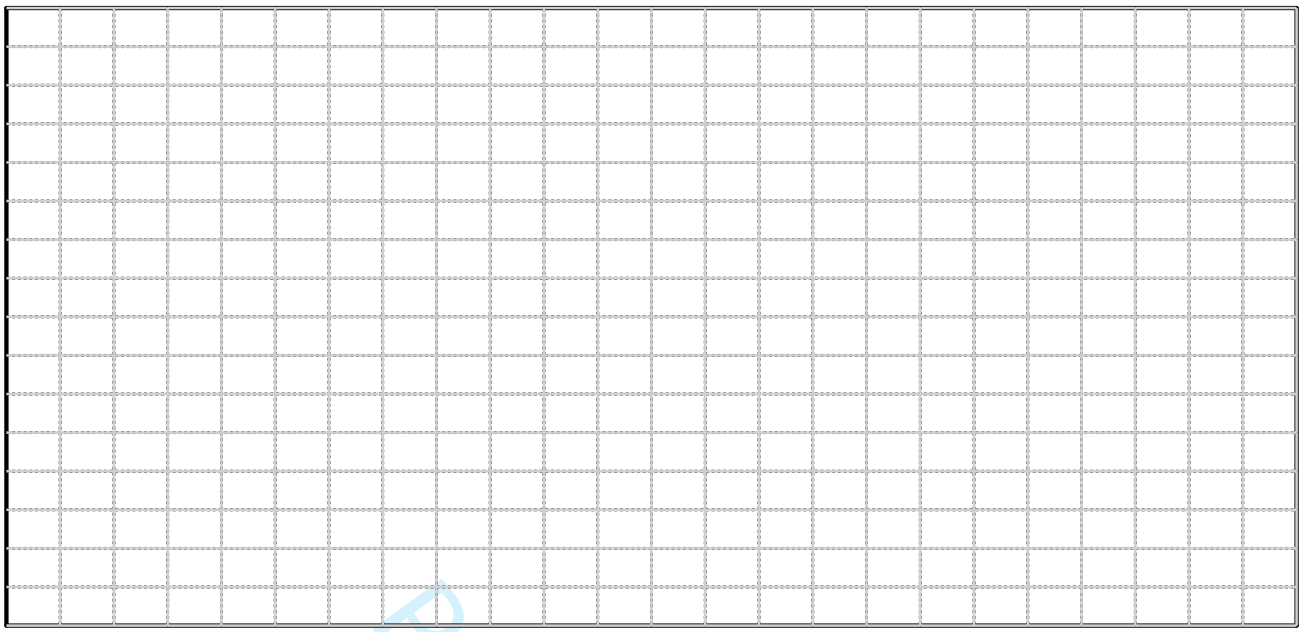

Dictyococcites bisectus	Dictyococcites bisectus (>10µm)	Dictyococcites perplexus	Dictyococcites productus	Discoaster 5-ray	Discoaster adamanteus	Discoaster asymmetricus	Discoaster barbadiensis	Discoaster bergenii	Discoaster berggrenii	Discoaster blackstockae	Discoaster brouweri	Discoaster calcaris	Discoaster deflandrei	Discoaster diastypus	Discoaster lodoensis	Discoaster loeblichii	Discoaster musicus	Discoaster pentaradiatus	Discoaster prepentaradiatus	Discoaster quinqueramus	Discoaster saipanensis	Discoaster surculus	Discoaster tamalis
											A							F					
											R							R					
			F								F							F					
			R								C							C					
			F								F												
			C								A							C				R	
			F								F							R					
			F								C							R					
	*		R				*				R												
			R								R												
*			F				*														*		
			F	R			*				R							R				R	
			R				*				R		*								*		
*			F				*														*		
*			R				*				R		*										
			F				*				R												
*			C											*									
			F																				
			R																				
			F																				
			F								R							R					
*		*	C				*				R												
			R				*																
			R				*				R												
			R				*						*										
			R				*						*					R			*		
			C								F												
			F								C							F				R	
			R	R																			
			R				*																
*			F				*																
			R				*																
*			F																				
			F				*											R					
			F								F							F				R	
*			F																				
			C															R					
			F															R					

			C								R		*		*			R					
			F								F							C				R	
			C								R							C					
			C								R							F					
			C								R							F				R	
			A								R							F					
			C								F							C					
			C								F							C				R	
			A								F							F					
			C				*				F							R					
			C			R					F							F					
											C							C				R	F
	*		C								C		*					F				R	R
	*		C								C											R	
	*		C								C							F				C	
			A								F							F					
			C															F				R	
			C								F							C					
			A								F							C				R	
			C								C							C					
			C								F							F					
			C			R					C							C				R	
						R					C							C		R			
			C								C							C				R	R
			R								C							F				R	
			C								R							R					
			C																				
			F																				
			F																				
			F																				
			F																				
			C								F							R					
			C							R	A							C				R	R
			R						R										R				
			F								R												
			F				*				R		*					R			*	R	
*			F				*						*						R			R	
*			R								R							R					
*			R				*											R		R	*		
			R				*				R									R		R	
		C									R							R		R			
		R	C								R							R		R		R	
*																				R			
											R											R	
	*	R	F				*											R					
		R	F															R					
		R	F								R							R		R		R	
*		F	F								R									R			
		F	F								R							R		R		R	
*		C	F	R							R							R		R			

			F				*				R							R				R	
*		R	F	R																R			
*		F	F	R			*				R									R	*		
		F	F	R			*						*					R			*		
		F	F								R							R		R			
		R	F				*													R	*		
	*		C								F							R				R	
		F	C								R							R		F		F	
*		F	F								R	R						R		R		R	
*		F	C						R		F							F		R		R	
*		R	F																		*		
*			F				*				R									R			
				R							R							R		F		R	
			C						R		F							R		R		R	
		F	C						R		R							R		R	*	R	
*		R	F								R							R		R		R	
*		F	F								R							R					
		F	C	R							R							R		R	*		
*		F	F				*				F							R		R			
		C	C								C							C				R	
		F	A								C							F		F		R	
		F	C						C		C	F	*					C		C		C	
*			A			R			C		C							C		F		F	
		C	C								C							C		F		F	
	*	F	C						R		F							F		R		R	
		C	C				*	R			A		*					A		R		C	
		C	C					R	R		C						*	C		F		F	
		F	C		R				F		F							C		R		F	
		C	C								C		*				*	C				F	
		C	A								C						*	A				C	
		C	C								C						*	C				C	
	*								F		C	F					*	C		R		F	
		C	C								C							C				C	
		C	A								C						*	C		R		F	
		C	A								C							R		R		F	
		C	C			R					C							F				R	
*		C	C								C						*	F		R		C	
		C	C				*	R	R		C						*	C		C		C	
			F								C	F	*					R				F	
		F	C				*		R		C							F		R		C	
		C	A								F		*					R		R		C	
*		F	C							R	C							F				C	
		C	C								C	C								R		C	
		C	C						F		F		*				*	F		C		F	
		F	C						C		C	F						F		C		C	
			R			R			C		F	C						F		C		C	
		C	A								F	F						C		C		C	
		C	C						C		R	F						C		C		F	
	*		C						F		R	R						R		C		F	
		R	C					R	F		R	F						F		F		R	

			A						C		F	F						F		C		C		
			F				*		C			C								C		C		
			A						C		F	C						F		C	*	C		
		C	A						C		F	F						F		C		F		
		C	C				*		A	R	C	F					*	C		A		F		
		C	C				*		C		F	R						C		C		F		
		C	A						A		R	F						C		A		F		
			C					X	C		C	F						F		A		F		
		C	V					R	C	R	R	R					*	F		C		R		
		C	C	R				R	C		F	F						R		A		F		
		C	C					X	C		F	F						R		C		F		
			F						F		C	F						F		A	*	F		
			A				*	X	C		F	F	*					R		C		R		
		C	A					X	F		C	C	*					F		C		C		
		C	C					F	A	R	R	R						F		C		F		
		C	V						C		F	R						F		C		R		
		C	A	R				R	C		C	C						F		C		C		
*	*		F								R									R				
*			F	R			*				R													
*		R	F																	R				
*		R	F						R		R							R		R		R		
*			F				*											R		R				
*		F	C						R		F							R		F		R		
			F				*	R	R		R									R		R		
			C						A		C	R						F		C		F		
	*	F	C						F		F	F						F		C		F		
		C	C	R				R	C		C							F		C		F		
		C	A					R	C		F	F						F		C		F		
			A					F	A		C	F						C		C		C		
			C					F	A		C	F						F		C		F		
		C	C					F	C		F	F						F		C		F		
				R				R	C		C	C						F		F		C		
		C	C	R				R	C		C	C						R		C		C		
			C	R					C		A	C						C		C	*	C		
			C					R	F		F	R					F	R				F		
		C	A						C		C	R						R		C		R		
		C	A						C		C							F		C		F		
		C	A						C		C	R						R		F				
*		C	C	F					R		C	F				R		R	*	R				
*		F	C	R			*		F		F	F	*					R		F				
			C								R	R								R				
	*		F										*											
			C				*				R													
		R	F		R																			
			F																					
*		F	C																					
	*		C										*											
		R	F								R													
			C				*		R		R												R	
			F																	R				

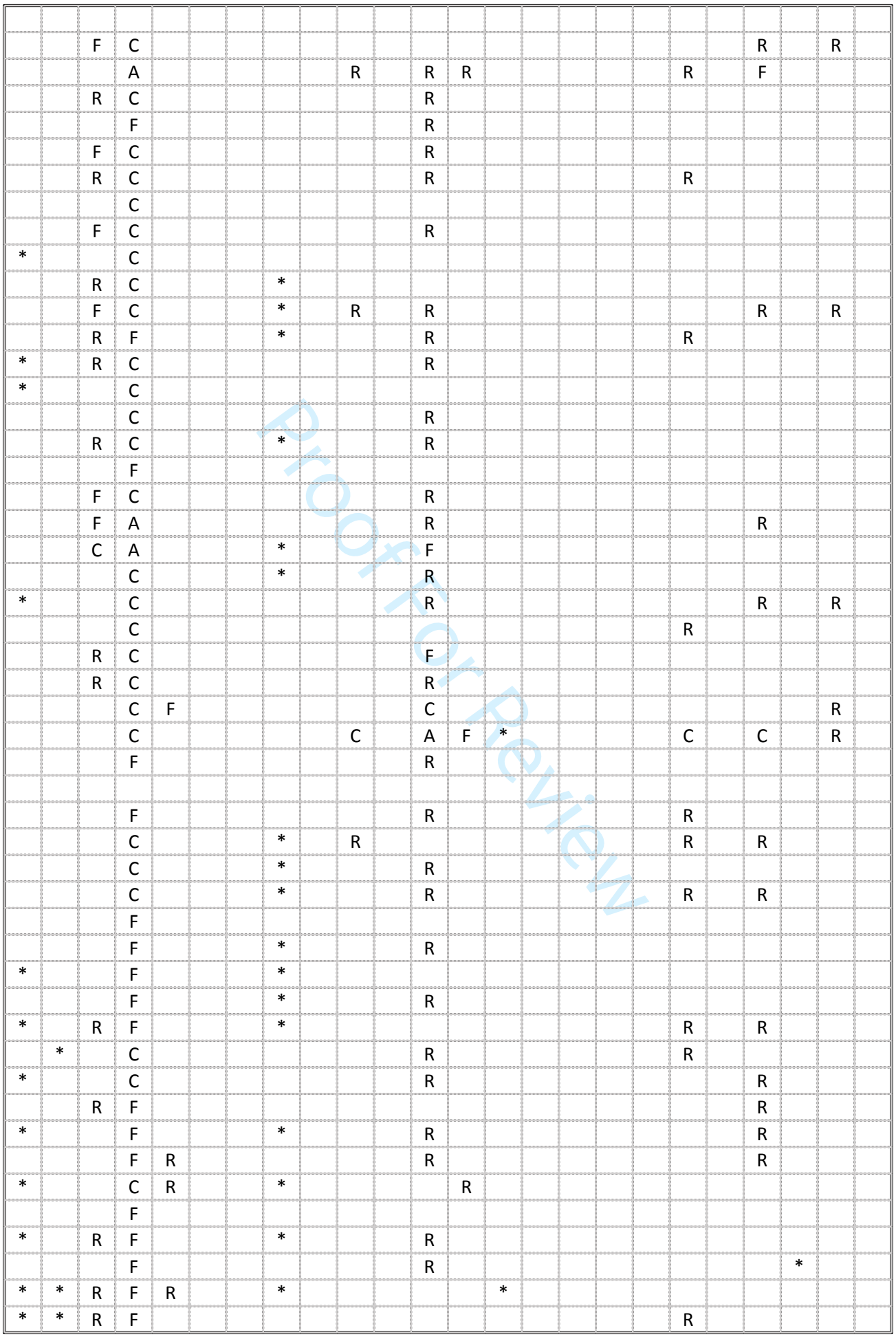

*			F				*																
			F								R												
		R	F																				
*		R	F				*				R		*										
*			F								R									R			
*		R	F				*																
		R	F																				
			F	R							R							R		R			
			R																		*		
			F				*				R							R					
		R	F																				
			F																				
	*	R	F																		*		
			F															R					
		R	F				*														*		
*			F																				
		R	F																				
			F																				
			F								R												
*		R	F																				
	*		F																				
			R				*													R			
			C															R		R			
		R	F				*						*								*		
			F				*				R												
		R	F				*				R									R			
			F										*										
*			F				*				R									R	*		
*																							
			R				*				R												
			C				*				R									R			
*			F																				
			F																				
			F										*										
			F								R		*										
			F				*													R			
			F				*													R			

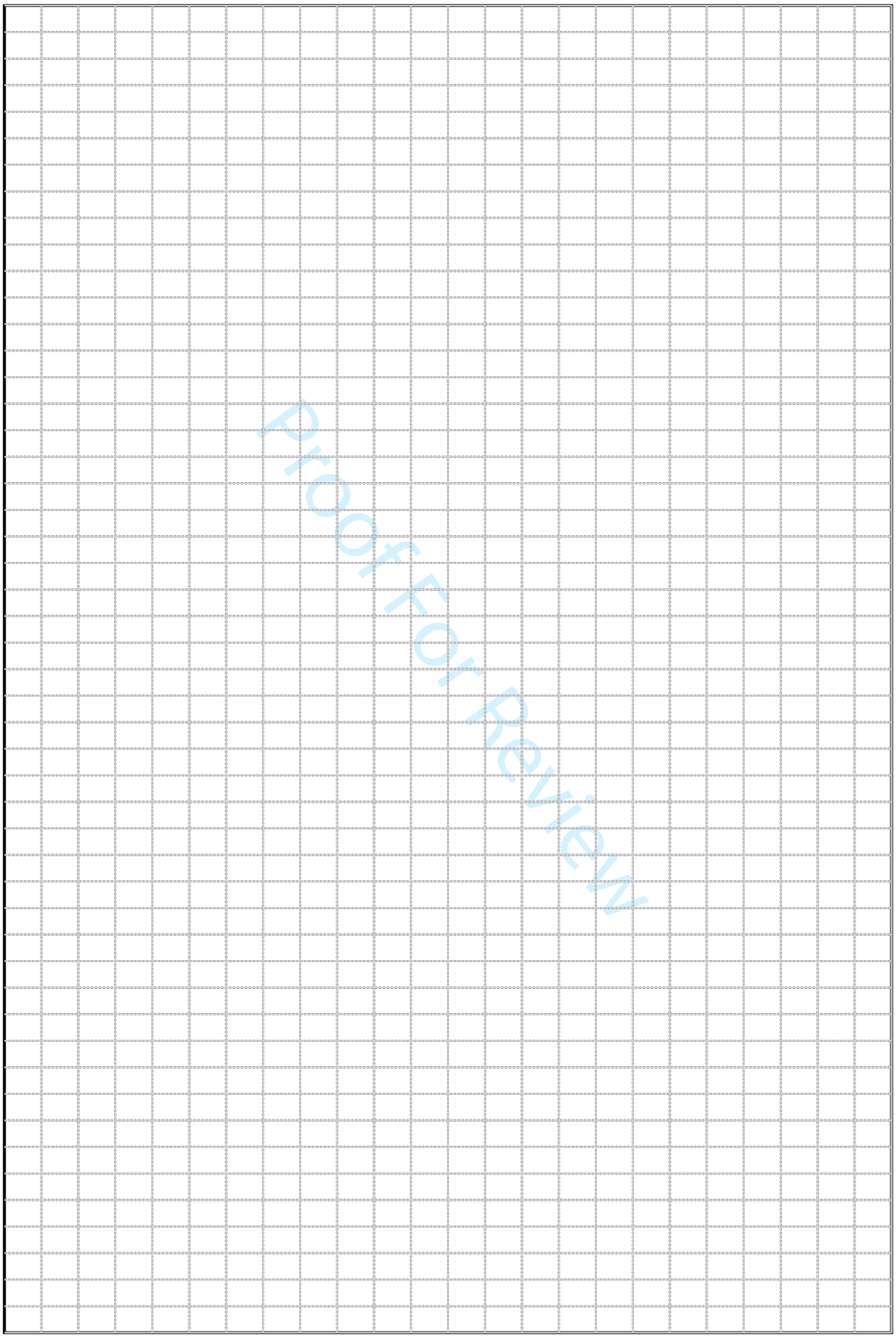
Proof For Review

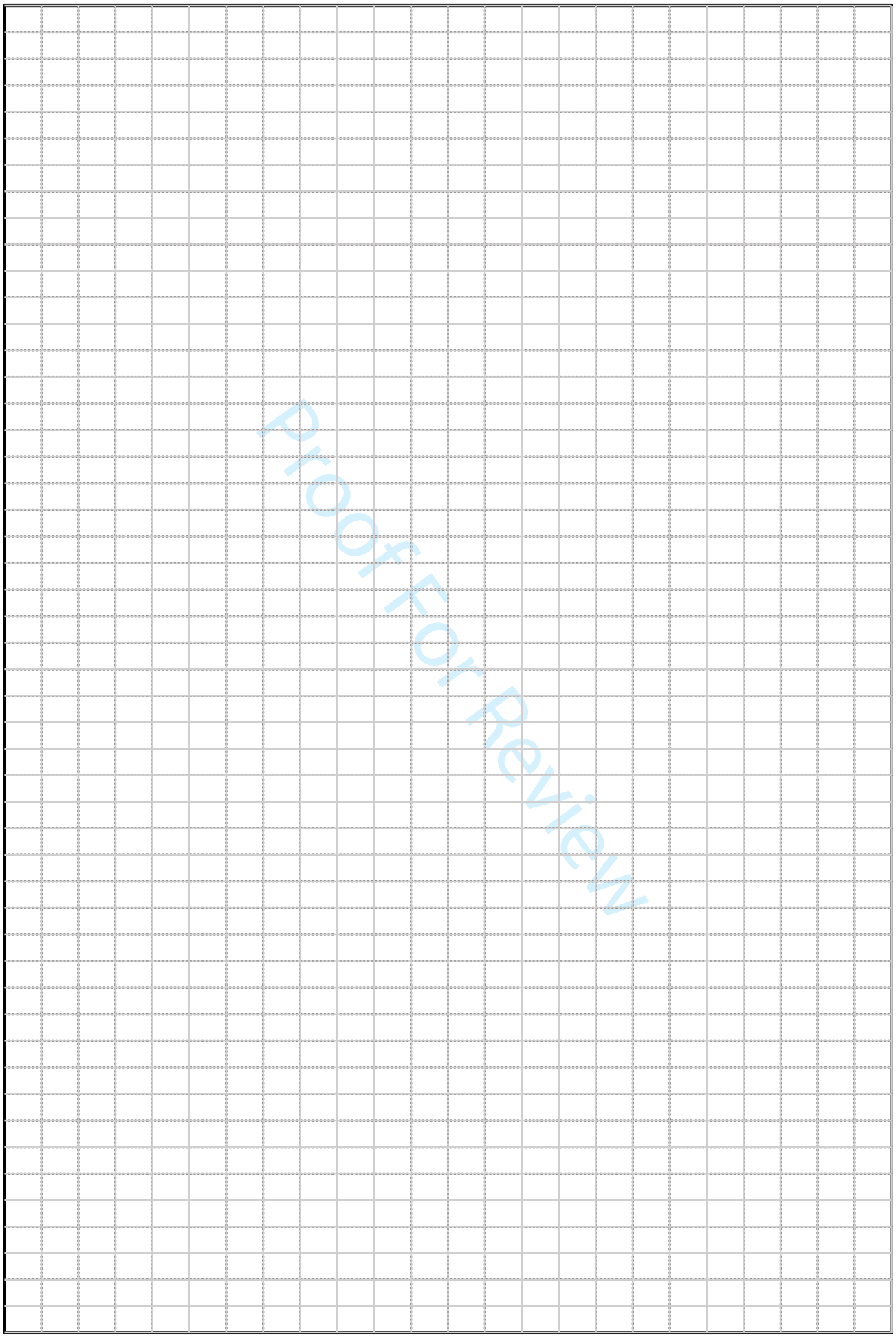
Proof For Review

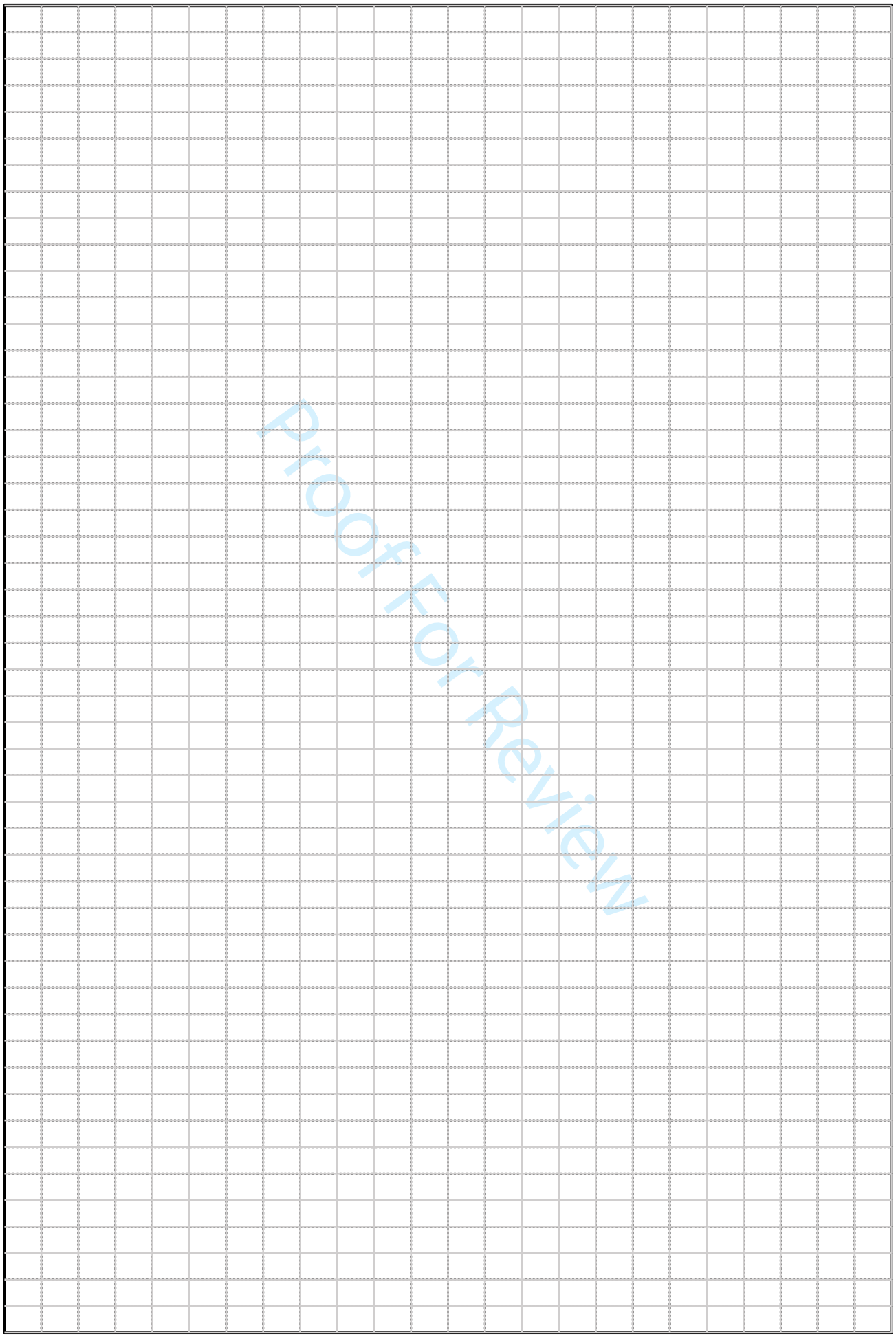
Proof For Review

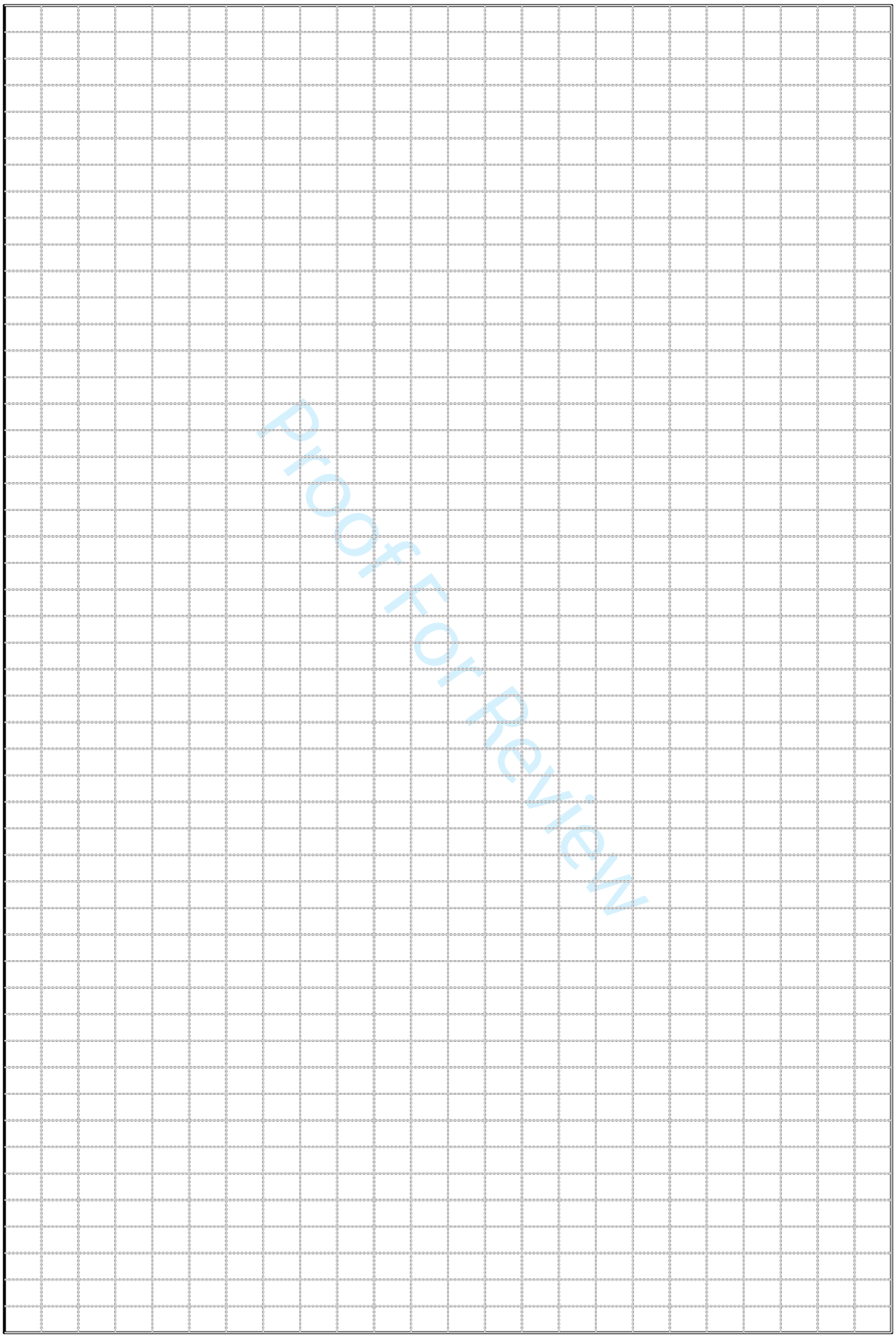
Proof For Review

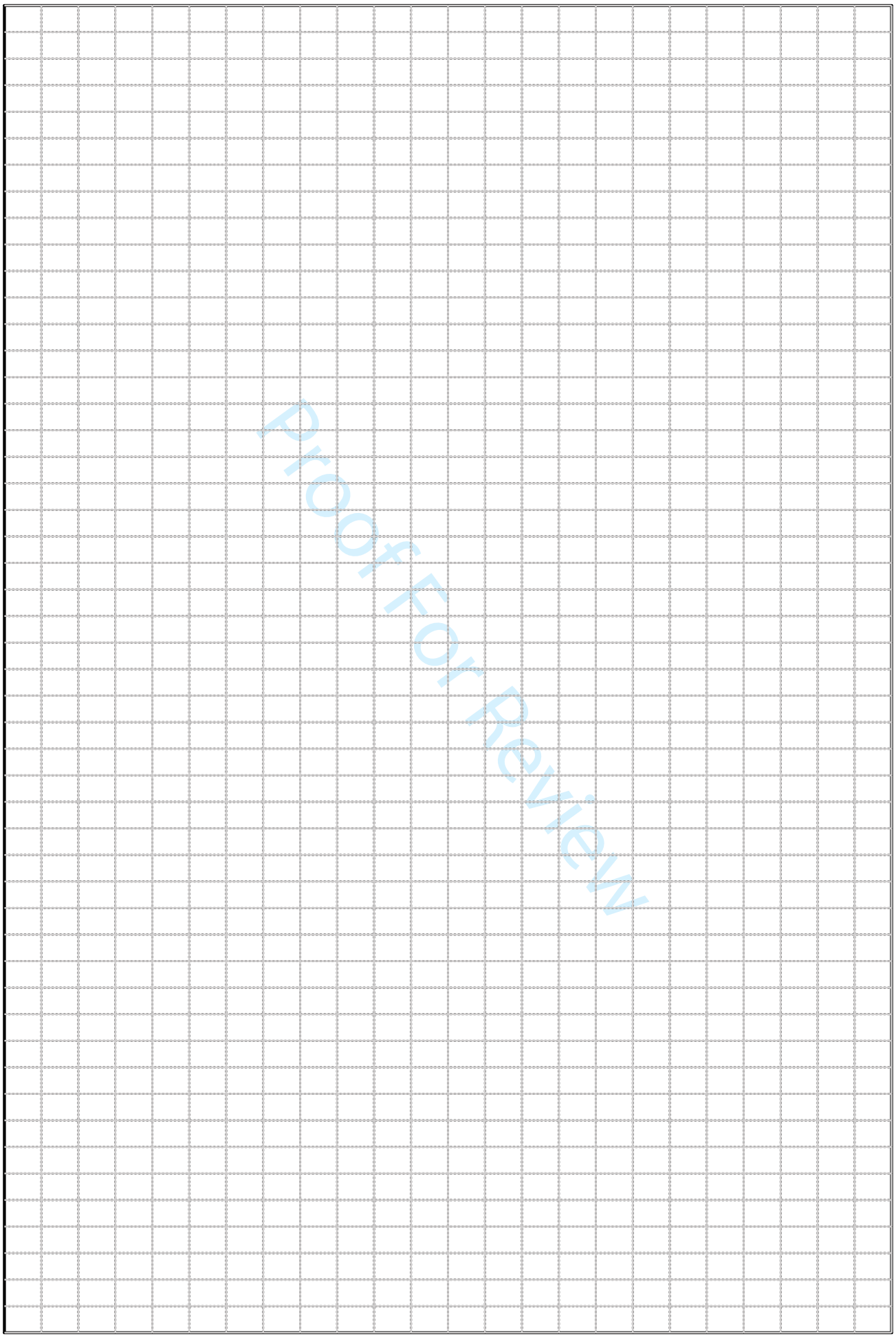
Proof For Review

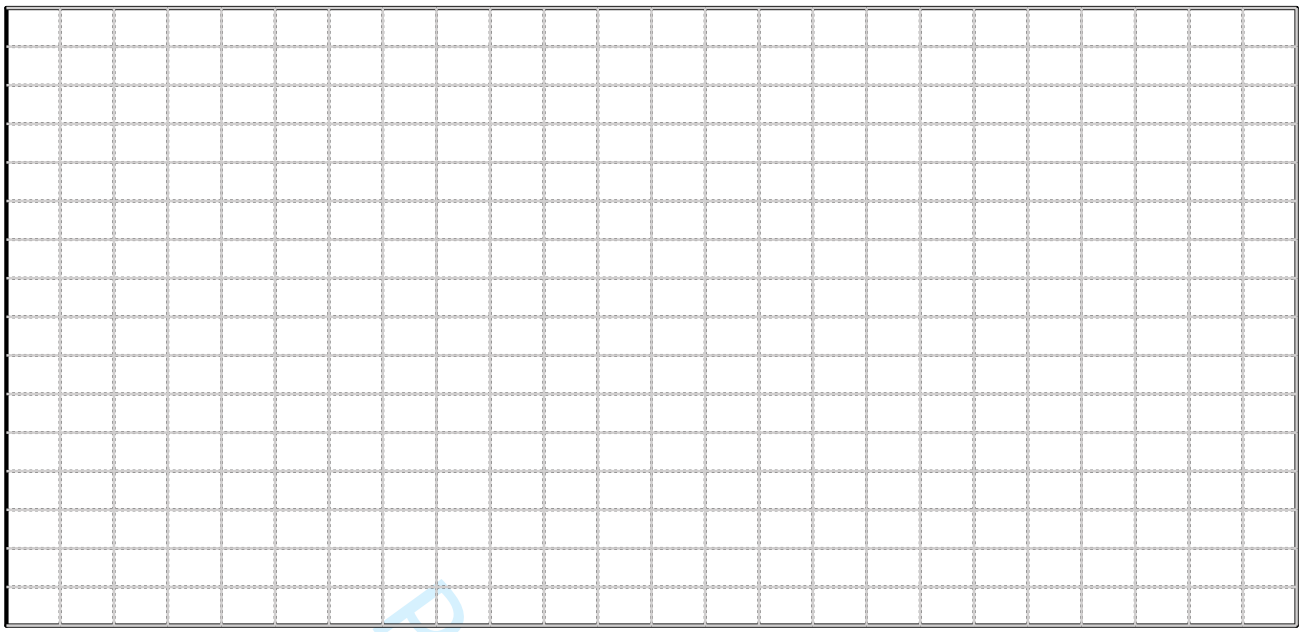

Discoaster tanii	Discoaster triradiatus	Discoaster variabilis	Discoaster wemmelensis	Fasciculithus spp.	Florisphaera profunda	Gephyrocapsa caribbeanica (3-4)	Gephyrocapsa oceanica (3-4)	Gephyrocapsa spp. (<3)	Helicosphaera bramlettei	Helicosphaera carteri	Helicosphaera euphratis	Helicosphaera granulata	Helicosphaera intermedia	Helicosphaera lophota	Helicosphaera orientalis	Helicosphaera sellii	Helicosphaera stalis	Nicklithus amplificus	Pontosphaera discopora	Pontosphaera enormis	Pontosphaera exilis	Pontosphaera japonica	Pontosphaera multipora
	R									C						F							
										C						F			R			R	
										C						R			R			R	R
	R									C						R			R			R	R
										F						F			R			R	
	R									R						R						R	
										C						F			R			R	
										R						R							
									*										R			R	
				*					*														
										R												R	
										R	*		*			R			R				
										R			*									R	
										R						R			R			R	
										F						R			R				
													*								*	R	
*	R									R						R						R	
										R			*			R			R				
	R									R												R	
										R						R			R			R	
							R		*	R									R			R	
				*						R													
										R									R				
													*	*		R			R			R	
										R													
										F						F							
		*								R	*			*					R		*		
										R			*						R				
*	R									R						R						R	
										R												R	
										F						R						R	
										F						F						R	
										R													
										F						R							
										F						R							

		*								F						R			R				
										R													
		*								F						R			R			R	
										C						F			F			F	
										F						R			F			F	
										F						F						F	
										F						F			R			R	
	R	F								C						F			F			F	
	R	R								C						C			R			F	R
										C						C			F			F	
										C						C			F			F	
	R	F					R			C		F											
		F								C						F			F				R
		F								C						F			F			F	R
	R	F								F			*						F				
		F								F						F						R	
		R								F						F			R				
		F								F						F							
	R	F						C		C						C							
		F								R			*			F							
		R								F						F			R				
		R								F													
	R	R			C			F		C													
	R	F								C						F							
		F								F						F			F			F	R
							R			F													
										R													
																			R				
																						R	
																						R	
										F						R							
		R								F			*			R							
	R	C								F						R							
													R			R							
										R												R	
		R								R													
										F						R			R			F	
										R												R	
										R													
										R													
	R									R													
	R									R									R				
										R	*		R										
		R								R													
										R					R								
										R													
										R												R	
		R																					
										F													
		R								F													

	R							R								R						R	
										R													
								R		R												*		
										R		*	R											
		R								R							R							
		R								F			R				R					*		
										F						R						R		
		R								R														
	R									F														
										F												R		
										R														
										F				*					R					
	R	R								R							R		R					
		R								F										*			R	
										R														
										R														
		R								R														
	R									F							F							
	R	F								C							F		R					
		R								C	*					F								
	F	R								F													R	
	F	F								F														
	R	F								C							R	R						
		R							*	F						F			R					
	R	F								C									R					
	R	F								F													R	
										R													R	
	F	F																						
	R	F								R														
	R	R								F														
	R									R						R							R	
	F	R								F														
	R	F								R														
	R	R								R								R						
		R																						
	R	F								R														
	R	F								F														
	R									F								R						
	R	F								F														
	F	F								F													R	
	R	F								F				R										
	F	R																R						
	R	R								F									R					
	F		*							F														
	F	F								R														
	F	F								F														
	R	F								R														
		R								F									R				R	
										C									R				R	

	F	F								R													
	F	F																					
	R									R			R										
	R									R													
	F	F								R													
	F																						
	F									R													
	F	R																					
	R	R								R													
	R	R								R													
	R	R								R													
	R	F								F													
	R	R								F													
	R	F								R													
	F	R								R													
	R	F								R													
	R	R								R													
										R													
										R			R				R						
										R			R										
										R			R		R								
		R								R			R		R		R						
										R													
	F	R																					
	R									F													
	R	R								C													R
	R									F													
	R									R													
	R	R								F			R										
	R									R													
	R	R								F													
	R	R								F			R										
	R	F								C			R										
		F			F					R													
	R	F								F													R
	R	R								F													R
	R									F			R										R
	R	F								C									R				R
		F								C													C
										C					R								R
										R													
																	R						
										R				*									
										F				*	R								
										F			R	*									
										R			R		R								
										R				*	R								

										R													
										F									R				
										F									R				
										R													
										F			R						R				
										R													
										R													
										R			R										
										R													
										R													
										F			F			R							
										R													
										R												R	
										F						F							
										R													
										R			R										
										R													
										R													
										F													R
		F								C			F										R
										F													
										R													
										R	*												R
										F													
										R													R
	R									R													
	F	F								F						F							
										R					R								
										F													
										R	*		R										
										R													
										R									R				
													R										
										R													
										R					R								
										R													
										F			R										
										R	*		R										
										R													
										R													R
										R													
		R								R	*										*		
										R													
													R										R
										R									R				
										R									R				
										R									R				

										R													
										R													
										R													
										R													
										F									R				
										R	*								R				
										R	*												
													R										
										R													
										R													
										R			R										
										R													
		R								R													
										R													
										R			R										
	R									R													
										R	*		R										
										R													
										R			R										
										R													
										R			R										
											*												
										R			R										
										R													
										R			R										
										R											*		
										R			R										
		R								R													
										R													
																			R				
										R			R										
										R											*		

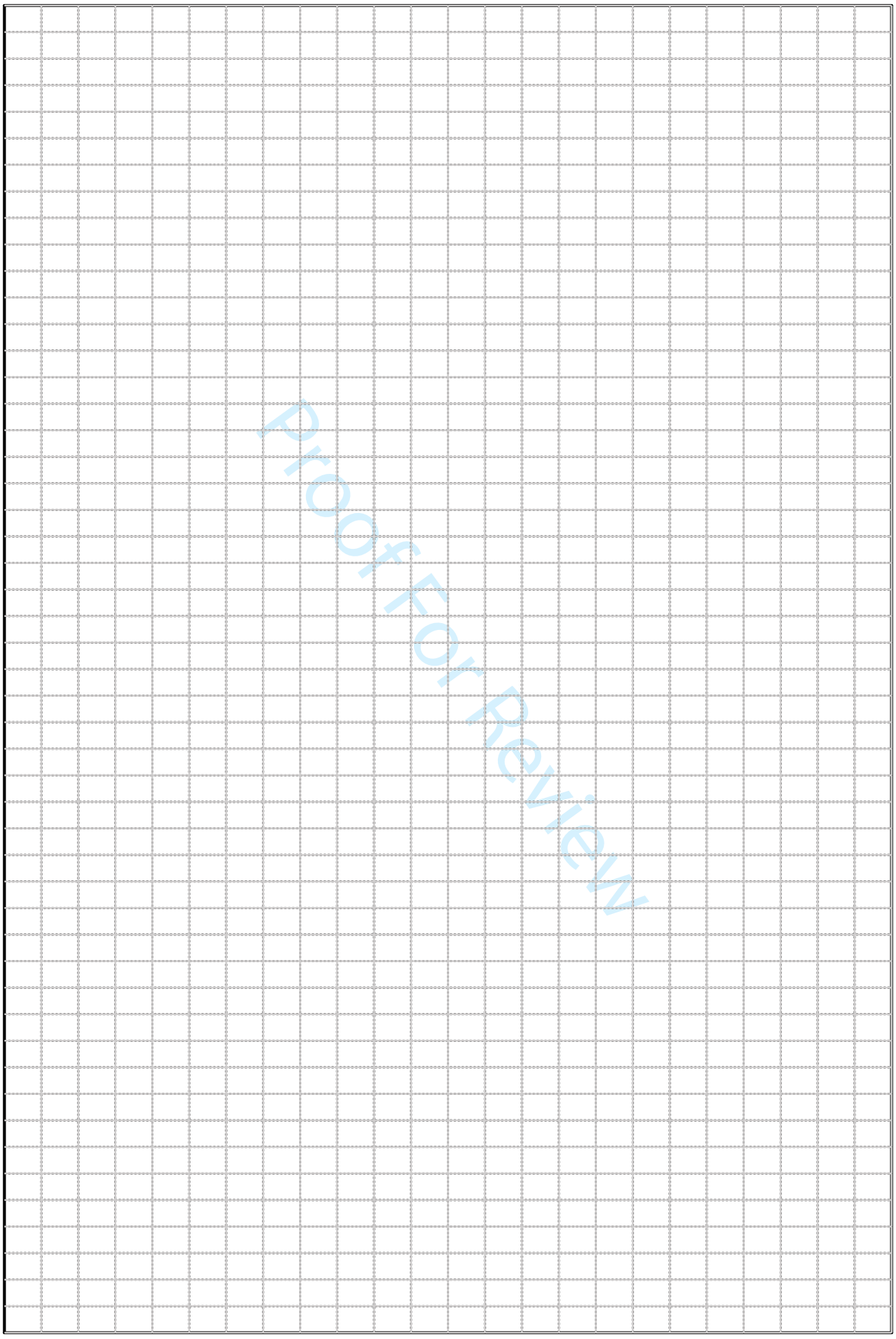
Proof For Review

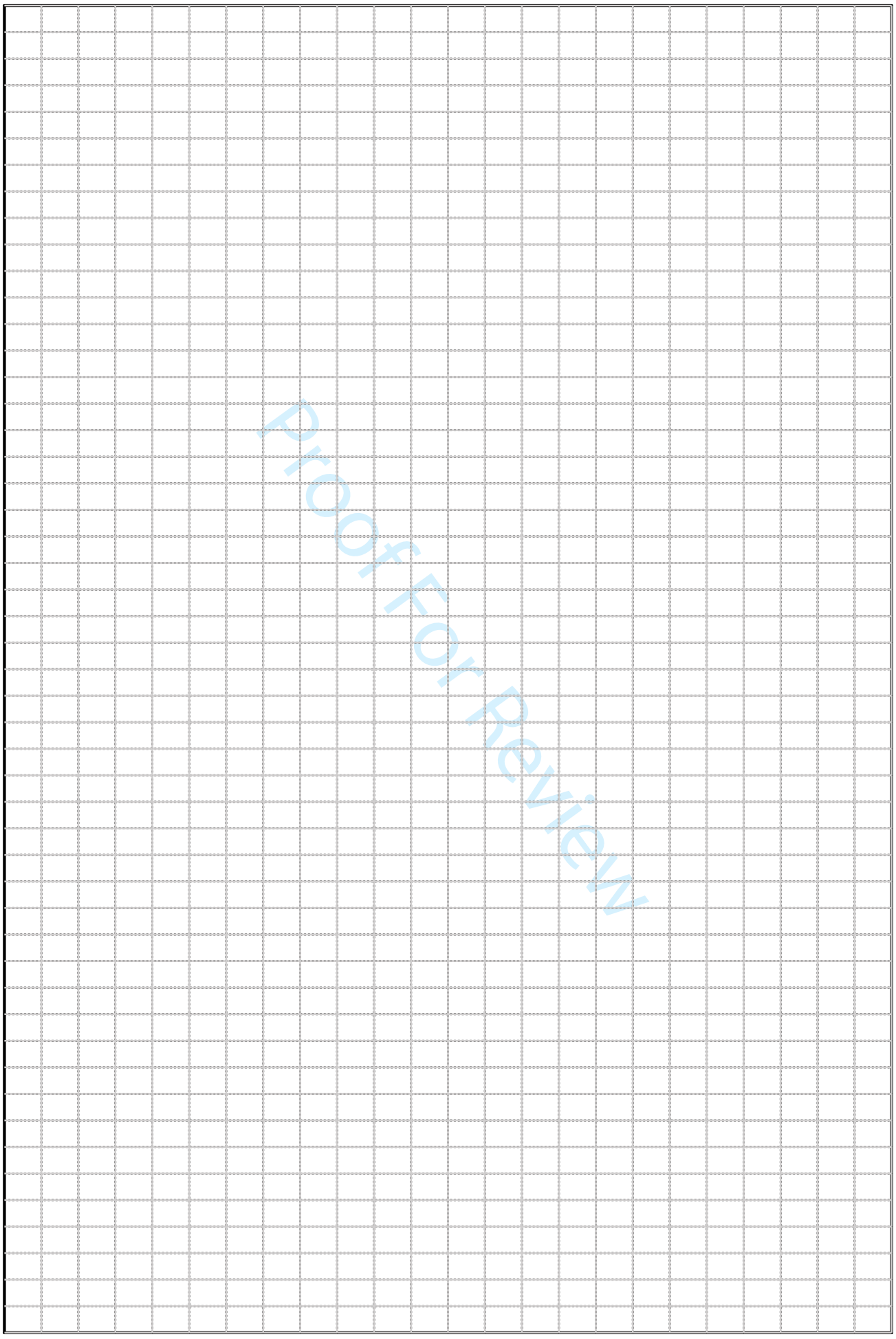
Proof For Review

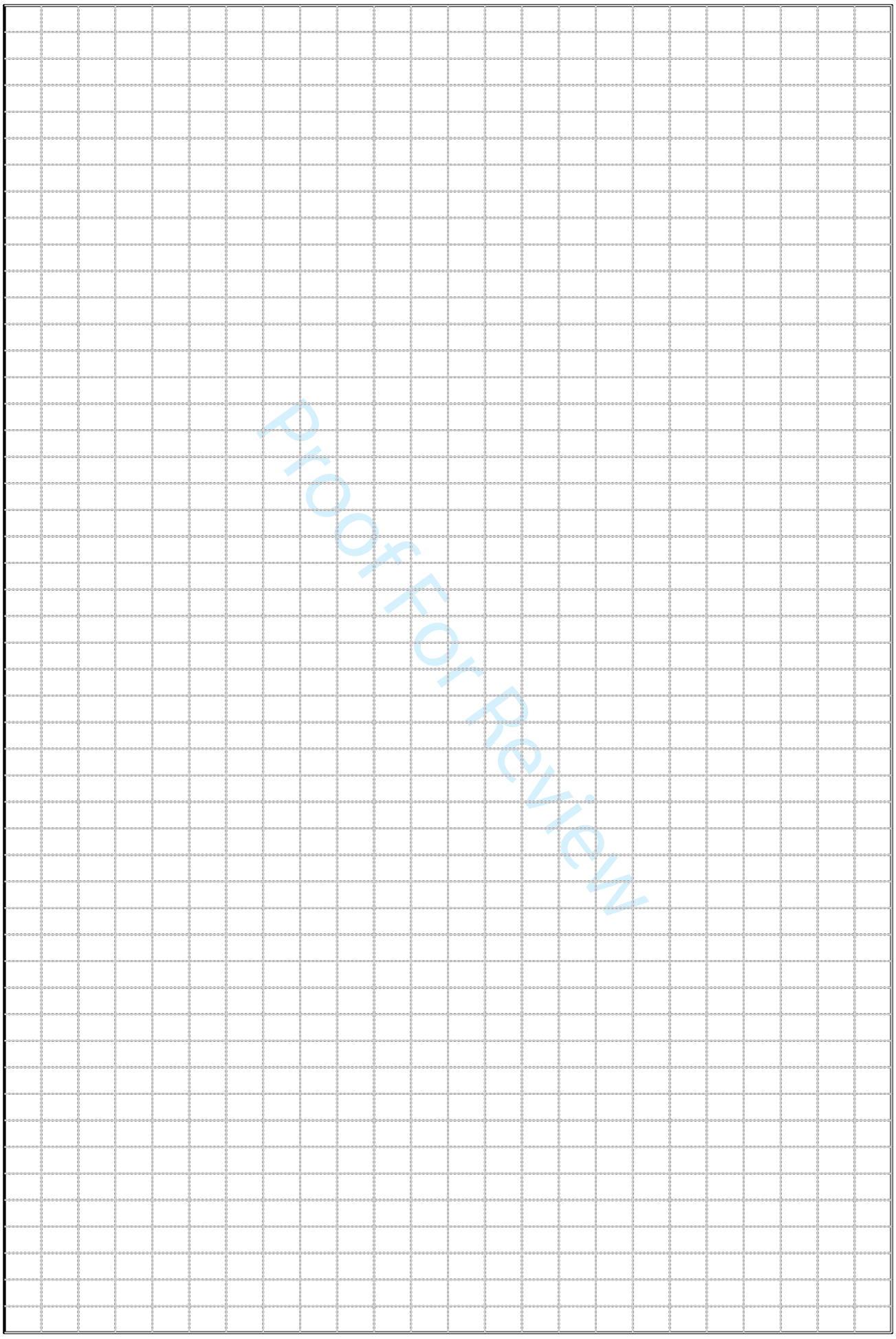
Proof For Review

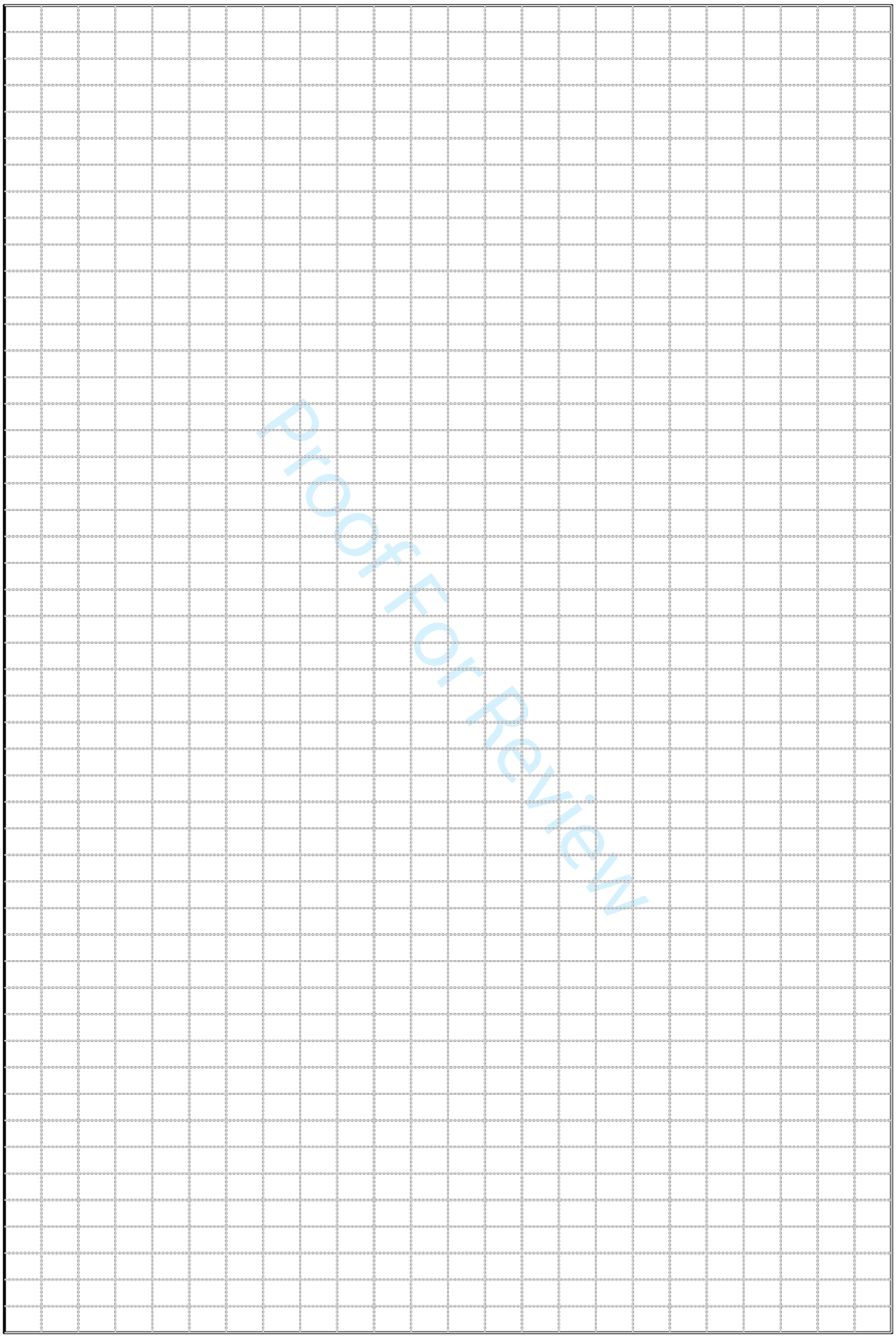
Proof For Review

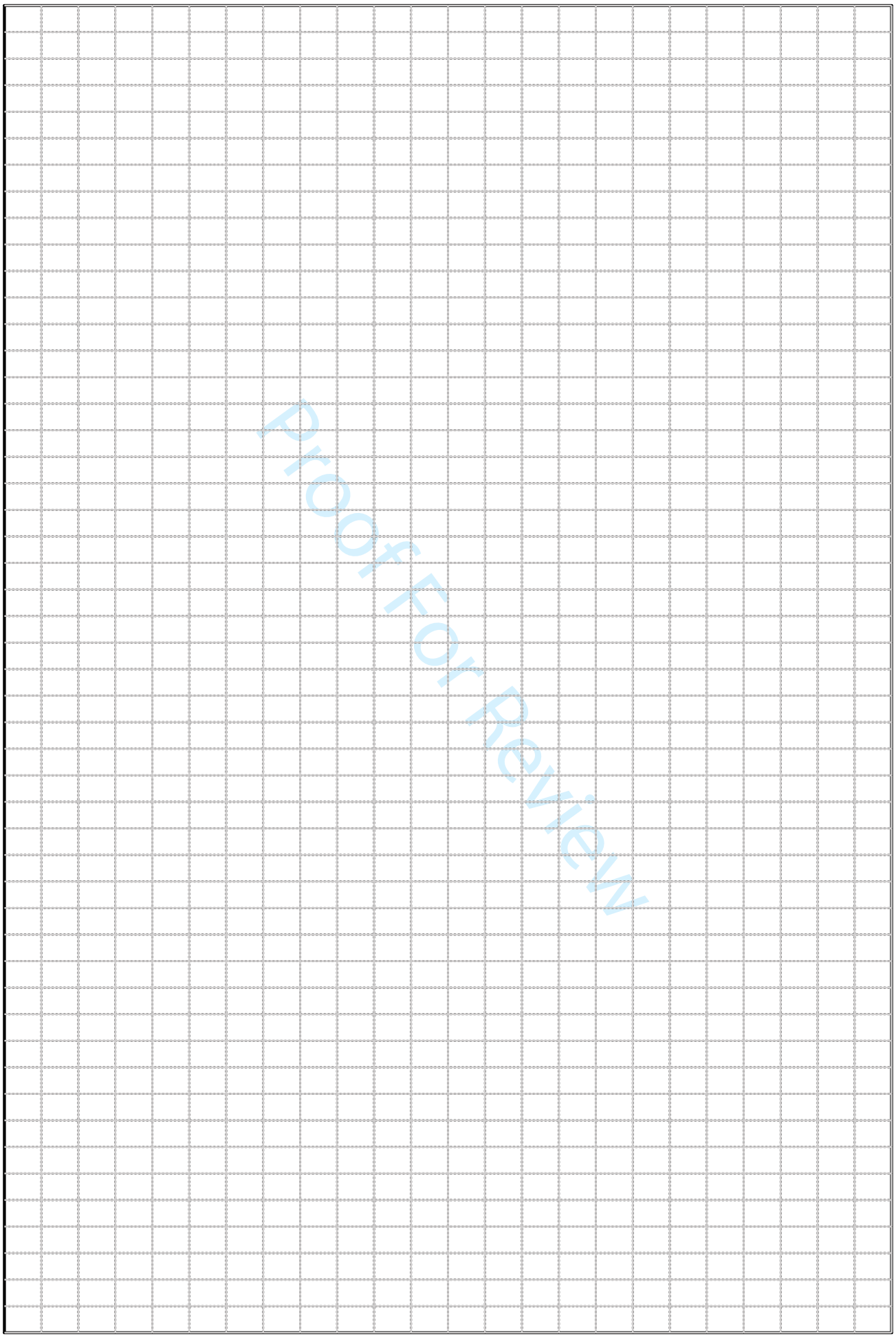
Proof For Review

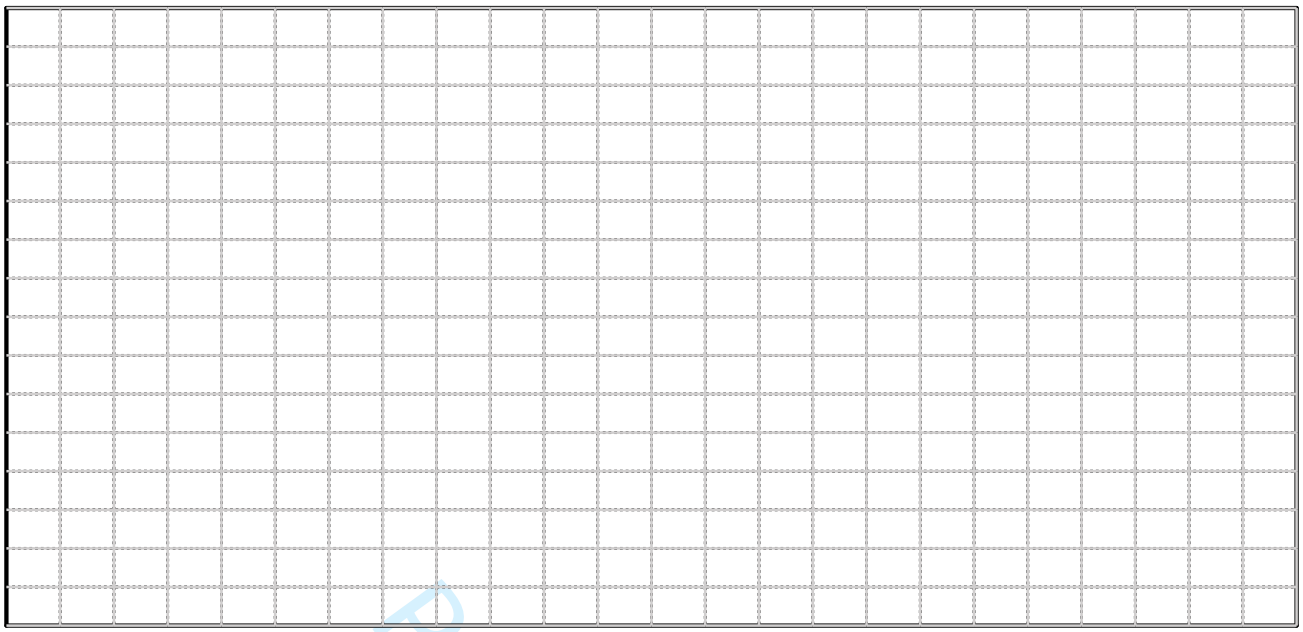

Pontosphaera spp.	Prinsius bisulcus	Prinsius martinii	Pseudoemiliania lacunosa	Pseudoemiliania ovata	Reticulofenestra daviesii	Reticulofenestra erbae	Reticulofenestra gelida	Reticulofenestra haqii	Reticulofenestra haqii (<3)	Reticulofenestra lockeri	Reticulofenestra minuta	Reticulofenestra minutula	Reticulofenestra pseudoumbi (>7)	Reticulofenestra pseudoumbil (5-	Reticulofenestra reticulata	Reticulofenestra rotaria	Reticulofenestra umbilicus (>14)	Rhabdosphaera spp.	Scyphosphaera spp.	Sphenolithus abies	Sphenolithus ciperoensis	Sphenolithus conicus	Sphenolithus disbelemnos
			C	C				A	C		F	C											
			C	C				C	C		C	C						R					
			F	C				C	C		C	R											
			F	F				C	A		C	C		*				R					
				F				C	C		F	C											
			R	F				V	V		V	A							R				
								C	A		A	C								*			
			R	R				C	C		C	F		*									
		*						F	F		R			*									
						*		R	R		R												
								F	F	*	F	F											
								F	C		F	R	*										
								F	C		F	R								*			
				R		*		R	C		C												
								F	F		F	R		*			*						
						*		F	C		F									*			
	*	*						C	F		F	F			*								
								F	R		F	R			*								
								F	C		F	R											
								C	C		F	F		*						*			
								F	C		F	F											
								C	C		F	F		*	*								
								R	F		R										*			
								F	F		R	R											
				R				F	F		F	R		*									
								R	F		F				*								
								C	R			F		*									
				C				V				A		*									
								R	F		F	R									*			
								R	R		R	R												
						*		F	F		R	F		*									
								F	F		R	R												
						*		F	C		F	F												
			F	R				F	C		F	R												
			F	F				C	C		C	F												
								F	F		R	F		*	*	*								
			R					F	C		F				*									
			R						C		F	F									*			

			F	F				C	A		C	F			*								
			F	R				F	C		F											
			F	C				C	A		C	F											
			C	C				C	A		A	F			*			R					
			F	C				C	A		C	C											
			F	C				C	A		A	F											
			F	F		*		A	A		C	C		*	*								
			F	C				A	A		A	F		R					R	F			
			F	F				C	A		C	C		R						F			
			C	F				C	A		A	C		F						F			
			F	C				A	A		A	C		F						C			
				C				C	A		C	A		F						C			
			C	C				A	V		A	C		C				R		A			
			F	F				C	A		A	C		C						A			
				F				C	A		C	C		F						C			
			C	C				C	A		C	C		F						C			
			R	F				C	C		C	F		F						C			
			F	C				C	A		A	F		R						A			
			C	C				A	A		C	C								C			
			F	F				A	A		A	C								C			
			F	F				C	A		C	C		R						C			
			F					A	V		A	C					*			A			
R				C				C			A	A		F						C			
			F	F				C	A		C	F		R						C			
			R	R				A	A		A	C	R	F						A			
				R				A	C		C	C		F	*					F			
			R	R				F	C		F	F		R						F			
								F	C		F			R						F			
			R					F	C											F			
			R	R				F	C		F			R						R			
				F				C	C		C				*					F			
			R	F				C	A		A	C		F						C			
								A	V		V	F		C						A			
								F	C		F	C	R	F						F			
								F	C		F			R						F			
								F	F		R			R						F			
								F	C		F			C						F			
								F	C		F	R		F	*					F			
			R					C	C		F			F						F			
								F	F			R	F	F	*			R		C			
					*			C	C		F	C	R	F						C			
								C	C		C	F		F						F			
	*							F						R						F			
								F	F			R		F						R			
			R	R			F	C	C		F	F	R	F						C			
	*				*			F	C		C	C		F						F			
								F	C		F		R	F						F			
	*							C	C		C	C		R						C			
								C	C		A	F		F						F			
					*			C	A		A		R	F						C			

	*	*		R			F	C	C		C	F	R	F				R		C			
								C	C		C			F						F			
								C	C	*	C	F		R						C			
								C	C	*	C			F						C			
	*							C	C		C	F		R						C			
					*			C	C		C	F		R		R				F			
							F	A	A		A	C	C	F						A			
					*			C	A		F	F		C		R				C			
								C	C		C		R	F		R				C			
							F	A	C		A	C	F	F						C			
								F	F		F			F						C			
								C	C		C		R	F						F			
								C	C		C		R	F		R				C			
		*					F	C	C		C	C	F	C	*					C			
								C	A		C			R						C			
								C	C		C	F		R						C			
								C	A		C	F	R	F		R				C			
					*			C	C		F	F	R	R						F			
								C	A		C	C	R	C		R				C			
					*		R	A	A		A	C	R	F						A			
								A	V		V	A	R	C						A			
							C	A	C			C	C	A						A			
							C	A	A		V	A	C	A		*				C			
								A	V		V	A	F	A						A			
							F	C	A		A	C	C	C						A			
							F	A	V		A	C		A		R				C			
								V	V		V	A		C						C			
							F	C	V		A	C	F	C						C			
								A	V		V	C		C						C			
							F	A	V		A	C	R	C						A			
							F	A	V		V	A	R	C						A			
							C	C	C			V	A	A						A			
							C	A	V		V	A		C						C			
								A	V		V	A		C				R		A			
							F	A	V		A	A		C						A			
							F	F			C	F	F	C						C			
							F	V	V		V	A								A			
							F	A	A		C	C	F	C						A			
							R	A	F			C	F	A						A			
								A	V		A	C	R	F						C			
								V	V		V	A		C						A			
								A	V		A	C		C						A			
							R	C				C	R	A						A			
							R	A	A		A	C	R	F						A			
							F	A				F	C	V						A			
							F	C				F	F	C						A			*
							C	A	V		V	A	F	C						A			
							F	A	A		A	C	F	C						A			
								C	C		F	F		F						C			
								C	A		C	C	R	F						A			

							R	A	A		A	C	F	F						A			
							F	C				A	C	C						A			
							R	A	V		V	C	C	C						A			
							F	A	V		V	A	F	C						A			
							F	A	A		C	A	F	C						A			
							C	A	A		A	F	F	C						A			
							C	A	V		A	A	F	C						V			
							F	C	A		A	C	F	F						C			
							F	A	V		V	A		F						C			
							F	C	V		A	C	R	C						A			
							C	A	V		V	C	F	C						A			
							C	F	A		A	A	C	F						A			
								V	V		V	A		R						A			
								A	V		V	C		R						A			
								A	A		A	C		R						C			
								A	V		V	A		F						A			
								V	V		V	A		C						C			
	*							F	F		F									R			
R								F	F		F	R		R						R			
								F	C		F	F		R						F			
								C	C		C	F		R						C			
		*						F	C		C	F				R				C			
							R	C	C		C	F		R	*					C			
					*			F	F		C	F		R						F			
								A	A		C	C		F						A			
								A	V		V	C		C						A			
								A	V		V	A		R						A			
								A	V		A	A		R						A			
								A	V		A	A								A			
R								A	V		A	A								A			
							F	A	V		V	C		F						A			
								A	V		V	A								A			
							R	A	V		A	A		R						A			
								A	V		A									A			
								A	C			C		F						C			
								A	A		A	C		R						A			
								V	V		V	A		R						A			
								V	V		V	C		R						C			
							C	A	V		A	A	F	C						A			
								C	A		C	C		R						C			
							R	C	A		C	C		R						C	*		
		*						F	C		F	F		R						F			
R								F	C		F			R		R				R			
						*		C	C	*	F	F								F			
								F	F		F		R	R						R			
								F	C		C	R		R									
R									C		C									R			
								F	F		F									R			
		*						C	C		F	F											
								F	C		F									R			

									C		C							R				
								F	A		A							C				
								C	C		R	F		R				F				
								F	C		C	F		R				F				
								F	C		C	F						R				
								C	C		C	F		R				R				
								F	C		C							R				
								C	C		F	F		R				F				
								F	C		C											
								F	C		C	F		R				R				
		*						C	A		C	C		R				C				
								R	C		C			R				R				
								F	C		C	R		R				R				
								C	C		F	C										
								F	C		C							R				
								F	C		C							F				
									F		F											
								F	C		C	R										
								C	A		A	C		R				F				
								V	V		C	C						C				
									C		F			R				R				
								F	C		C	F		R				R				
									C		F											
								F	C		C			R				F				
								F	C	*	F			R				R				
								F	A		F			R								
							R	C	C			F		R				C				
								F	C		F			R				F				
									R			R										
R								F	F		F		R					R				
R								R	C		C			R				F				
								F	F		F			R				F				
								F	C		F			R				C				
								R	F		R							R				
									F		F			R				R				
		*						R	C		F			R				F				
								R	F		R	R					R	F				
								R	F		F							R				
								F	C		F							F		*		
R								R	C		F			R				F				
R								R	F		F			R				F				
								F	F		R	R						R				
R									F		F			R				R				
								R	C		F			R				F				
R								R	F		F		R	R				F				
R	*							F	F		F			R		*		R				
R								F	C		F							F				
								R	F		R			R				F				
R								F	F		F	R		R								

R								R	F		F		R	R						R			
								F	C		F	F								R			
							R	F	F		F									F			
R								F	F		F			R						C			
R									F		F									C			
R								F	F		F									R			
								F	C		C	R								R			
								F	C		C	R		R						F			
								F							*					R			
							R	R	F		F	F		R						R			
								F	F		F			R						F			
								R	F		F			R	*					F			
								R	F		F									R			
								F	C		C		R	R						F			
R									F		F			R						F			
									F		F									F			
						*		F	C		F			R						F			
								F	F		F	R								F			
								F	C		F			R						F			
								R	F		F		R							F			
								F	F		R									R			
R									F		F									R			
R								F	C		F			R						F			
						*		R	C		C									F			
		*						F	F		F									F			
		*						R	C	*	F									F			
R								F	C		R		R		*	*				F			
						*		R	F		F									F			
									F		F												
R		*						R	F		F			R						R			
									C		F									F			
R									F		F			R						F			
R								R	F		F			R						F			
						*		R	C		C			R						C			
									F		F				*					F			
								R	F		F									C			
R		*				*		F	F		F	F								F			

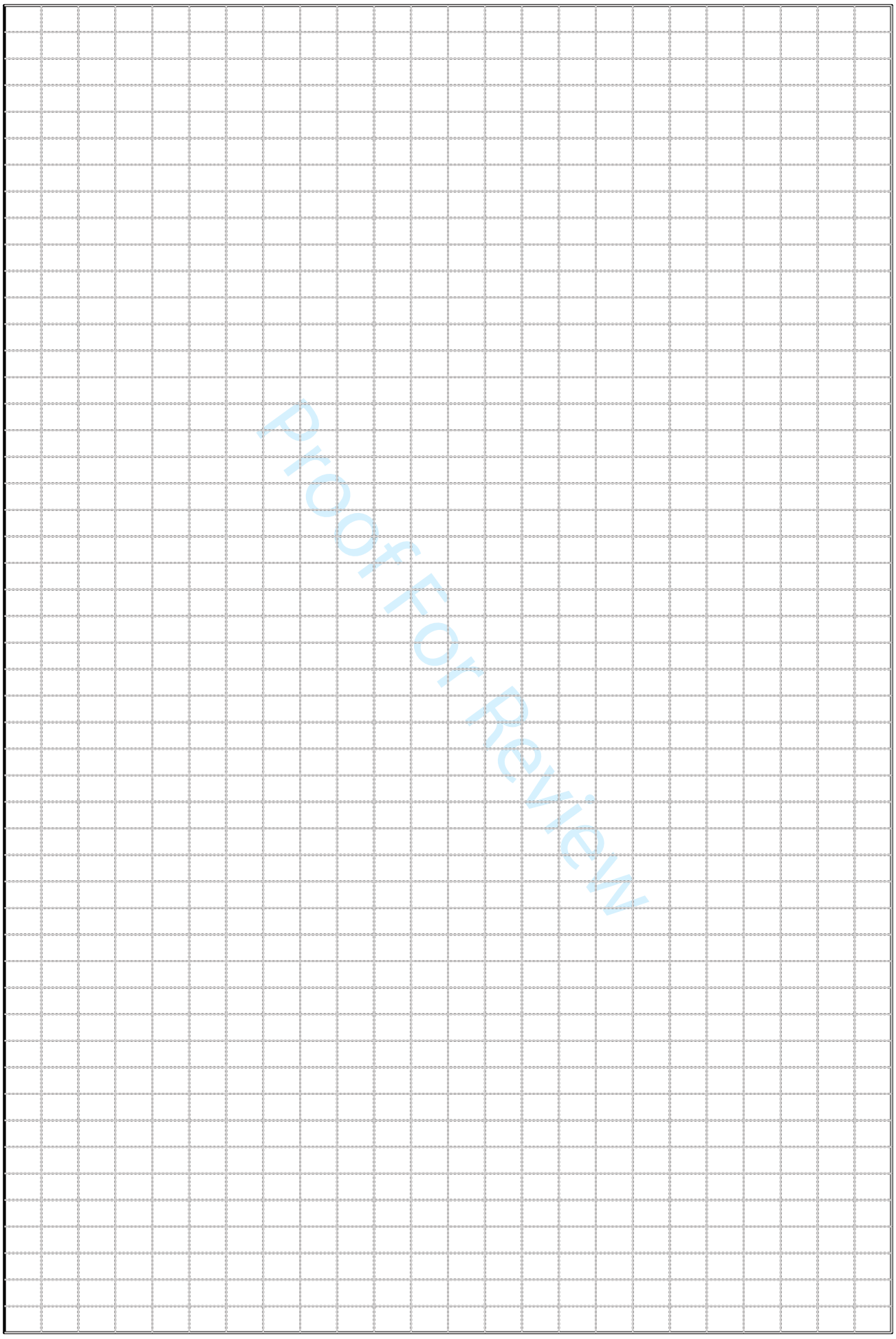
Proof For Review

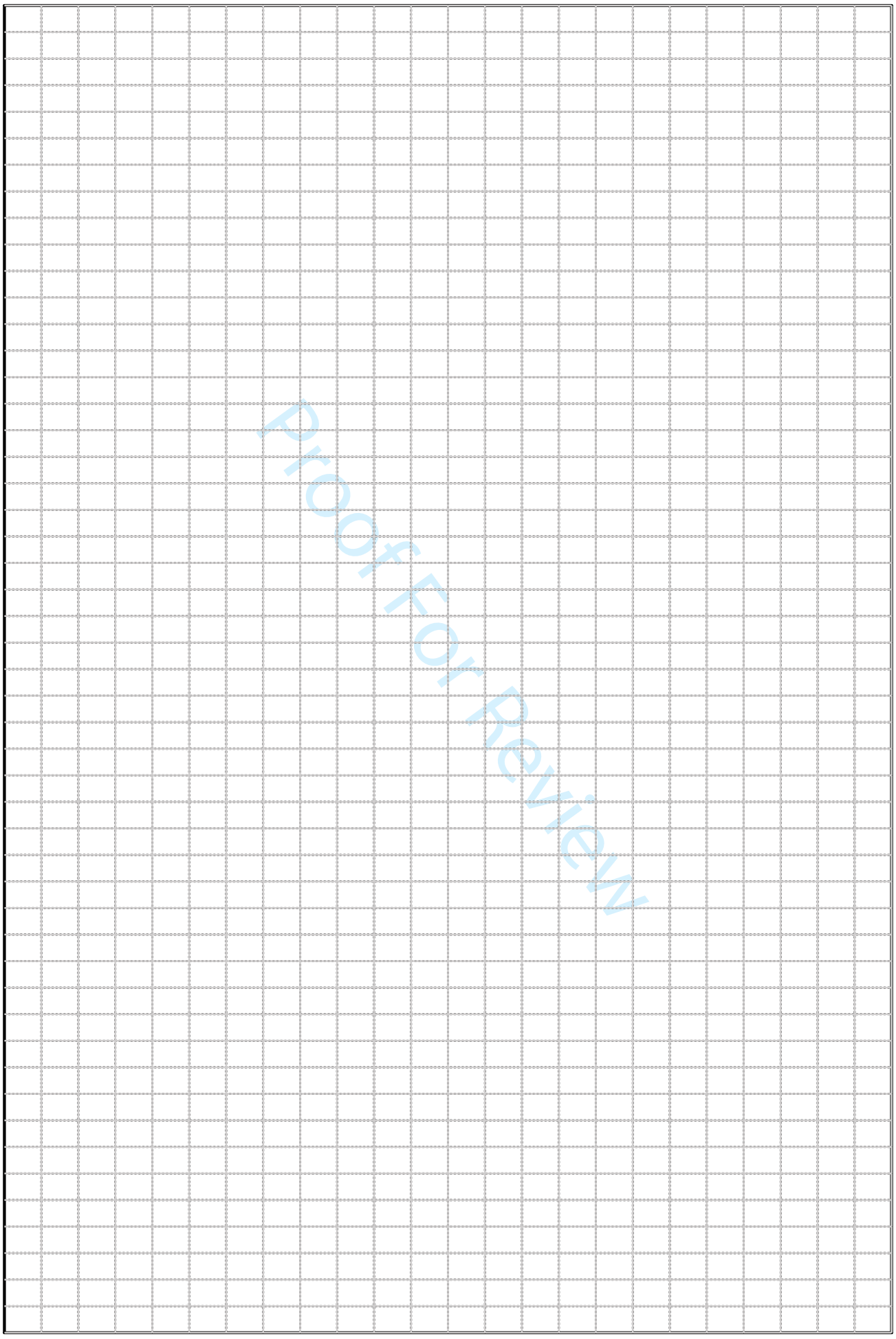
Proof For Review

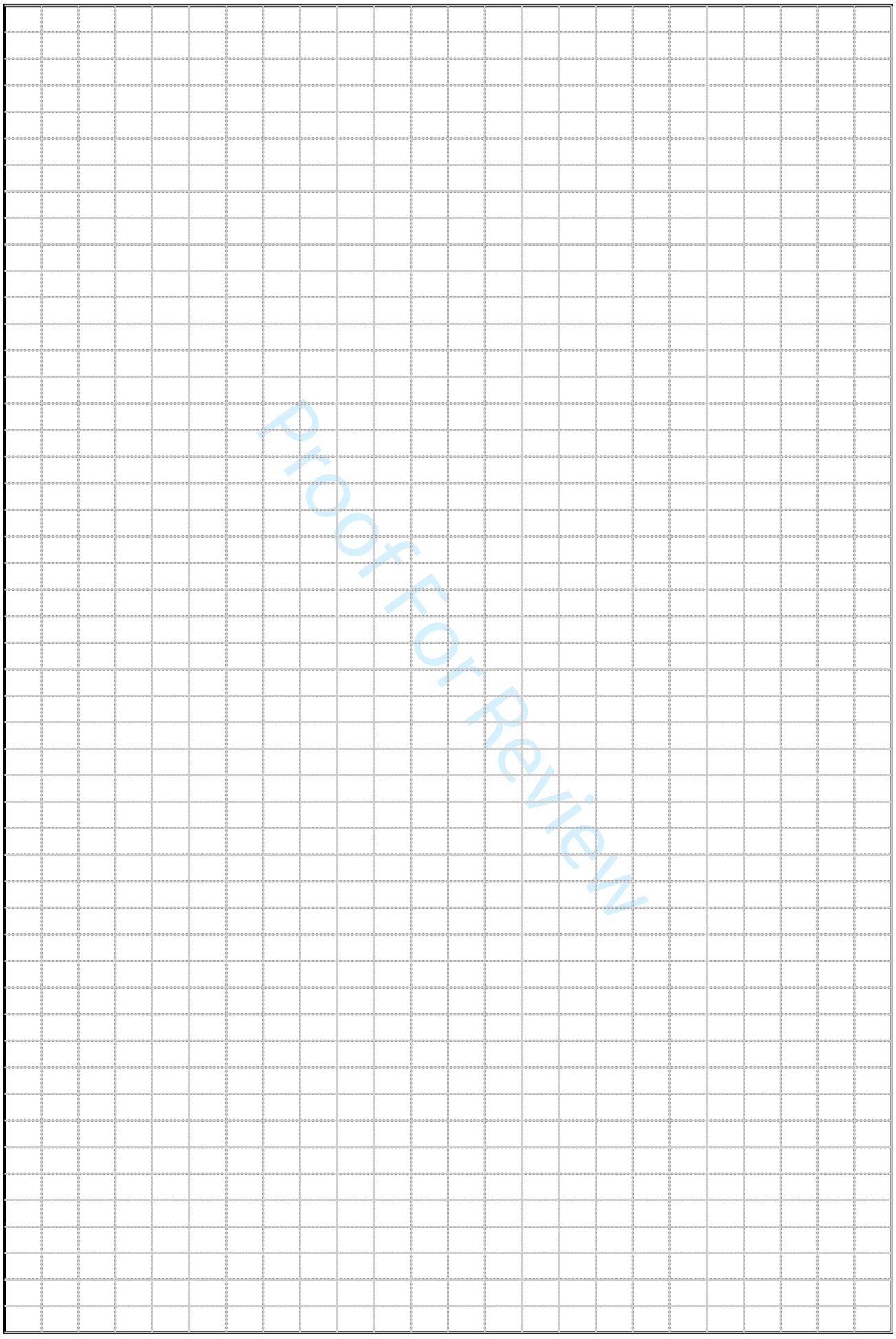
Proof For Review

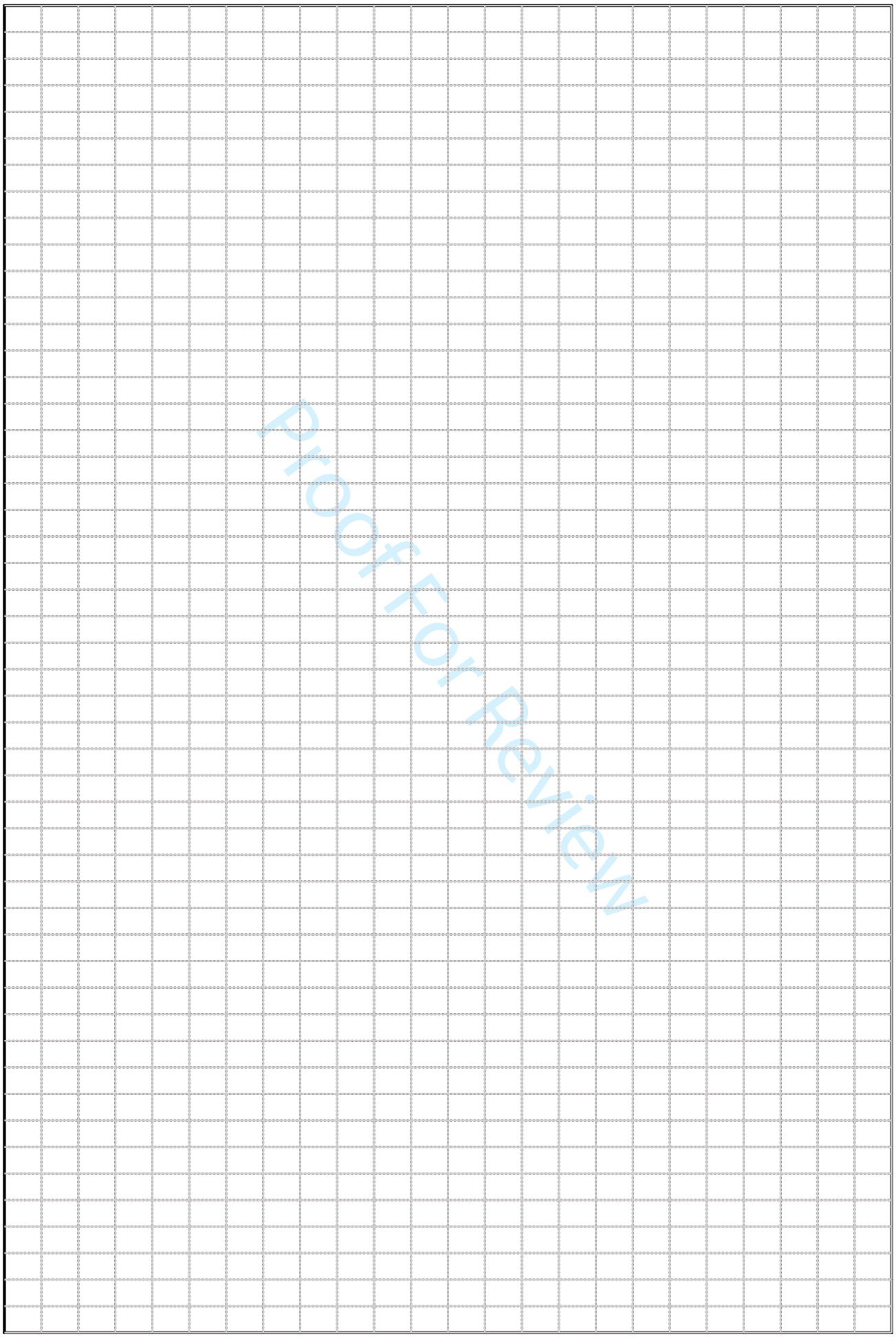
Proof For Review

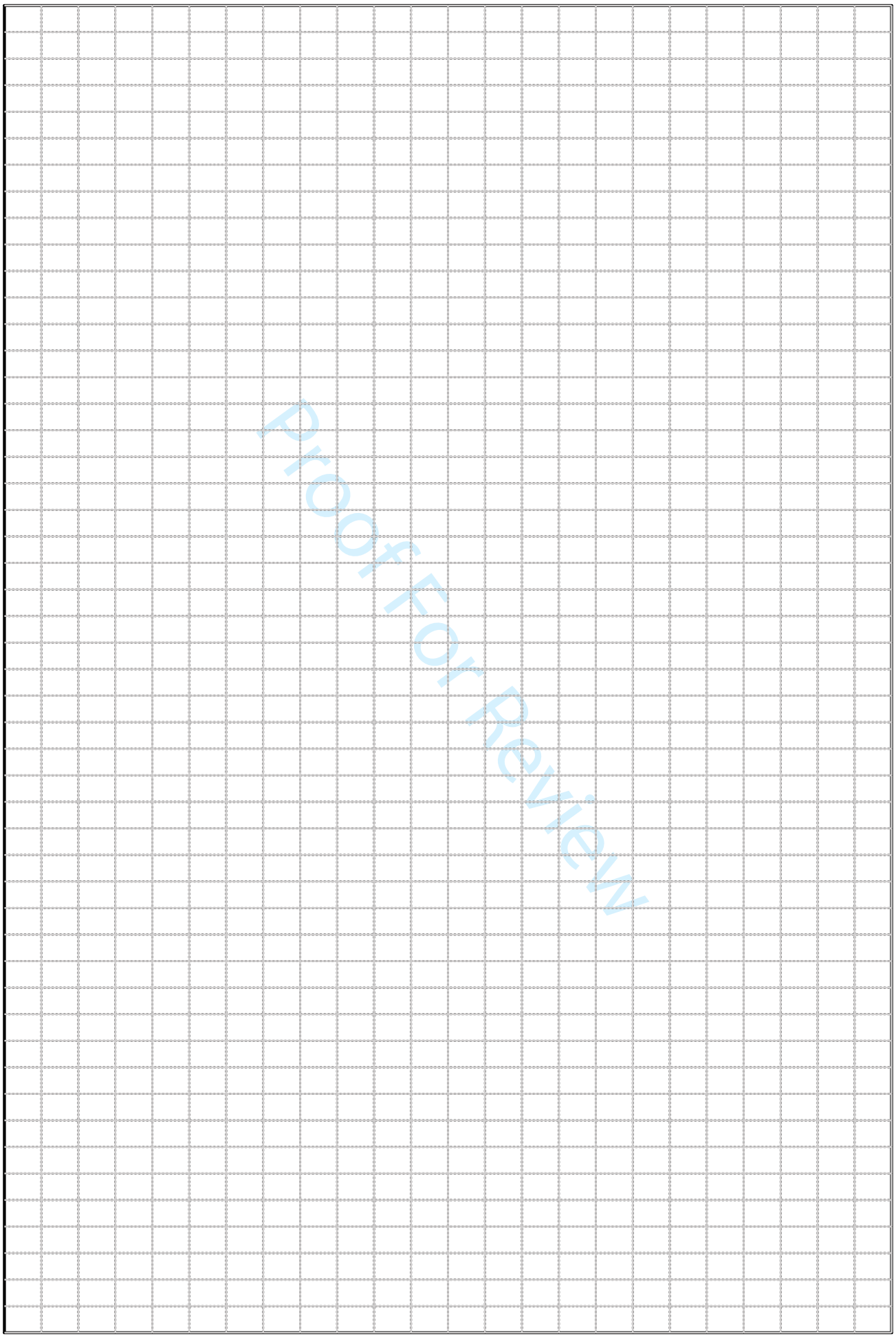
Proof For Review

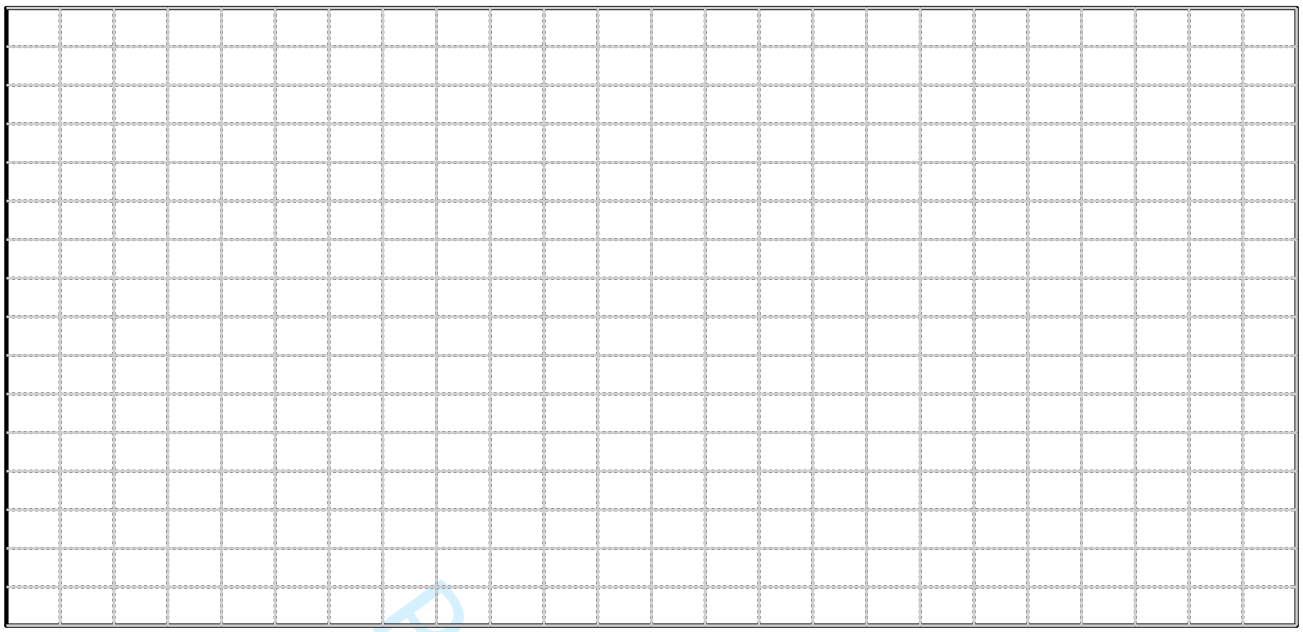

Sphenolithus dissimilis	Sphenolithus editus	Sphenolithus furcatolithoides	Sphenolithus moriformis	Sphenolithus obtusus	Sphenolithus orphanknollensis	Sphenolithus predistentus	Sphenolithus radians	Sphenolithus spiniger	Syracosphaera spp.	Thoracosphaera spp.	Toweius callosus	Toweius pertusus	Toweius rotundus	Tribrachiatus orthostylus	Triquetrorhabdulus rugosus	Umbilicosphaera foliosa	Umbilicosphaera hulbertiana	Umbilicosphaera jafari	Umbilicosphaera rotula	Umbilicosphaera sibogae	Uniplanarius sp.	Zeugrhabdotus sigmoides	Zygrhablithus bijugatus
										R													
									R	R						F	R			F			
									R	R						R				C			
									R	R						R				F			
									R										F				
									R	R										R			*
									R	R						R				R			
										R													
			*							R		*					R						*	
			*							R													*	
			*	*			*						*				R						*	
			*	*						R													*	
			*							R		*					R						*	
			*			*				R				*										*
*			*																				*	
			*							R	*								R		R			
			*							R	*		*				R		R					
										R														
			*							R											R			
*																			R					
			*							R	R						R			R				*
*			*							R									R	R	R		*	
										R											R			
			*							R	R													*
			*	*							R						R							*
			*	*							R											*		*
*																								
			*	*							R						R							*
			*								R						R					R		*
*											R	*		*										
			*								R				*		R							*
																	R		F					
			*	*						R	F		*				R					R		
											R						R							
*										R														
			*	*					*		R						R							*
*			*								R						R						*	

			*								*				F				R		*	*
			*							R											
										F					R							
									R	R					F				C			
									R	F					F				F			
									R	R					F				F			
										R							R	F				
									R	F					F				R			
									R	F					F		F		F			
									R	F					C				F			
										F					F				F			
*										F					F			C	F			
									R	R					C			C	F			*
										F					F			C	C			
										R					F		F		R			
										R					F		R					
										F					F			R				
									F	F					F			F			*	
										R					F		R					
										R					F			F	R			
										F					F			R	F			
										R					F			R	R			
			F							R					R			C	C			
										R					F		R	F	R			
										R					R				R			
	*		*							R							F					
			*							R					F			R				
			*							R												*
			*						R								R			*	*
			*												R					*	*
			*							R			*		R						*
			*							R					R							
			*							R				*								
			*				*			R				*			R	R				*
			*							R								R		*	
*			F							R												
			*							R		*						R				
													*					R	F			
			*							R												
										R										*		
			R							F								F		*		
			*				*			F								R	F			
			*							R		*					R					
			*	*					R			*							R			
										R				*			R					
	*		*							R										R			

			F						R		*											
	*		*																			*
			*							R		*										
			*							R							F	R		*		
			*							R							R		R	*		
			*																R				*
			C							R							R	F				
			*															R					*
			*			*				R													*
			F				*			R	*		*					F					
			*							R											*	*	
										R							R		R	*	*	
			*														R						
			C								*		*				R				*	*	
	*		*															R			*	*	
			*							R										*			
			*							R													*
	*		*																				*
*	*		*							R							R	R	R	*			
									R	R													
										R								R	F				
			C							F													
			C							F					R			F					
									R										F				
										R							R	F					
			F															F					
									R														
			*							R													
			C																				
			*							R													
										R													
			F																				
			*							R								R					
			*														R		F				
			C							R													
			*																				
*									R														
*			*															R	R				
										R								F					
*															R				F				
			C							F													
			F												F								
															F								
*										R					F			R		R			
*			*							R													
*										R					R			R		R			

*										R					F					R			
			C												F								
*			*							R					R								
*									R						F					F			
*			*												R					F			
															F								
*			*							R					F								*
															X			F					
*			*												R								
			*												F								
*										R					R								
			F							R					X			R	R				
*															R								
*										F					F								
*										R					F								
*															F								
*															R								
			*																			*	
			*							R													*
			*													R		F		R			
			*	*						R								R			*	*	*
			*									*				R		R		R			
*				*															R			*	
			F															F					
*										R					R								
*															R								
*										F					R				R	R			
*															R					F			
*															F								
*										R					R			R					
*																							
																		R	R	R			
*															R			R		R			
															R								
			F															C	F				
*															R				R	R			
*																				F			
*			*												R					F			
*			*							R					R					F			
			*							R					R					R			
*			*												R			R	R	R		*	
*			*							R										R			
			*							R										F	*		
			F					*		R								F	F				
*			*																			*	
*										F		*								R	*		
			*																	R			
		*	*							R		*											*
			F									*						F					
*			*																				

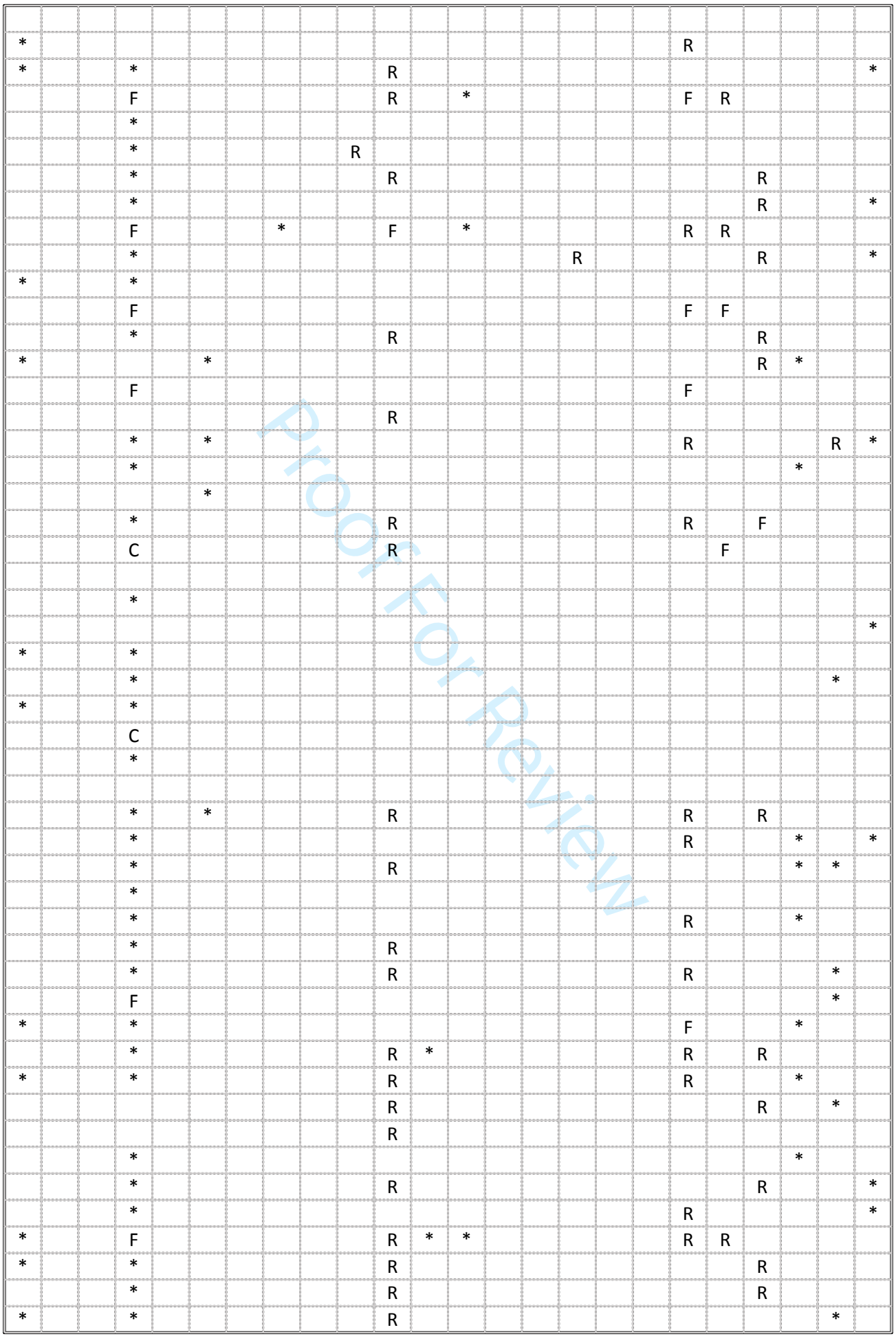

*										R												*	*
*			R		*		*			R								R					
*			*				*											R			*		*
*																						*	
*			*		*					R										R			
*			*							R										R			*
										R											*	*	
*			*							R													
			R							F													
			*							R										R		*	
			*							R													
*			*	*																			*
			*								*							R					
			*	*	*					R										R			*
										R												*	
*										R											*		
										R													
			*		*					R										R	*		
*			*	*						R												*	
*			R					R										F					
										R		*											
	*		*		*					R		*									*		*
			*																	R		*	
			*																R			*	*
			*							R		*								R			
			F											*					R				
			*							R		*									*		
			*							R		*											
										R								R					
			*		*													R		R		*	
*																		R					
										R		*								R			
												*						R					
											*	*							R	R			
	*						*			R												*	
			R															F					

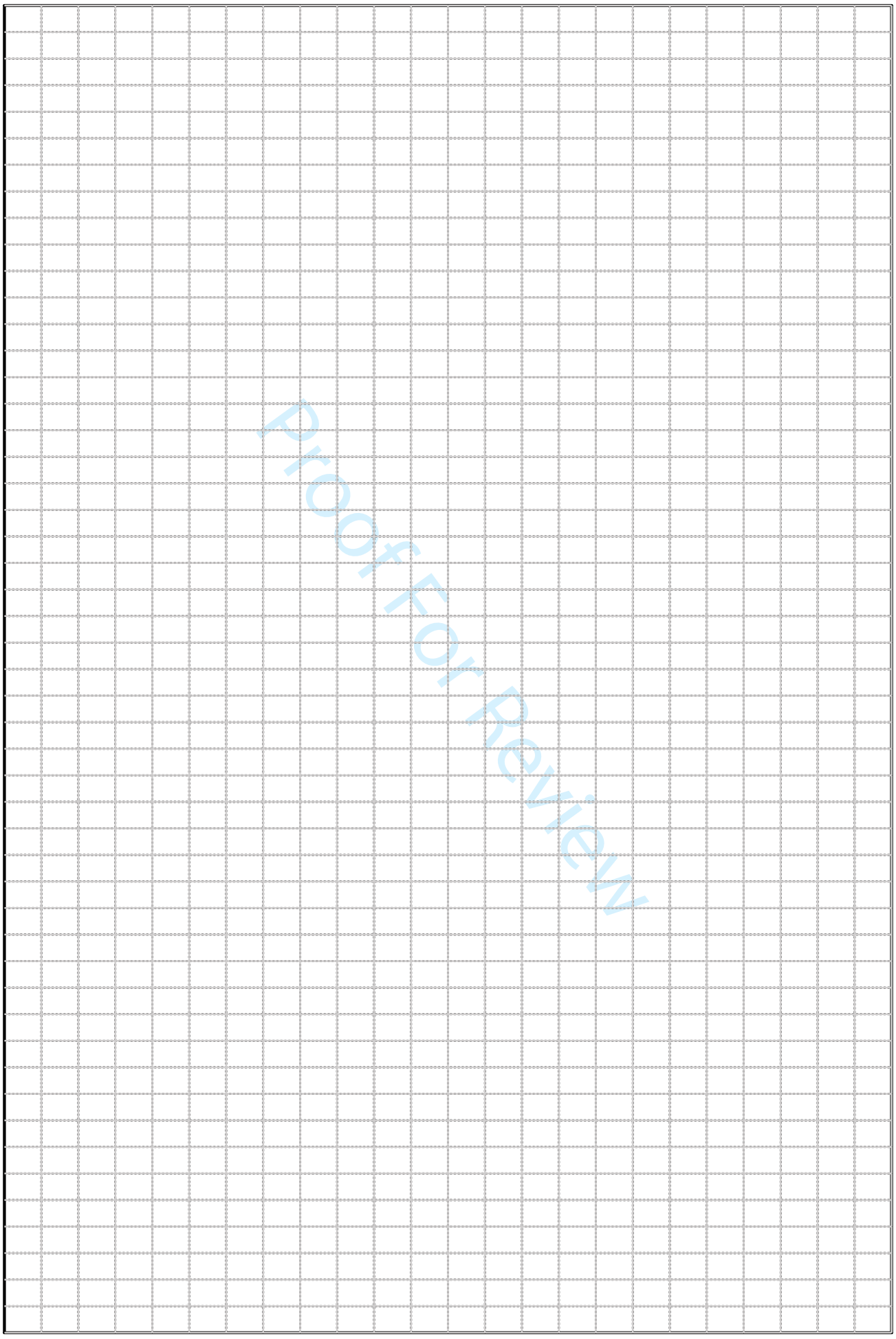
Proof For Review

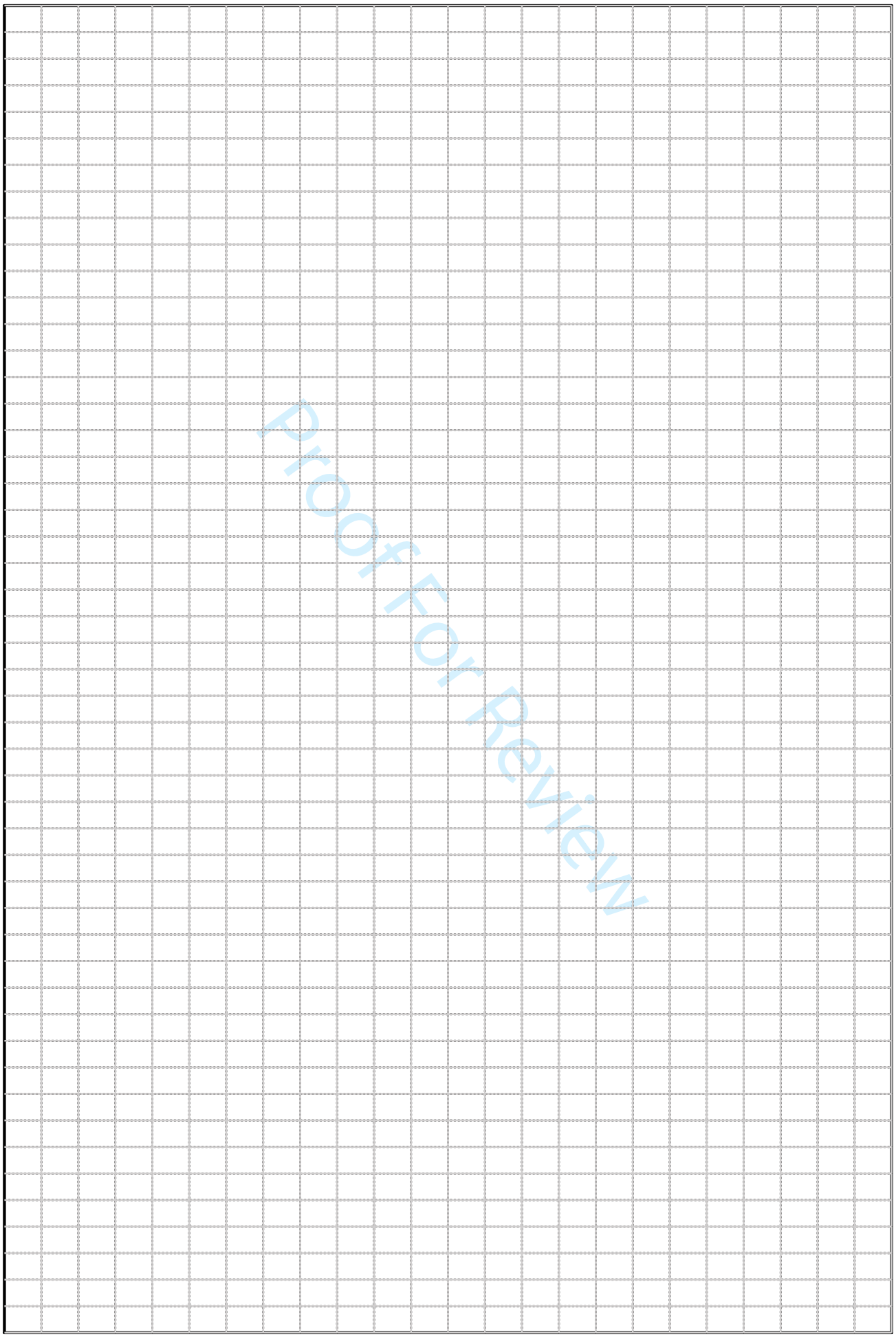
Proof For Review

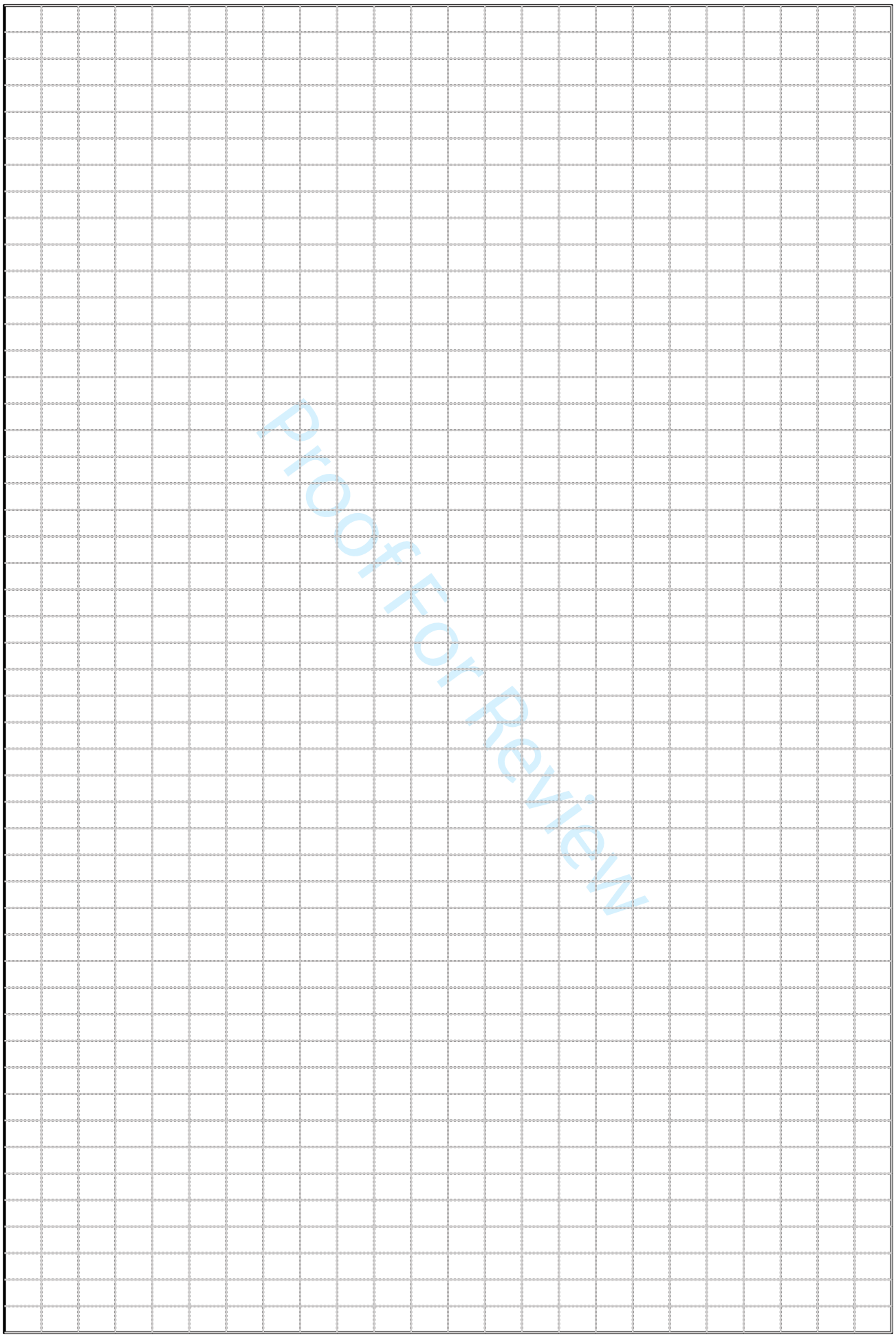
Proof For Review

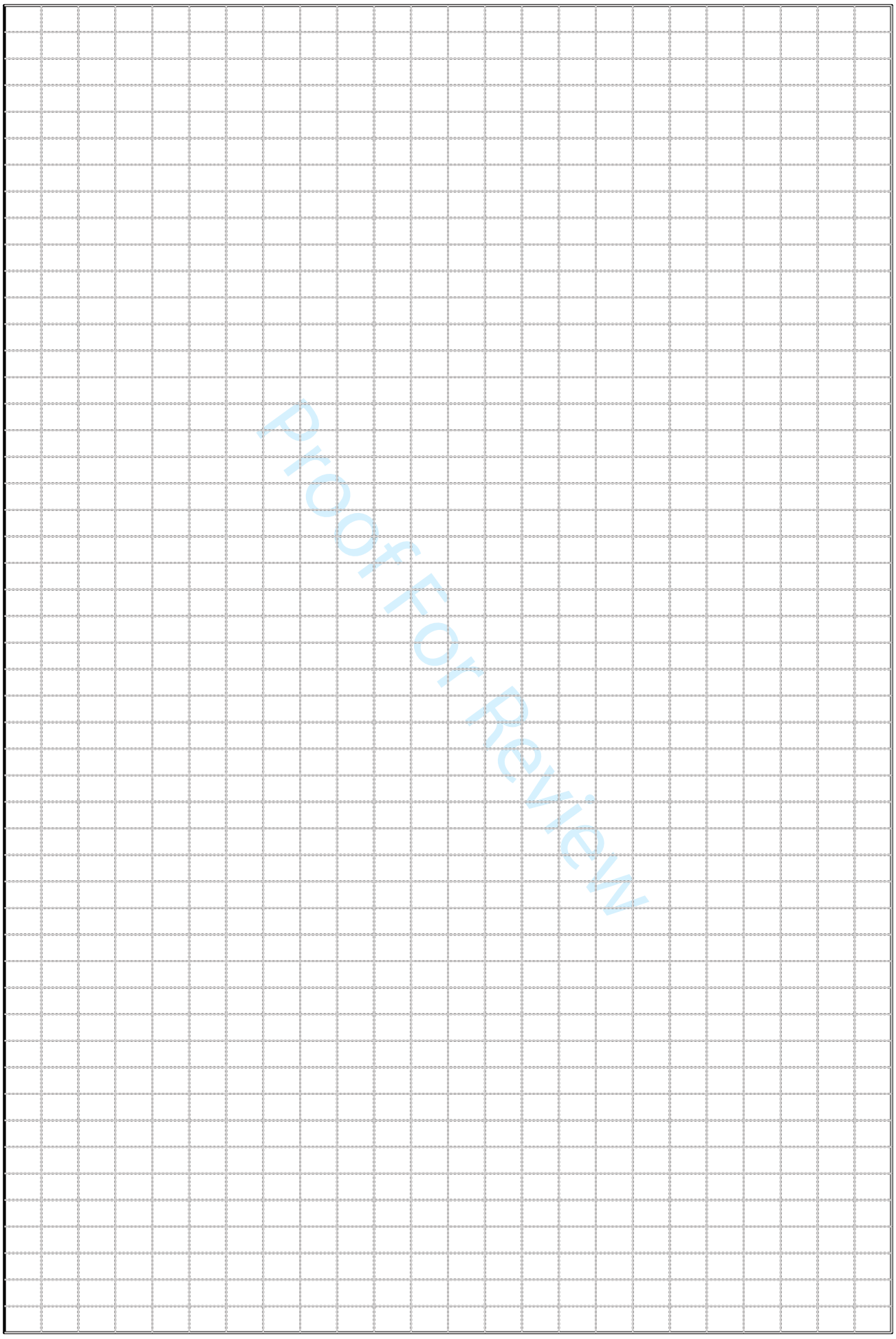
Proof For Review

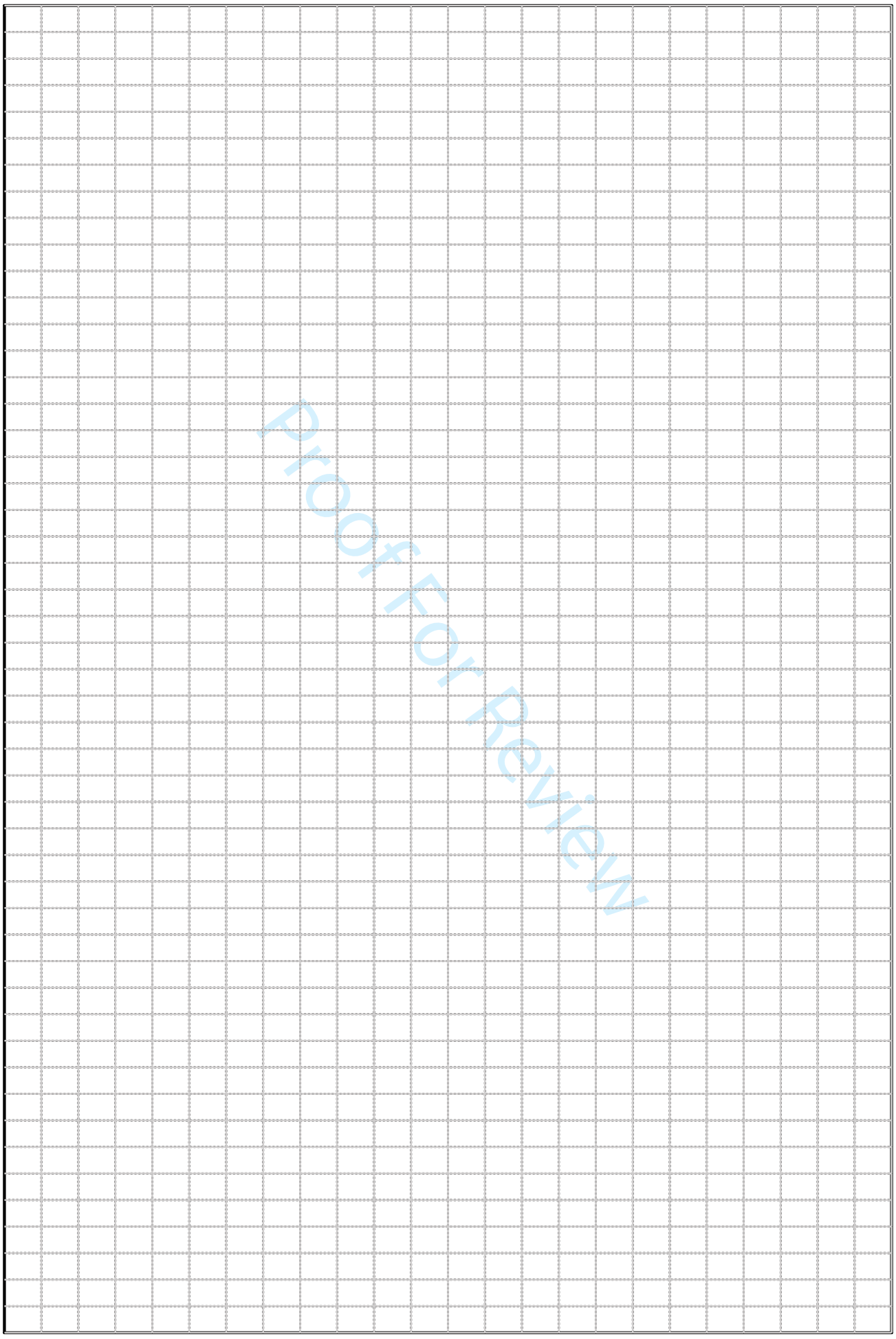
Proof For Review

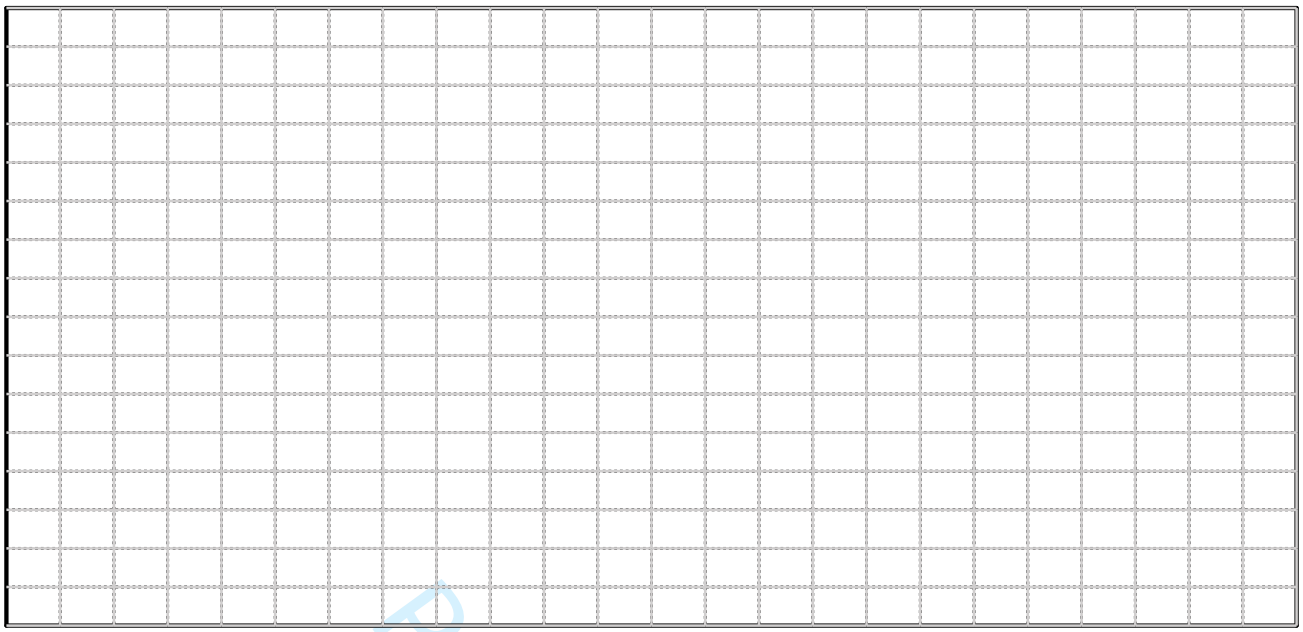

Reworked Cretaceous	
C	
C	
C	
C	
C	
C	
F	
F	
F	
F	
F	
F	
F	
F	
F	
C	
C	
C	

C	
R	
R	
F	
R	
F	
R	
R	
F	
R	
R	
R	
R	
R	
C	
C	
C	
C	
C	
R	
F	
C	
C	
C	
C	
C	
C	
C	
C	
C	
C	
C	
C	
C	
C	

C	
C	
C	
C	
C	
C	
C	
C	
C	
C	
C	
C	
C	
C	
C	
R	
R	
F	
R	

F	
R	
R	
R	
C	
C	
C	
C	
C	
C	
F	
R	
R	
R	
F	
F	
C	
C	
C	
C	
C	
C	
C	

F	
F	
R	
C	
C	
C	
C	
C	
C	
C	
C	
C	
F	
C	
F	
C	
C	
F	
C	
C	
R	
C	
C	
C	
C	
C	
C	
F	
F	
C	
F	
C	
C	
F	
C	
C	
F	
C	
C	
C	

C	
C	
C	
C	
C	
C	
C	
C	
C	
C	
F	
C	
C	
C	
C	
C	
C	
C	
C	
C	
F	
C	
C	
C	
F	
C	
C	
C	
C	
C	
C	